SINGLE-CRYSTAL COMPOSITES: GEL-INCORPORATED SINGLE-CRYSTALS GROWN FROM HYDROGEL MEDIA

A Dissertation

Presented to the Faculty of the Graduate School

of Cornell University

In Partial Fulfillment of the Requirements for the Degree of

Doctor of Philosophy

by

Hanying Li

February 2010

SINGLE-CRYSTAL COMPOSITES: GEL-INCORPORATED SINGLE-CRYSTALS GROWN FROM HYDROGEL MEDIA

Hanying Li, Ph. D.

Cornell University 2010

In Nature, organisms produce single-crystal composites of calcite crystals with incorporated biomacromolecular matrices. In order to understand this phenomenon, we have developed a model system of agarose-incorporated calcite single-crystals grown from agarose hydrogels.

Annular dark-field scanning transmission electron microscopy (ADF-STEM) and electron tomography reveal how random three-dimensional networks of agarose nano-fibers (diameter: 13 ± 5 nm) are incorporated into single-crystals of synthetic calcite by allowing both high- and low-energy fiber/crystal interface facets to satisfy network curvatures. The effects of gel concentration, gel strength, and the concentration of calcium ions on the amount of incorporated polymers have been investigated qualitatively by scanning electron microscopy (SEM) and quantitatively by thermogravimetry analysis (TGA). The results show that gel-grown calcite crystals have two states: without and with polymer incorporation. Crystals switch from the former state to the latter one when gel strength and/or crystal growth rate increase, suggesting that at the growth fronts there are two competitions: a force competition between a disjoining force, a hydrodynamic force, and the resistance of the gel network and a mass competition between growth fronts screened and unscreened by the gel fibers. The interplay between these two factors determines if the gel polymers are incorporated by the growing crystals.

TEM observation shows that agarose/calcite single-crystal composites become porous single-crystals after removal of the incorporated polymers by pyrolysis at 300^{o}C. The specific surface area (5.8 $m^2 g^{-1}$ for crystals grown from 3 w/v % gels) measured by Brunauer, Emmett and Teller (BET) method is around 100 times higher than that of the non-porous calcite single-crystals with the same size.

In addition to calcite, we prepared gel-grown glycine and calcium tartrate single-crystals and found that these two crystals also incorporated gel polymers. These results imply that gel-incorporation might be a general phenomenon for crystallization in gels.

This work presents an approach for modifying the internal structures of crystals and synthesizing single-crystal composites and porous single-crystals. Potential uses for the gel method include the preparation of materials that require both high crystallinity and high surface areas such as photovoltaic materials.

BIOGRAPHICAL SKETCH

Hanying was born 1980 in a small village, Huang Keng, in China. After four years of field fun, he accidently moved to a large city, Xiamen, where it was possible for him to get much better education at a cost of leaving his parents. Taken care by his aunts and uncles, Hanying grew up very well in Xiamen. Admiring his ambitious father, he stood out in high school, especially showing his exceptional understanding on chemistry. In 1998, he attended the department of polymer science and engineering at Zhejiang University (ZJU) where he met Wenjing, who became his wife. In ZJU, he initiated his research experience by doing a summer research project in Prof. Mujie Yang's lab. Then, he joined Prof. Mang Wang's group where he achieved his B.E. and M.E. degrees, studying nano-science and organic semiconductors in collaboration with Prof. Yue Wang and Prof. Yuguang Ma at Jilin Unviesity. In 2005, he started his Ph. D. study with Prof. Lara Estroff at Cornell University, working on biomineralization of calcite in close collaboration with Prof. David Muller at Cornell and Prof. Fiona Meldrum at University of Leeds. After his defense in Dec. 2009, he will join Prof. Zhenan Bao's lab at Stanford University as a postdoc scientist, getting new experiences on organic electronics and optoelectronics.

I would like to dedicate this Ph. D. dissertation to my father, Zongqing Li, and my aunt, Liqin Li, for their profound and constant love.

ACKNOWLEDGMENTS

I am grateful to my Ph. D. life at Cornell. It is intensive and concentrated, full of persistence, longing, inspiration and excitement. I would like to thank everybody who has been supporting me in this four-and-a-half-year long journey.

Prof. Lara Estroff is my great advisor. Her supervision is going to benefit significantly my whole scientific career. Especially, with her help, I have been getting opportunities to communicate with the top scientists in the world to get a "big picture" of my research field. My groupmates have been very supportive. Ellen Keene, Debra Lin, Jason Dorvee, Miki Kunitake, Dat Tran and I have years of overlap and I appreciate their kind helps. Especially, Dat helped me a lot settle down well in Ithaca. And Ellen helped read through this dissertation, providing very useful suggestions.

My research benefits greatly from collaborations and I am grateful to all my collaborators. Especially, Prof. David Muller and Huolin Xin at Cornell contributed their topping STEM method, making it possible to upgrade my work. Prof. Fiona Meldrum and Dr. Yi-Yeoun Kim at University of Leeds shared their deep understanding on particle-incorporation inside crystals. Chung-Han Wu and Dr. Hon Hang Fong at Cornell found applications in electronics for my materials. Dr. Barbara Aichmayer and Anna Schenk at MPI contributed their expertise on interface study using SAXS.

Many thanks to people who help me carry out my experiments. The CCMR facility managers taught and helped me a lot, especially Dr. Maura Weather, John Hunt and John Grazul. Hiroaki Sai and Marleen Kamperman provided kind helps with BET and SAXS measurements.

My research has been moved forward by encouragements, discussions and suggestions. Especially, I appreciate the communications with Prof. Jack Blakely, Prof. Uli Wiesner, Dr. James De Yoreo, Prof. Alexander Chernov, Prof. Katsuo

Tsukamoto, Prof. Juan Manuel Garcia-Ruiz, Prof. Pupa Gilbert, Dr. Nico Sommerdijk, Prof. Rizhi Wang, Dr. Boaz Pokroy and Prof. Zhenan Bao.

My life in Ithaca has been made colorful and full of sweet memories by my friends. Especially, I am grateful to Wenteng Shao, Yong Chen, Steven Tin, Ying Xing, Pengsheng Ji, Jing Sha, Seth Schweitzer, Jingzhou Liu, Kai Xue, David Lou and Qinwen Cai.

My family has been supportive, motivating and inspiring. My wife, Wenjing, gave up her nice job and easy living enviroments in China to accompany me at Cornell. I deeply appreciate her love.

Last, I would like to thank the people, who initially encourage and help me to join top university, especially my friend, Bin Zhu, Prof. Hongzheng Chen and Prof. Jingzhi Sun.

TABLE OF CONTENTS

LIST OF FIGURES

LIST OF TABLES

CHAPTER 1

INTRODUCTION TO CRYSTAL GROWTH IN GELS

The study of crystal growth contributes to our understanding of the structure of matter at atomic scales, the development the solid state science, and the production of crystalline materials with high performance. Crystallization is a common phenomenon ranging from bone formation in Nature to silicon wafer fabrication. Crystal growth has maintained a high level of interest for decades with connection to various disciplines including physics, chemistry, biology, and mineralogy. Although the mechanisms by which crystals grow are complex and not well understood, it is widely accepted that crystallization is determined by both the intrinsic properties of crystals, such as the nature of bonding, and the growth conditions, such as the surrounding medium.[1, 2]

Crystals can be grown from solution, melt and vapor. Gels have been used to grow crystals for more than one century.[3] Crystal growth in gels is a modification of crystal growth in solution. The major difference is, in a gel, solution is compartmentalized in small cavities by a porous solid, the gel network.[3] Various types of crystals have been prepared in gels and many studies have shown that gel-grown crystals are superior to their solution-grown counterparts, in terms of size, quality (such as defect density), and mosaicity.[4-8] Empirically, gels present several advantages as media for crystal growth: 1) generally, spontaneous nucleation is reduced and only a limited number of nuclei form; 2) convection is suppressed and mass transport is dominated by diffusion; 3) gel networks sustain the growing crystals, preventing sedimentation. For these reasons, gels have been called, “the best and most versatile growth media” for crystal growth.[3]

Crystal growth in gels has been widely used to prepare single-crystals for structural characterization,[9] to synthesize porous materials,[10] to study the interaction

between matrix and crystals,[11] and to simulate crystallization in microgravity condition[12]. Early work on crystal growth in gels has been reviewed and collected in Henisch's book (1988)[3] and Lefaucheux and Robert's review (1994)[12]. Herein, I introduce mainly the work done in the past twenty years, emphasizing the biological relevance of crystal growth in gels and studies associated with gel-crystal interactions.

1.1 Gel methods

1.1.1 Crystallization techniques

Crystallization in gels usually involves a chemical reaction or physical mixing between two components (A&B). Typical methods for crystal preparation are double diffusion (or counter-diffusion) and single diffusion. When double diffusion is used, two solutions are physically separated on two sides of a gel (Fig. 1.1ai). Diffusion of the two components from opposite ends of the gel results in crystal formation near the center of the gel where the two reagents meet. A variation of the double diffusion method is to incorporate the two components in two connected gels (Fig. 1.1aii). Crystals then form nearby the interface between these two gels. In contrast, in a single diffusion set-up, one component is incorporated in a gel and the other one is either in the supernatant solution or a gas accessible to the gel (Fig. 1.1b). Generally, both double and single diffusion methods are used to grow insoluble crystals such as barium sulfate from chemical reaction of two soluble components,[13, 14] and single diffusion method is used to prepare soluble crystals such as ammonium sulfate by adding precipitants (such as nonsolvent) to reduce solubility.[15]

Crystallization in gels can also be induced by a change in physical parameters, such as temperature. In this case, the solute for crystallization is gelled and supersaturation is reached by changing the parameter (such as reducing the

temperature). This method is usually used to grow soluble crystals such as sodium bromate.[16]

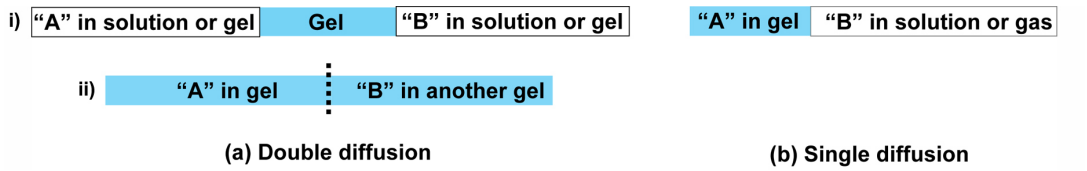

Figure 1.1: Two typical gel methods used to grow crystals formed from mixing or reacting of two components (A & B): a) double diffusion and b) single diffusion.

1.1.2 Gels used for crystallization

Both chemical and physical gels are used for crystal growth. In chemical gels, polymer chains are linked together by chemical bonds, while in physical gels, non-covalent interactions such as H-bonding, salt bridge, and van der Waals force hold the polymer chains together. Agarose is a typical physical gel, while polyacrylamide (PAA) is a widely-used chemical gel. Silica gels, the most commonly used gel media, could be either chemical or physical gels since the type of bonding in silica gels is still unresolved.[3]

Varied techniques have been used to study the network structures of gels, including visualization methods (such as scanning electron microscopy (SEM), transmission electron microscopy (TEM), and atomic force microscopy (AFM)) and methods relying on models (such as light scattering,[17] neutron scattering,[17] X-ray scattering[18] and electrophoresis[19]). Here, I only discuss the studies of gels used for crystal growth using visualization methods. As gels are associated with a large amount (usually >90%) of liquid, visualization of the gel networks rely on advanced imaging techniques, especially with regards to sample preparation such as critical point drying.

1.1.2.1 Silica gels

Silica gels are the most widely used gels for crystal growth.[3] Tetra-methoxysilane (TMOS), tetra-ethoxysilane (TEOS), and sodium metasilicate are typical chemicals used to prepare silica gels. There are three stages to form a silica gel. First, silicic acid is produced by hydrolysis of the silanes or by neutralization of metasilicate, with by-products of alcohols or sodium salts (Fig. 1.2). Second, polymerization of silicic acid leads to 3-D chains that form silica beads. Finally, these silica beads connect together into 3-D gel networks. The linking between the silica beads is still unknown and could be either electrostatic or covalent or the combination of the two. Therefore, it is difficult to categorize silica gels as either chemical or physical gels.[20]

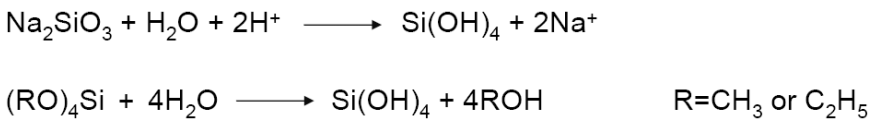

Figure 1.2: Reaction scheme of the formation of silicic acid.

Halberstadt et al. examined silica gels (made from sodium metasilicate) by SEM and observed cellular structures with sheet-like cell walls with varying surface roughness and porosity (Fig. 1.3a, b).[21] Pore size was estimated, ranging from less than 100 nm to several microns. In contrast to sheet-like morphology, sphere aggregates were observed in TEM (Fig. 1.3c, d). [22] Favard et al. reported that networks of silica gels (made from TMOS) were composed of connected spheres of 30 nm (for 5% TMOS gels) and 10 nm (for 10% TMOS gels). Pore sizes were measured to be 210 nm (5% TMOS) and 60 nm (10% TMOS).[22]

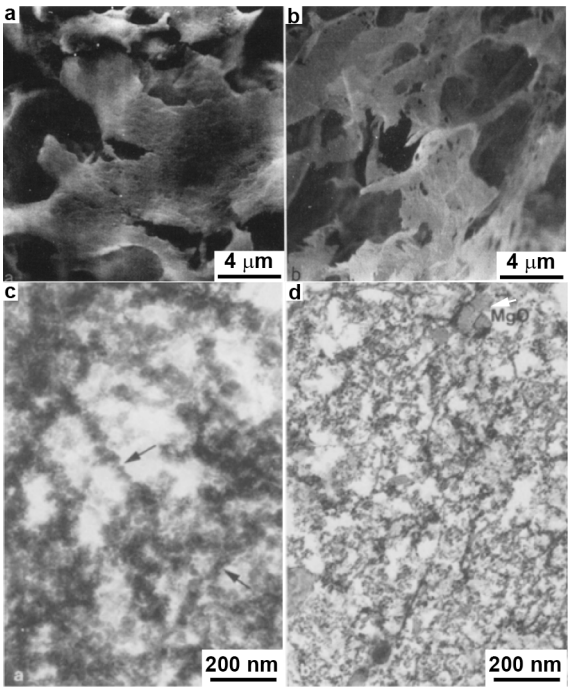

Figure 1.3: (a, b) SEM images of (a) dense and light (b) silica gels.[23] (c, d) TEM images of Pt-C replica of (c) 5% and (d) 10 % TMOS gels.[22] Arrows in (c) highlight the silica spheres and the arrow in (d) indicates the MgO particles that were used to label the gel surface where the gels was vitrified without ice formation and the inherent gel structure was maintained during the preparation of TEM samples.[24]

1.1.2.2 Agarose gels

The molecular structure of agarose is a linear polysaccharide consisting of alternating 1,3-linked β-D-galactopyranose and 1,4-linked 3,6-anhydro-α-L-galactopyranose. Agarose powder is soluble in hot water and the warm solution gels on cooling to gelling temperature (~40^{o}C). The gels melt at temperatures (~85^{o}C) that are higher than the gelling temperature. During the process of gelation, polymer chains form helices (double or single helix) that subsequently aggregate into three dimensional (3-D) bundles (Fig. 1.4).[25, 26] Both the gelling and melting temperatures can be reduced by chemical modification such as partial hydroxyethylation.[27]

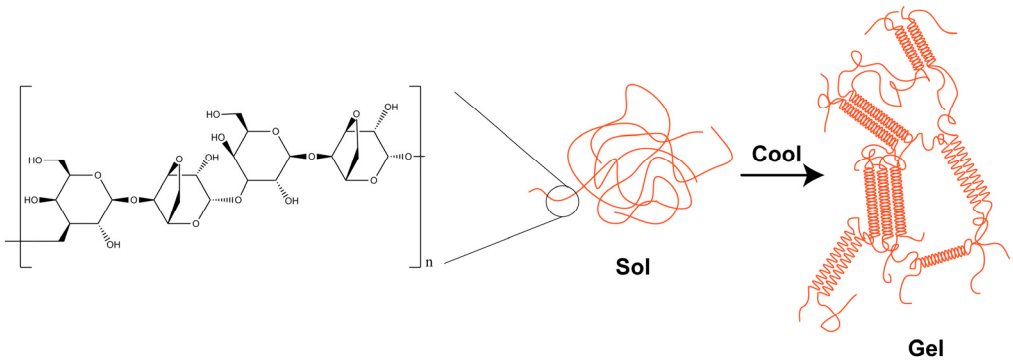

Figure 1.4: Chemical structure of agarose and its structure evolution during gelation.[25, 26]

The network structure of agarose gels has been widely studied. Zhou et al. measured the pore size of critical point dried agarose gels by SEM (Fig. 1.5). [10] When the gel concentration is increased from 0.5 wt% to 5 wt%, the pore sizes decreased from 180 nm to 55 nm.

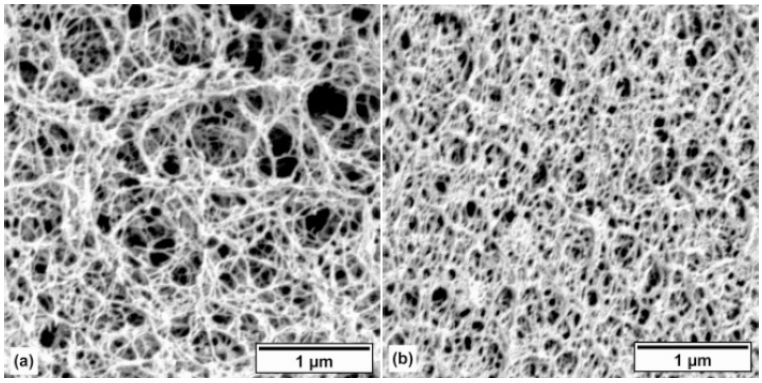

Figure 1.5: SEM images of critical point dried agarose gels: (a) 0.5 wt%; (b) 2 wt%.[10]

Compared to SEM, TEM provides better spatial resolution and thus more structural information. Typically, freezing techniques are used to vitrify the gel (such as in liquid helium) and the gel network is exposed after fracture or by sublimating the frozen liquid in vacuum. Then replicas (e.g., Pt-C) of the exposed gel structure are

prepared for TEM observation.[24] Using such techniques, Waki et al. observed dots that were believed to be the image of the replicas of agarose fibers protruding out from the freeze-fractured surface (Fig. 1.6a, b).[28] The number of fibers per unit area and the mean square radius of the fibers were measured in the TEM images of gels at different gel concentrations (0.25-4 w/v %). Physical parameters of the gels were calculated based on these two measured data, as well as a model, including fiber density, water content, and total length of fiber per unit volume. In addition, the authors found that gels prepared with Tris-borate buffer had larger pore sizes than those gels made in water. Whytock et al. also studied the structure of agarose gels.[29] Instead of "dots" as Waki et al. reported,[28] they observed fibrous networks in TEM (Fig. 1.6c, d). The discrepancy is possibly due to the different methods of TEM sample preparation. Whytock et al. freeze-etched their samples before shadowing them with Pt/C, while Waki et al. did not. Measurements of the diameters of the fibers showed an increase from 5.6 nm to 8.8 nm with increasing gel concentration (0.3-2 w/v %). This trend is contradictory to Waki's report[28] where fiber diameters decreased from 5.6 nm to 3 nm as gel concentration increased from 0.25 % to 4 w/v%. In addition to replica techniques, the structure of agarose gels has been examined in stained, ultramicrotomed, thin sections. Using this technique, Griess et al. observed fibrous structures with fiber widths of 15-30 nm.[30] The interfiber distances were measured and they decreased from 300 nm to 68 nm as the gel concentration increased from 0.4% to 2.5%. For derivatized (hydroxypropyl) agarose gels, the interfiber distance were smaller.

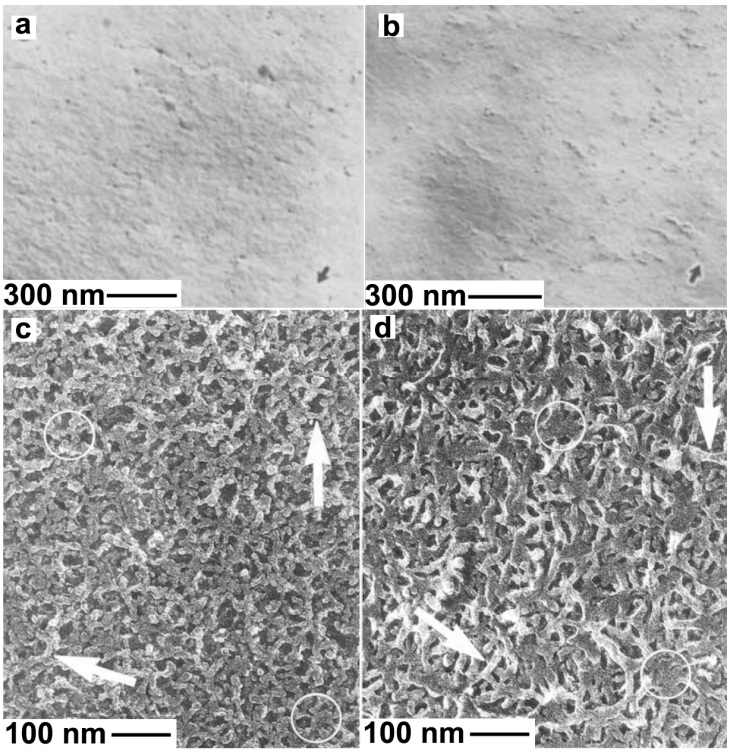

Figure 1.6: TEM images of (a, c) 0.5 % and (b, d) 2 % agarose gels. (a, b) were reported by Waki et al. [28] Arrows show the direction of shadowing for replicas. (c, d) were reported by Whytock et al.[29] Arrows highlight the fibers with two clear shadowed sides, while circles indicate where the sides of fibers are obscure.

Agarose gels were also investigated by AFM. Compared to SEM and TEM, AFM has the advantage that it does not require high vacuum so that experiments could be carried out in an aqueous environment to eliminate potential artifacts introduced by drying samples. Maaloum et al. studied the structure of agarose gels by AFM (under aqueous conditions) and observed porous structures (Fig. 1.7).[19, 31] The pore size decreased from 530 ± 185 nm to 201 ± 36 nm and the size distribution became narrower when the gel concentration increased from 0.7% to 5%. Empirically, pore size, a, as a function of gel concentration, C, showed a power law dependence, $a \sim C^{-0.6}$. The effect of ion strength on pore size was also examined by introducing Tris-borate-

EDTA buffer into the gels. The results showed that pore size increased and the pore size distribution became wider as the ionic strength increased.

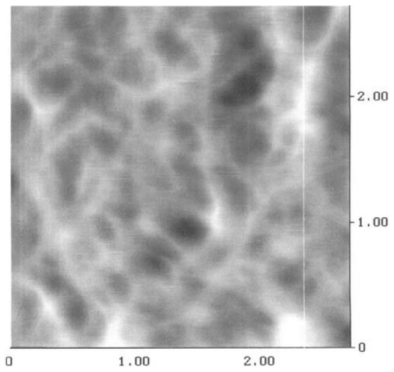

Figure 1.7: An AFM image (3 μm by 3 μm) of a 3% agarose gel.[31]

1.1.2.3 Polyacrylamide (PAA) gels

PAA is a typical chemical gel that is also used for crystal growth. The chemical composition is polyacrylamide polymers and the 3-D gel network is formed by interconnecting covalently-linked PAA chains by crosslinking reactions.

Blank et al. studied the structure of PAA gels using SEM.[32] Gels with 2.5 wt% of PAA had a porous structure with pore sizes of 2-10 μm (Fig. 1.8a, b). Denser gels (4 wt% PAA) were less porous with larger pores (2 – 15 μm). The gel structure was not uniform in size, as can be seen by comparing Fig. 1.8a and Fig. 1.8b.

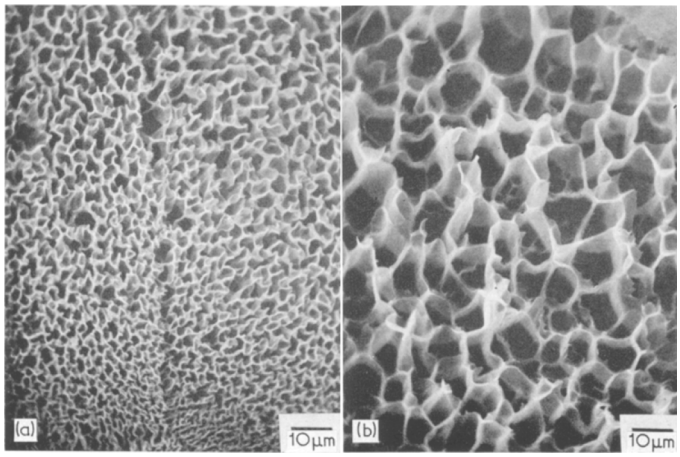

1.8: SEM images of a 2.5 wt% PAA gel.[32]

Ruchel et al. studied the structure of PAA gels by TEM and observed cellular morphologies.[33] Effects of gelation conditions were investigated, including acrylamide concentration, cross-linking ratio, different cross-linkers, and catalyst concentration. Qualitatively, pore sizes were inversely proportional to acrylamide concentration, and the percentage of cross-linking showed a non-linear effect. About 5% cross-linking resulted in minimum pore size, while more or less cross-linking led to larger pore sizes. Hsu et al. also observed PAA gels by TEM.[34] PAA gels and solutions with 5% PAA were examined and compared. TEM images showed that the structure of PAA solution is more homogeneous than that of PAA gel. This difference was reconfirmed by photodiffraction and the reason was attributed to the aggregation of cross-linkers during gelation.

The above work gives abundant information about the network structure of gels. However, caution is warranted when this information is referred to interpret crystallization in gels. Firstly, gel structure might be changed during the process of sample preparation for SEM or TEM examinations resulting in artifacts.[24, 28, 32, 33, 35] Secondly, the recipe (especially the solution composition) used to prepare the gel

samples for structural characterization is usually different from that for crystal growth. This difference might result in structure modification. Finally, gels are not equilibrium structures and their network structures are known to evolve with time.[23]

1.2 "Structure" of liquids in gels

For crystal growth in gels, it is important to consider the structure of the solvent molecules in the gels since it may be different from that of bulk solvent (e.g. water in hydrogels). Differences in solvent structure will lead to differences in solubility and activity of solutes and affect supersaturation levels and diffusion of the solutes for crystallization in gels.

In gels, liquids are trapped within solid networks. The interaction at the solid/liquid interface changes the structure of liquids nearby the interfaces. For example, water in hydrogels has been studied.[36-41] The water in hydrogels is different from the bulk water and has been divided into three categories: bound water, free water, and intermediate water. [42, 43] The bound water interacts strongly with the solid network and has aggregation structures different from bulk water. The free water is similar in structure to bulk water. The intermediate water interacts weakly with the solids and is the state between the first two types. Supporting evidences for these three types of water include thermal expansion,[44] specific conductivity,[45] infrared spectroscopy,[46, 47] nuclear magnetic resonance (NMR),[48, 49] differential scanning calorimetry (DSC),[43] and Raman spectroscopy.[39, 50] For example, Lee et al. studied the water in poly (2-hydroxyethyl methacrylate) (pHEMA) gels, using multiple techniques.[43] For dilatometry measurements, gels with high water content (50%) showed a sharp volume change at 0^{o}C, while gels with low water content (20%) did not have this kind of thermal expansion. Gels with medium water content exhibited an intermediate behavior. These results were consistent with the model of the three types

of water in gels. A specific conductivity study gave activation energies for specific conduction and the relationship between activation energy and water content in gels clearly indicated three different zones, implying the existence of three possible types of gelled water. DSC verified the three different behaviors of gelled water. Gels with low water content (20%) showed no phase transitions (-15 ^{o}C to 24^{o}C), indicating that the gelled water were mainly bound water. As water content increased, the phase transition exist and transition temperature gradually shifted and reached near 0^{o}C at high water content (60%).

1.3 Effects of gels on crystallization

When crystals grow in gels, the gels define the space for the initiation of crystallization and serve as media to supply the "nutrients" to the growing crystals. The effects of gels on crystallization occur both during crystal nucleation and growth, including general and specific effects. General effects apply to all gel/crystal systems, such as the effects associated with mass transport. The specific effects involve interactions between the gel networks and the crystals. This category of effects depends on a specific gel-crystal pair.

1.3.1 Nucleation in gels

Generally, gels strongly suppress spontaneous nucleation, as compared with solution. In gels, the solution is isolated into small cavities by the gel network and convection is suppressed. "Nutrients" are supplied to the growing nuclei by diffusion-dominated mass transport among the cavities, leading to a reduced probability that the nuclei reach the critical size required for growth. Therefore, nucleation in gels takes place only when "nutrients" accumulate to a fairly high threshold supersaturation.[51, 52]

In addition to the confinement effect, there are other specific effects on nucleation. For example, Vidal et al. studied the crystallization of hen egg white lysozyme (HEWL) in silica[20] and agarose[53, 54] gels using small angle neutron scattering (SANS). Interestingly, silica gels inhibited HEWL nucleation, while agarose gels promoted it. For the silica system, HEWL molecules were found to absorb onto the silica network, resulting in a lower concentration of free HEWL and thus a lower nucleation rate as compared to gel-free solution. For the agarose system, nucleation was promoted, possibly because gels contributed to the formation of large HEWL clusters. More recently, Van Driessche et al. measured the two dimensional (2D) nucleation rate of HEWL in agarose gels using laser confocal microscopy combined with differential interference contrast microscopy and found that 2D nucleation rates were enhanced by agarose fibers.[55]

Another effect of gels on nucleation is seen in Petrova and Swift's work looking at enantiomeric selectivity of sodium chlorate (an achiral molecule adopting chiral forms (*d* or *l*) in crystalline solids) crystals grown in agarose gels.[56] While solution-grown crystals yielded a 1:1 statistical distribution of *d*- and *l*-enantiomers, large enantiomeric excesses were observed in gel-grown crystals. The magnitude and direction of the enantiomeric excess could be controlled by changing the gelation or crystallization conditions including gel concentration, temperature, and co-solvent. The mechanism of enantiomer selection was ascribed to intermolecular interactions between the gel and crystal surfaces that inhibited the formation of the two enantiomers to different extents.

Gels can also influence polymorph selectivity. Xiao et al. grew calcium carbonate in chitosan sols and gels and found that calcite, the most stable polymorph formed in sols while in gels, vaterite, the least stable polymorph, formed.[57] The phase selection was suggested to relate to different interactions between the crystals and

chitosan chains with different flexibility. Similarly, Daiguebonne et al. [58] reported that the reactions of Erbium or Nickel ions with polycarboxylate ligands in agarose gels resulted in polymorphs different from those grown in hydrothermal conditions. Pauchet et al.[59] found that silica gel was suitable to grow form III of (±)-modafinil, a metastable polymorph that had not been obtained in solution growth. One possible explanation for the appearance of metastable polymorphs in gels is Ostwald's "rule of stages", which predicts that metastable phases should precipitate prior to the stable phases in a system deviated from thermodynamic equilibrium.[1, 2] The high level of threshold supersaturation in gels, therefore, may favor the nucleation of the metastable phases.

1.3.2 Morphology of gel-grown crystals

Once nuclei reach their critical sizes, they start to grow under the influence of the surrounding gels. The effect of gels on crystal growth is expressed in the morphology of the crystals. One prominent effect of gels on crystal morphology is a destabilization of the polyhedral shape. This effect results from the specific mode of mass transport, the way in which growing crystals are fed. In gels, convection is suppressed and mass transport is dominated by diffusion, leading to a roughly spherical concentration contour surrounding growing polyhedral crystals where corners and edges are better supplied than the face centers.[60-62] Once critical supersaturation is reached, 2-D nucleation takes place at the corners and edges and crystals lose their morphology stability with overgrowth at the corners and edges and depression at the face centers. Therefore, the gel-grown crystals often show skeletal, hopper-like or star-shape morphologies (Fig. 1.9).[9, 63-66] In gels with high gel concentration, the very high level of threshold supersaturation leads to adhesive-type growth mechanisms, resulting in dendritic or branched crystals.[2, 64]

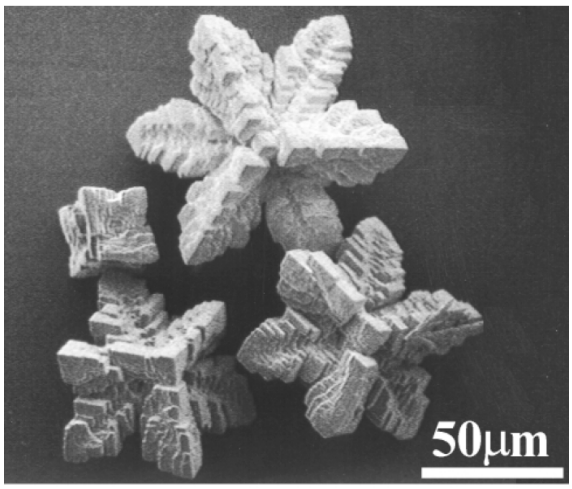

Figure 1.9: A SEM image of star-shaped calcite crystals grown from a 1 % agarose gel.[63]

In addition to mass transport, specific chemical interactions between gels and crystals might play a role determining crystal morphology, possibly similar to the effects of varied additives on crystal morphology through stereochemical recognition and/or step-specific interactions.[67-71] For example, Petrova et al. prepared asparagine monohydrate crystals in several different gel media including agarose, carrageenan, and gelatin.[72] Gel-grown crystals exhibited morphologies different from their solution-grown counterparts and the morphology depended on the gel media. The morphological dependence was interpreted in terms of possible gel-crystal interactions. In other work, when grown in gelatin, PAA gels or PAA gels with sulfonic acid groups, calcite crystals are expressed in morphologies (such as pseudo-octahedral) different from the typical rhombohedra (Fig. 1.10).[73-75]

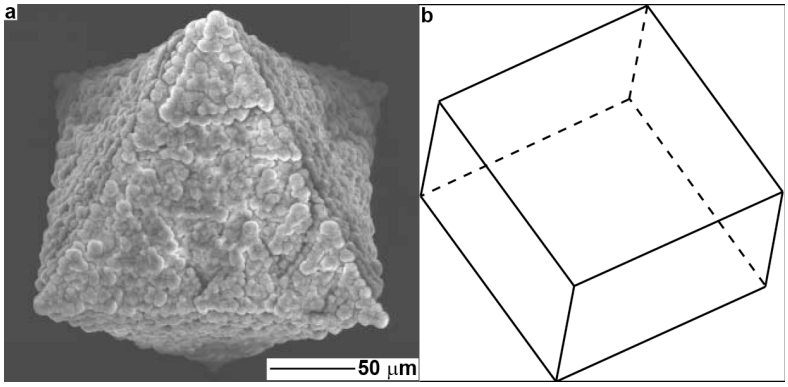

Figure 1.10: (a) A SEM image of a pseudo-octahedral calcite crystal grown from a PAA gel.[74] (b) A model of the typical morphology of calcite crystal expressed by six $\{10\bar{1}4\}$ faces.

1.3.3 Gel-incorporation

During crystal growth, the surrounding gel networks become physical obstacles for the growing crystals. In order to continue to grow, the crystals must either push away or incorporate the gel networks. Gel rupture (or "cusp" formation) has been observed around crystals, indicating that crystals can push away and break the gel networks to make space.[76, 77] For most of the cases of crystallization in gels, the gel networks are pushed away by growing crystals, resulting in "pure" crystals.[3]

There are exceptions, however, where crystals incorporate the gel networks rather than push them away. In 1969, Nickl and Henisch found that calcite crystals grown from silica gels actually incorporated the gel matrix and became gel/single-crystal composites.[78] Dissolution of the gel-grown crystals in acids provided direct evidence of gel incorporation (Fig. 1.11). More recently, Huang et al. showed that when grown in gelatin gels, calcite crystals also incorporate the gel materials.[75] In addition, Garcia-Ruiz et al. reported that gel-grown protein (lysozyme, ferritin and thaumatin) crystals can incorporate the gel (silica and/or agarose) matrix.[9, 79] In the

case of HEWL crystals grown from silica gels,[9] two effects of gel incorporation on the properties of crystal were found. First, the morphology of the crystal was controlled by the amount of incorporated gel. With increasing gel concentrations, the shape of protein crystsals evolve from faceted polyhedrons to spheres, possibly, because the incorporated gel fibers reduce the surface energy anisotropy. Second, the incorporated gel reinforced the crystals and enhanced their resistance to dehydration, benefiting structural characterization by X-ray.

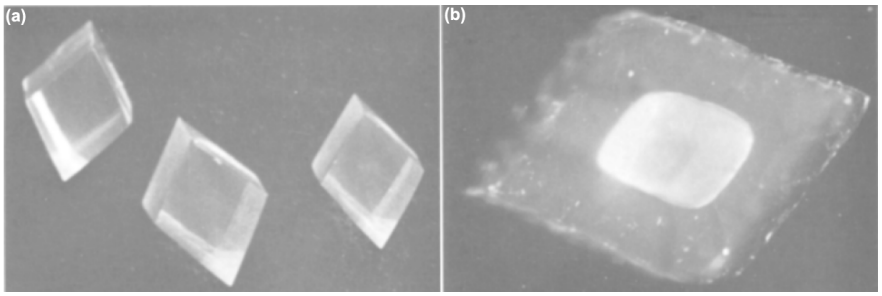

Figure 1.11: (a) Calcite crystals grown from a silica gel. Edge length: 2.5 mm; (b) A gel-grown calcite crystal after partial dissolution in acid. The incorporated gel network was left around the centered residual crystal, maintaining the same shape as the original crystal. Original edge length: 2.5 mm.[78]

The mechanism of gel incorporation is still not clear. Intuitively, the incorporation might be due to chemical interactions (or good wetting) between the gel network and the crystal.[9, 55] However, good wetting might not be necessary. Khaimov-Mal'kov suggested that gel incorporation was associated with the mechanical properties of the gel network. The incorporation (or lack thereof) of the gel matrix into the growing crystal was determined by the competition between the crystallization pressure and the gel strength.[76, 79] Gels that were strong enough to resist the crystallization pressure would be incorporated, while weaker gels would be pushed

away (or broken). In addition to wetting and the mechanical properties of the gel, growth kinetics might be another factor related to gel incorporation phenomena.[80] The investigation of particle incorporation into growing crystals has shown that there is a critical growth rate beyond which particles are incorporated.[1, 80-83] Possibly, this kinetic effect also applies to gel incorporation. (see Chapters 6 and 7 for further discussion.)

1.3.4 Gels as porogens

The porous, continuous network structure of gels is another characteristic that has been exploited for crystal growth. Gels are used as porogens to template materials by growing polycrystalline materials in the gel networks. After removing the gel networks, porous materials with aggregates of tiny crystals are obtained. For example, using gels (agarose, gelatin, and PAA) as a porogen, porous TiO_2, SnO_2, ZrO_2, SiO_2, In_2O_3 and Nb_2O_5 materials have been prepared. [10, 84-86] Among them, porous TiO_2 was studied in detail and materials with specific surface area of 5-100 m^2g^{-1} were obtained, exhibiting efficient photocatalytic activities (Fig. 1.12). [10, 85-89]

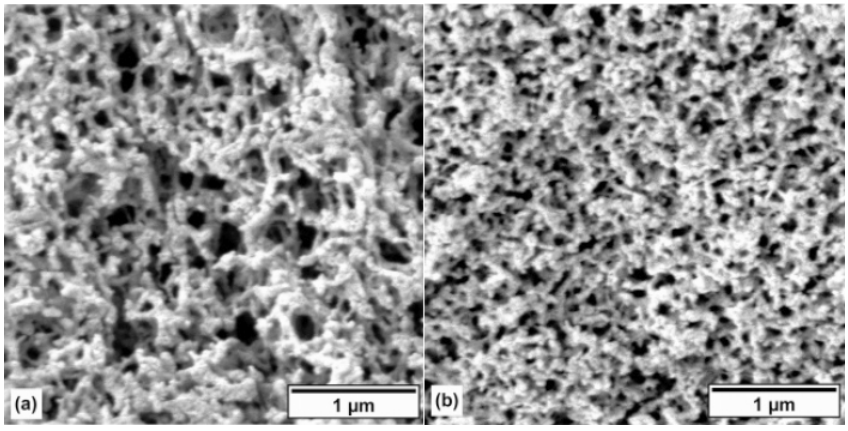

Figure 1.12: SEM images of porous TiO2 obtained using (a) 0.5 wt% and (b) 2 wt% agarose gel templates. [10]

1.3.5 Preventing sedimentation

Once a gel is set, the gel network mechanically supports the weight of the gel, preventing collapse. This solid-like behavior of gels supports crystals where they are nucleated, eliminating the detrimental effects of sedimentation on crystal growth, such as dramatic change of local concentration and contacts with container walls or other crystals. When coupled with other techniques, gels with their ability of suppressing sedimentation exhibit extra controls on crystal growth. For example, femtosecond lasers[90, 91] and electric fields[92] have been used to control nucleation spatially and temporally in agarose gels, making it possible to pattern the gel-grown crystals (Fig. 1.13).[91]

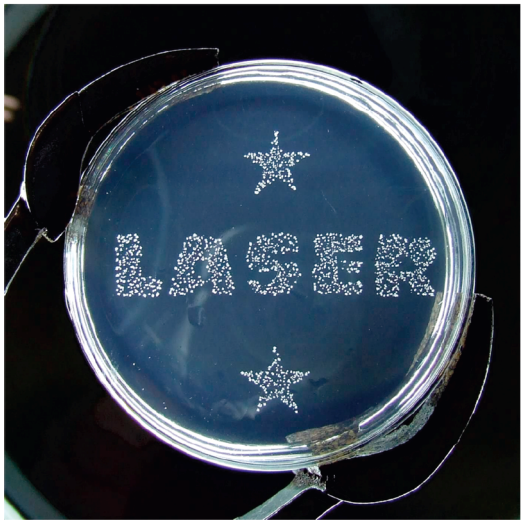

Figure 1.13: Photograph showing spatial control of KCl crystallization in an agarose gel, using laser-induced nucleation and optical mask techniques. The diameter of the dish was 9 cm.[91]

1.4 Gels and biomineralization

In Nature, organisms have been constructing hard skeletons (biominerals) using crystalline materials for the past 550 million years.[71, 93] Calcium carbonate

($CaCO_3$) is one of the most abundant biominerals and has been widely studied.[71] $CaCO_3$ exists in a variety of polymorphs, of which calcite, aragonite, vaterite and amorphous calcium carbonate are significantly relevant to biominerals (Figure 1.14).[71, 93]

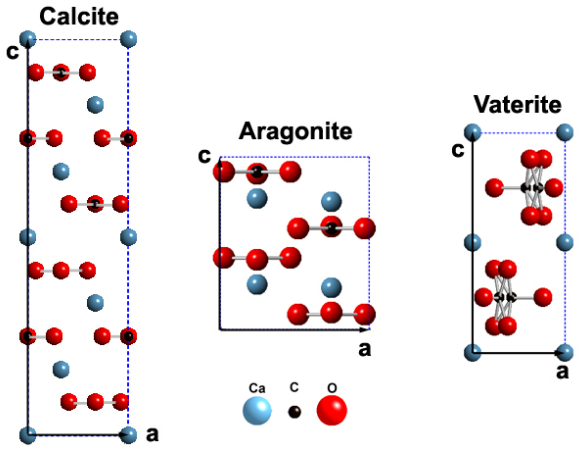

Figure 1.14: Crystalline structures of calcite, aragonite, and vaterite. Calcite (a = b = 4.99 Å, c = 17.06 Å), the most stable polymorph under ambient conditions, is in the hexagonal space group of $R\bar{3}c$; aragonite (a = 4.96 Å, b = 7.96 Å, c = 5.74 Å), a slightly less stable polymorph, is in orthorhombic *Pmcn* group; vaterite (a = b = 4.13 Å, c = 8.48 Å), a kinetic polymorph, is in hexagonal *P63* group.

The biominerals often contain occluded organic matrices so that they are, in nature, organic/inorganic composites. The presence of organic materials provides biominerals with improved mechanical properties and more elaborate morphologies than their counterpart pure synthetic crystals.[71, 94] For example, mollusk nacres (mother-of-pearl) are 3000 times more fracture resistant than a single crystal of its compositional inorganic material (aragonite).[95, 96] And sea urchin spines and plates are porous single crystals of high-Mg calcite with micrometer-sized pores (10's of μm) in

contrast to the faceted single crystals of calcite (Fig. 1.16)[97-99]. It is believed that organisms control the formation of biominerals using organic matrices.[71]

Crystal growth in gels is relevant to biomineralization in three ways: First, some organisms possibly use gels or gel-like materials as the media for biomineralization; second, the gel method could be a platform with which to study matrix-incorporation in biominerals; finally, gels have been used as biologically-relevant media in which to assay the role of matrix macromolecules in biomineralization. The last aspect has been reviewed by Silverman and Boskey[100] and the former two aspects will be discussed here.

1.4.1 Gels associated with biominerals

Recently, researchers have described protein-based hydrogels as the primary component of the organic matrices associated with a variety of biominerals. For example, in the organic matrix for nacre formation, three major organic components (chitin, silk-like protein, and acidic glycoproteins) assemble to form a 3-D micro-environment (Fig. 1.15).[101, 102] Based mainly on cryo-TEM observation, Levi-Kalisman et al. suggested that the silk-like component existed as a hydrogel.[101] In subsequent work, when a fractured nacre was investigated in a wet-mode environmental SEM, the silk-like protein exuded as a diluted gel materials that gradually condensed into films.[103] The effects of a silk-like hydrogel on biomineralization are not clear, but it is possible that the silk-like proteins are involved in the polymorph selection (nucleation). Falini et al. studied the effect of biogenic organic matrix on the polymorph selection of calcium carbonate.[102] They found nacreous polymorph, aragonite, formed only when chitin, acidic glycoprotein, as well as silk protein were present in the crystallization assay. When silk protein is absent, another polymorph, vaterite, was obtained.

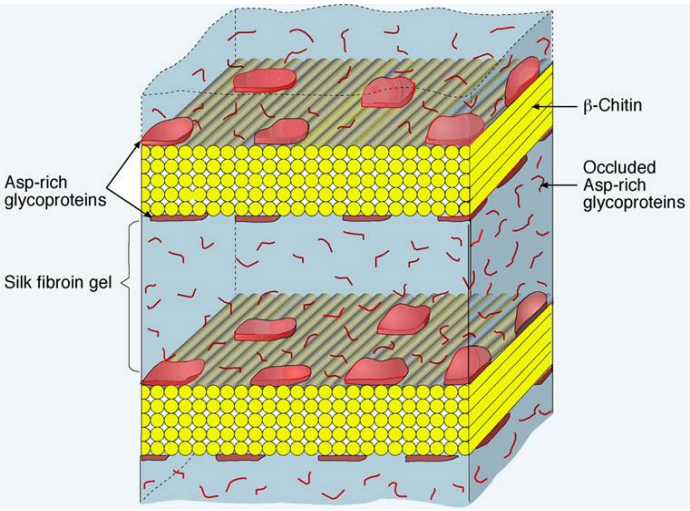

Figure 1.15: A schematic representation of the microenvironment assembled from the three organic components associated with nacre.[101]

In addition to silk-like hydrogels in nacre, amelogenin gels are associated with the organic matrix in tooth enamels[104] and gelatinous materials are supposed to be important for the biomineralization of otolith[105]. Further work is required to elucidate why organisms use hydrogels to produce these biominerals.

1.4.2 Gel-grown and biogenic single-crystal composites

Another relevance of crystal growth in gels to biomineralization occurs in the structural similarity between gel-grown and biogenic single-crystal composites. In Nature, organisms fabricate calcite single crystals with occluded biomacromolecules such as proteins and polysaccharides. Typical examples are the skeletal parts of echinoderms (e.g., sea urchins and brittle stars) that incorporate organic materials at different length-scales. The dorsal arm plate of a brittle star is a single crystal of calcite with incorporated micrometer-sized organic tissues (Fig. 1.16a).[106] Sea urchin spines and plates are high-Mg calcite single crystals, which incorporate not only

micrometer-sized cellular tissue networks but also smaller intracrystalline proteins (Fig. 1.16c).[99] One component of sea urchin teeth is high-Mg calcite plates that are single crystals with 20 v/v% nano-cavities (10 to 225 nm) possibly filled with a hydrated organic phase (Fig. 1.16b).[107] Similar to the skeletal parts of echinoderms, prisms from the calcitic layer of mollusk shells (such as *Atrina rigida*) are single crystals of calcite with incorporated proteins and other biomacromolecules (Fig. 1.16d).[108] As Henisch et al. pointed out,[3, 78] the biogenic calcite crystals and gel-grown calcite crystal are similar in the sense that they all incorporate the surrounding materials (biomacromolecules or gel networks, section 3.3) during crystallization. Therefore, gel-grown calcite is a promising platform to study calcite biomineralization in terms of the calcite-organics interfacial structure, the organic-incorporation mechanisms, and the mechanical properties corresponding to the incorportation.

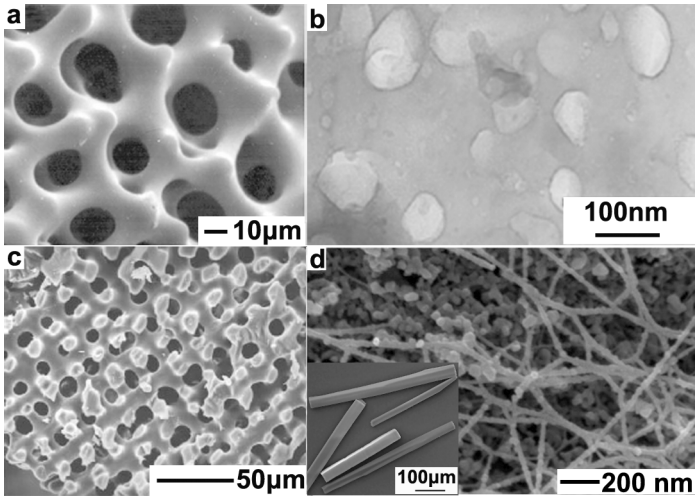

Figure 1.16: (a, c, d) SEM images of (a) a dorsal arm plate of a brittle star[106], (c) a sea urchin plate[99] and (d) a prism (from mollusk shell) etched by acetic acid[108]. Inset in d, a SEM image of prisms before etching. (b) a TEM image of a sea urchin tooth[107].

1.5 Summary and outlook

During the past 20 years, interesting trends have emerged from the studies of crystal growth in gels. Specifically, research has now shown that gel networks are not just inert media surrounding growing crystals. Chemical and physical interactions between gels and crystals play significant roles in crystallization. The gel method, therefore, is not only a traditional approach to prepare single crystals but also a useful platform to study matrix-crystal interactions. Potential uses for the gel method include the preparation of gel/single-crytsal composites as well as investigation on the effects of organic matrix on biomineralization processes.

1.6 Outline of the dissertation

In this dissertation, calcite crystal growth in agarose gels has been used to model biomineralization *in vitro*, with a focus on the structure and formation mechanisms of biomacromolecule-incorporated calcite single-crystal composites. The first part of this dissertation (Chaper 2) develops the model system of agarose-incorporated calcite single-crystals grown from agarose hydrogels. The second part (Chapter 3-5) describes the characterization of the internal structure of the gel-grown crystals. The third part (Chapter 6 and 7) assesses the mechanisms of gel-incorporation. The last part (Chapter 8) examines the generality of the gel-incorporation phenomenon.

REFERENCES

1. A. A. Chernov, *Modern Crystallography III: Crystal Growth*, Springer-Verlag, New York, 1984.
2. I. Sunagawa, *Growth, Morphology and Perfection*, Cambridge University Press, Cambridge, 2005.
3. H. K. Henisch, *Crystals in Gels and Liesegang Rings*, Cambridge University Press, New York, 1988.
4. B. Brezina and J. Horvath, *J. Cryst. Growth*, 1981, **52**, 858-863.
5. T. Y. Miller, X. M. He and D. C. Carter, *J. Cryst. Growth*, 1992, **122**, 306-309.
6. F. Sica, D. Demasi, L. Mazzarella, A. Zagari, S. Capasso, L. H. Pearl, S. Dauria, C. A. Raia and M. Rossi, *Acta Crystallogr.D*, 1994, **50**, 508-511.
7. O. Vidal, M. C. Robert, B. Arnoux and B. Capelle, *J. Cryst. Growth*, 1999, **196**, 559-571.
8. B. Lorber, C. Sauter, M. C. Robert, B. Capelle and R. Giege, *Acta Crystallogr.D*, 1999, **55**, 1491-1494.
9. J. M. Garcia-Ruiz, J. A. Gavira, F. Otalora, A. Guasch and M. Coll, *Mater. Res. Bull.*, 1998, **33**, 1593-1598.
10. J. F. Zhou, M. F. Zhou and R. A. Caruso, *Langmuir*, 2006, **22**, 3332-3336.
11. L. A. Estroff, L. Addadi, S. Weiner and A. D. Hamilton, *Org. Biomol. Chem.*, 2004, 137-141.
12. F. Lefaucheux and M. C. Robert, in *Handbook of Crystal Growth: Bulk Crystal Growth*, ed. D. T. J. Hurle, North-Holland, New York, 1994, pp. 1271-1303.
13. A. Fernandez-Gronzalez, R. Martin-Diaz and M. Prieto, *J. Cryst. Growth*, 1999, **200**, 227-235.

14. S. K. Arora, V. Patel, A. Kothari and B. Amin, *Cryst. Growth Des.*, 2004, **4**, 343-349.

15. C. M. Pina, L. FernandezDiaz and M. Prieto, *J. Cryst. Growth*, 1997, **177**, 102-110.

16. R. I. Petrova and J. A. Swift, *Cryst. Growth Des.*, 2002, **2**, 573-578.

17. C. Rochas, A. M. Hecht and E. Geissler, *Macromol. Symp.*, 1999, **138**, 157-163.

18. M. Djabourov, A. H. Clark, D. W. Rowlands and S. B. Rossmurphy, *Macromolecules*, 1989, **22**, 180-188.

19. M. Maaloum, N. Pernodet and B. Tinland, *Electrophoresis*, 1998, **19**, 1606-1610.

20. O. Vidal, M. C. Robert and F. Boue, *J. Cryst. Growth*, 1998, **192**, 271-281.

21. E. S. Halberst, H. K. Henisch, J. Nickl and E. W. White, *J. Colloid Interface Sci.*, 1969, **29**, 469-471.

22. P. Favard, J. P. Lechaire, M. Maillard, N. Favard, P. Andreazza, F. Lefaucheux and M. C. Robert, *Colloid Polym. Sci.*, 1992, **270**, 584-589.

23. Halberst.Es, H. K. Henisch, J. Nickl and E. W. White, *J. Colloid Interface Sci.*, 1969, **29**, 469-&.

24. P. Favard, J. P. Lechaire, M. Maillard, N. Favard, M. Djabourov and J. Leblond, *Biology of the Cell*, 1989, **67**, 201-207.

25. S. Arnott, A. Fulmer, W. E. Scott, I. C. M. Dea, R. Moorhouse and D. A. Rees, *J. Mol. Biol.*, 1974, **90**, 269-284.

26. J. M. Guenet and C. Rochas, *Macromol. Symp.*, 2006, **242**, 65-70.

27. K. B. Guiseley, (Union, ME), MARINE COLLOIDS INC, US, 1976.

28. S. Waki, J. D. Harvey and A. R. Bellamy, *Biopolymers*, 1982, **21**, 1909-1926.

29. S. Whytock and J. Finch, *Biopolymers*, 1991, **31**, 1025-1028.

30. G. A. Griess, K. B. Guiseley and P. Serwer, *Biophys. J.*, 1993, **65**, 138-148.

31. N. Pernodet, M. Maaloum and B. Tinland, *Electrophoresis*, 1997, **18**, 55-58.

32. Z. Blank and A. C. Reimschuessel, *J. Mater. Sci.*, 1974, **9**, 1815-1822.

33. R. Ruchel, R. L. Steere and E. F. Erbe, *J. Chromatogr.*, 1978, **166**, 563-575.

34. T. P. Hsu and C. Cohen, *Polymer*, 1984, **25**, 1419-1423.

35. H. H. Trieu and S. Qutubuddin, *Colloid Polym. Sci.*, 1994, **272**, 301-309.

36. B. Ratajska-Gadomska, B. Bialkowski, W. Gadomski and C. Radzewicz, *J. Chem. Phys.*, 2007, **126**, 184708.

37. Y. Sekine and T. Ikeda-Fukazawa, *J. Chem. Phys.*, 2009, **130**, 034501.

38. T. Singh, R. Meena and A. Kumar, *J. Phys. Chem. B*, 2009, **113**, 2519-2525.

39. B. Ratajska-Gadomska and W. Gadomski, *J. Chem. Phys.*, 2004, **121**, 12583-12588.

40. T. Goda, J. Watanabe, M. Takai and K. Ishihara, *Polymer*, 2006, **47**, 1390-1396.

41. F. V. Chavez, E. Persson and B. Halle, *J. Am. Chem. Soc.*, 2006, **128**, 4902-4910.

42. M. S. Jhon and J. D. Andrade, *Journal of Biomedical Materials Research*, 1973, **7**, 509-522.

43. H. B. Lee, M. S. Jhon and J. D. Andrade, *J. Colloid Interface Sci.*, 1975, **51**, 225-231.

44. M. Aizawa and S. Suzuki, *Bull. Chem. Soc. Jpn.*, 1971, **44**, 2967-2971.

45. J. Mizuguchi, M. Takahashi and M. Aizawa, *Nippon Kagaku Zasshi*, 1970, **91**, 723-726.

46. S. Morita, M. Tanaka and Y. Ozaki, *Langmuir*, 2007, **23**, 3750-3761.

47. H. Kusanagi and S. Yukawa, *Polymer*, 1994, **35**, 5637-5640.

48. C. F. Hazlewoo, B. L. Nichols and N. F. Chamberl, *Nature*, 1969, **222**, 747-750.

49. S. Katayama and S. Fujiwara, *J. Phys. Chem.*, 1980, **84**, 2320-2325.

50. T. Terada, Y. Maeda and H. Kitano, *J. Phys. Chem.*, 1993, **97**, 3619-3622.

51. P. Andreazza, F. Lefaucheux and B. Mutaftschiev, *J. Cryst. Growth*, 1988, **92**, 415-422.

52. A. Putnis, M. Prieto and L. Fernandezdiaz, *Geological Magazine*, 1995, **132**, 1-13.

53. O. Vidal, M. C. Robert and F. Boue, *J. Cryst. Growth*, 1998, **192**, 257-270.

54. K. Provost and M. C. Robert, *J. Cryst. Growth*, 1991, **110**, 258-264.

55. A. E. S. Van Driessche, F. Otalora, J. A. Gavira and G. Sazaki, *Cryst. Growth Des.*, 2008, **8**, 3623-3629.

56. R. I. Petrova and J. A. Swift, *J. Am. Chem. Soc.*, 2004, **126**, 1168-1173.

57. J. W. Xiao, Y. C. Zhu, Y. Y. Liu, H. J. Liu, Y. Zeng, F. F. Xu and L. Z. Wang, *Cryst. Growth Des.*, 2008, **8**, 2887-2891.

58. C. Daiguebonne, A. Deluzet, M. Camara, K. Boubekeur, N. Audebrand, Y. Gerault, C. Baux and O. Guillou, *Cryst. Growth Des.*, 2003, **3**, 1015-1020.

59. M. Pauchet, T. Morelli, S. Coste, J. J. Malandain and G. Coquerel, *Cryst. Growth Des.*, 2006, **6**, 1881-1889.

60. J. M. Garcia-Ruiz, M. L. Novella, R. Moreno and J. A. Gavira, *J. Cryst. Growth*, 2001, **232**, 165-172.

61. F. Lefaucheux, M. C. Robert and Y. Bernard, *J. Cryst. Growth*, 1988, **88**, 97-106.

62. M. C. Robert and F. Lefaucheux, *J. Cryst. Growth*, 1988, **90**, 358-367.

63. D. Yang, L. M. Qi and J. M. Ma, *Chem. Commun.*, 2003, 1180-1181.

64. Y. Oaki and H. Imai, *Cryst. Growth Des.*, 2003, **3**, 711-716.

65. K. M. Doxsee, R. C. Chang, E. Chen, A. S. Myerson and D. P. Huang, *J. Am. Chem. Soc.*, 1998, **120**, 585-586.

66. L. Fernandez-Diaz, J. M. Astilleros and C. M. Pina, *Chem. Geol.*, 2006, **225**, 314-321.

67. S. Mann, D. D. Archibald, J. M. Didymus, T. Douglas, B. R. Heywood, F. C. Meldrum and N. J. Reeves, *Science*, 1993, **261**, 1286-1292.

68. J. J. De Yoreo and P. M. Dove, *Science*, 2004, **306**, 1301-1302.

69. K. J. Davis, P. M. Dove, L. E. Wasylenki and J. J. De Yoreo, *Am. Mineral.*, 2004, **89**, 714-720.

70. C. A. Orme, A. Noy, A. Wierzbicki, M. T. McBride, M. Grantham, H. H. Teng, P. M. Dove and J. J. DeYoreo, *Nature*, 2001, **411**, 775-779.

71. P. M. Dove, J. J. DeYoreo and S. Weiner, eds., *Biomineralization*, The Mineralogical Society of America, Washington, DC, 2003.

72. R. I. Petrova, R. Patel and J. A. Swift, *Cryst. Growth Des.*, 2006, **6**, 2709-2715.

73. O. Grassmann and P. Lobmann, *Chemistry-a European Journal*, 2003, **9**, 1310-1316.

74. O. Grassmann, R. B. Neder, A. Putnis and P. Lobmann, *Am. Mineral.*, 2003, **88**, 647-652.

75. Y. X. Huang, J. Buder, R. Cardoso-Gil, Y. Prots, W. Carrillo-Cabrera, P. Simon and R. Kniep, *Angew. Chem., Int. Ed.*, 2008, **47**, 8280-8284.

76. V. I. Khaimov-Mal'kov, *Sov. Phys.: Crystallogr.*, 1958, **3**, 487-493.

77. J. I. Hanoka, *J. Appl. Phys.*, 1969, **40**, 2694-2696.

78. H. J. Nickl and H. K. Henisch, *J. Electrochem. Soc.*, 1969, **116**, 1258-1270.

79. J. A. Gavira and J. M. Garcia-Ruiz, *Acta Crystallogr.D*, 2002, **58**, 1653-1656.

80. A. A. Chernov and D. E. Temkin, in *Current Topics in Materials Science*, ed. E. Kaldis, North-Holland, New York, 1977, pp. 3-77.

81. A. A. Chernov, D. E. Temkin and A. M. Mel'nikova, *Sov. Phys. Crystallogr.*, 1976, **21**, 369-374.

82. D. R. Uhlmann, B. Chalmers and K. A. Jackson, *J. Appl. Phys.*, 1964, **35**, 2986-2993.

83. M. O. Kliya and I. G. Sokolova, *Sov. Phys. Crystallogr.* , 1958, **3**, 217-221.

84. J. G. Jia, X. W. Zhou, R. A. Caruso and M. Antonietti, *Chem. Lett.*, 2004, **33**, 202-203.

85. R. A. Caruso, M. Giersig, F. Willig and M. Antonietti, *Langmuir*, 1998, **14**, 6333-6336.

86. D. G. Shchukin, J. H. Schattka, M. Antonietti and R. A. Caruso, *J. Phys. Chem. B*, 2003, **107**, 952-957.

87. R. A. Caruso, M. Antonietti, M. Giersig, H. P. Hentze and J. G. Jia, *Chem. Mater.*, 2001, **13**, 1114-1123.

88. J. H. Schattka, D. G. Shchukin, J. G. Jia, M. Antonietti and R. A. Caruso, *Chem. Mater.*, 2002, **14**, 5103-5108.

89. X. Fan, H. Fei, D. H. Demaree, D. P. Brennan, J. M. S. John and S. R. J. Oliver, *Langmuir*, 2009, **25**, 5835-5839.

90. H. Y. Yoshikawa, R. Murai, S. Sugiyama, G. Sazaki, T. Kitatani, Y. Takahashi, H. Adachi, H. Matsumura, S. Murakami, T. Inoue, K. Takano and Y. Mori, *J. Cryst. Growth*, 2009, **311**, 956-959.

91. C. Duffus, P. J. Camp and A. J. Alexander, *J. Am. Chem. Soc.*, 2009, **131**, 11676-11677.

92. Z. Hammadi, J. P. Astier, R. Morin and S. Veesler, *Cryst. Growth Des.*, 2009, **9**, 3346-3347.

93. S. Weiner and L. Addadi, *J. Mater. Chem.*, 1997, **7**, 689-702.

94. S. Weiner, L. Addadi and H. D. Wagner, *Mater. Sci. Eng. C-Bio S*, 2000, **11**, 1-8.

95. J. D. Currey, *Proc. R. Soc. Lond. Ser. B-Biol. Sci.*, 1977, **196**, 443-&.

96. B. L. Smith, T. E. Schaffer, M. Viani, J. B. Thompson, N. A. Frederick, J. Kindt, A. Belcher, G. D. Stucky, D. E. Morse and P. K. Hansma, *Nature*, 1999, **399**, 761-763.

97. J. Aizenberg, J. Hanson, T. F. Koetzle, S. Weiner and L. Addadi, *J. Am. Chem. Soc.*, 1997, **119**, 881-886.

98. R. J. Park and F. C. Meldrum, *Adv. Mater.*, 2002, **14**, 1167-1169.

99. R. J. Park and F. C. Meldrum, *J. Mater. Chem.*, 2004, **14**, 2291-2296.

100. L. Silverman and A. L. Boskey, *Calcif. Tissue Int.*, 2004, **75**, 494-501.

101. Y. Levi-Kalisman, G. Falini, L. Addadi and S. Weiner, *J. Struct. Biol.*, 2001, **135**, 8-17.

102. G. Falini, S. Albeck, S. Weiner and L. Addadi, *Science*, 1996, **271**, 67-69.

103. L. Addadi, D. Joester, F. Nudelman and S. Weiner, *Chemistry-A European Journal*, 2006, **12**, 981-987.

104. J. Moradian-Oldak, *Matrix Biol.*, 2001, **20**, 293-305.

105. E. Murayama, Y. Takagi, T. Ohira, J. G. Davis, M. I. Greene and H. Nagasawa, *Eur. J. Biochem.*, 2002, **269**, 688-696.

106. J. Aizenberg, A. Tkachenko, S. Weiner, L. Addadi and G. Hendler, *Nature*, 2001, **412**, 819-822.

107. J. S. Robach, S. R. Stock and A. Veis, *J. Struct. Biol.*, 2005, **151**, 18-29.

108. F. Nudelman, H. H. Chen, H. A. Goldberg, S. Weiner and L. Addadi, *Faraday Discuss.*, 2007, **136**, 9-25.

CHAPTER 2

HYDROGELS COUPLED WITH SAMS: AN IN VITRO MATRIX TO STUDY CALCITE BIOMINERALIZATION*

2.1 Abstract

This work describes the control of the nucleation and growth of calcite crystals by a matrix composed of an agarose hydrogel on top of a carboxylate-terminated self-assembled monolayer (SAM). The design of this matrix is based upon examples from biomineralization in which hydrogels are coupled with functionalized, organic surfaces to control, simultaneously, crystal morphology and orientation. In the synthetic system, calcite crystals nucleate from the (012) plane (the same plane that is observed in solution growth). The aspect ratio (length/width) of the crystals decreases from 2.1 ± 0.22 in solution to 1.2 ± 0.04 in a 3 w/v% agarose gel. One possible explanation for the change in morphology is the incorporation of gel fibers inside of the crystals during the growth process. Etching of the gel-grown crystals with deinonized water reveals an interpenetrating network of gel fibers and crystalline material. This work begins to provide insight into why organisms use hydrogels to control the growth of crystals.

2.2 Introduction

Bio-inspired, mineralizing systems usually have focused on controlling either growth (crystal morphology) or nucleation (crystal orientation and density). In biomineralization, however, these two processes are controlled simultaneously. This work presents an experimental set-up, which combines hydrogels and self-assembled

* Reproduced with permission from [H. Y. Li and L. A. Estroff, *J. Am. Chem. Soc.*, 2007, **129**, 5480-5483.] Copyright [2007] American Chemical Society.

monolayers, to control both the nucleation and growth of calcite ($CaCO_3$) crystals. This approach provides the ability to tune the orientation, morphology, and materials properties of the resulting crystals.

2.2.1 Crystal Growth in Hydrogels

Recently, researchers have described protein-based hydrogels as the primary component of the organic matrices associated with a variety of biominerals, including tooth enamel,[1] the nacreous layer in mollusk shells,[2] and trout otoliths.[3] In both tooth enamel and nacre, there is a defined, and possibly patterned, nucleating surface at which crystal growth is initiated.[4,5] Synthetically, crystal growth in hydrogels[6-10] is an alternative to solution-based strategies[11-16] for controlling the morphology (growth) of crystals. One advantage of using gels as a media for crystal growth is that they provide a stable mass transport mechanism that is dominated by diffusion.[17-20] A disadvantage of gels is that this diffusion-limited mass transport among isolated pores makes it more difficult than in solution for a homogeneous nucleus to reach the critical size required for growth. In other words, gel media suppresses homogeneous nucleation by isolating the solutes in small pores.[17] Therefore, growth does not begin until the ions accumulate to a fairly high threshold supersaturation.

2.2.2 Crystal Growth on SAMs

In this work, to promote uniform nucleation in a hydrogel environment, we provide a defined, heterogeneous nucleating surface: a self-assembled monolayer (SAM) of ω-functionalized alkanethiols on gold (Figure 2.1). Functionalized surfaces, such as SAMs, can control the nucleation of minerals.[21-23] Several researchers have demonstrated that the identity and orientation of the terminal functional group on the SAM determines the crystallographic plane on which the crystals nucleate.[22-24] When

SAMs are combined with soluble additives such as Mg^{2+}, it is also possible to control the morphology of the crystals as a function of the nucleating surface.[25]

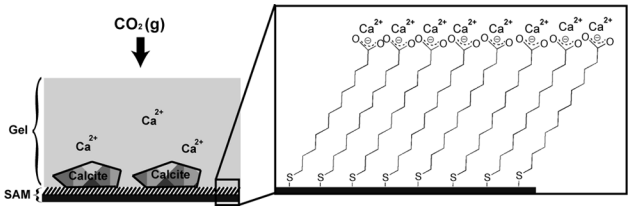

Figure 2.1: A schematic representation of the synthetic, organic matrix used to grow calcite crystals. An agarose gel containing $CaCl_2$ (7 mM) is formed on top of a carboxylate-terminated SAM (16-MHDA) on a gold-coated silicon wafer. The entire construct is then placed in a desiccator with $(NH_4)_2CO_3(s)$. The slow diffusion of $CO_2(g)$ into the gel results in the precipitation of calcite crystals. (The drawing is not to scale.)

2.3 Results and Discussion

2.3.1 Role of the SAM in controlling nucleation

Calcite crystals grown in the SAM-gel matrix (Figure 2.2c-h) are different than control crystals either grown on a carboxylate-terminated SAM in solution (Figure 2.2a,b) or in bulk agarose gel, in the absence of a SAM (Figure 2.2i). As compared to the crystals grown in bulk agarose gel, the polymorph distribution changes when the SAM is introduced. In bulk gel, a small number of vaterite spherulites form in addition to the star-shaped calcite crystals (Figure 2.3).[26] In contrast, when a carboxylate-terminated SAM (16-mercaptohexadecanoic acid (16-MHDA) on gold) is introduced into agarose gels of different concentrations (1 w/v% - 3 w/v%), calcite is the only

polymorph observed and the crystals grow primarily on the functionalized surface (as opposed to in bulk gel, Figure 2.4).

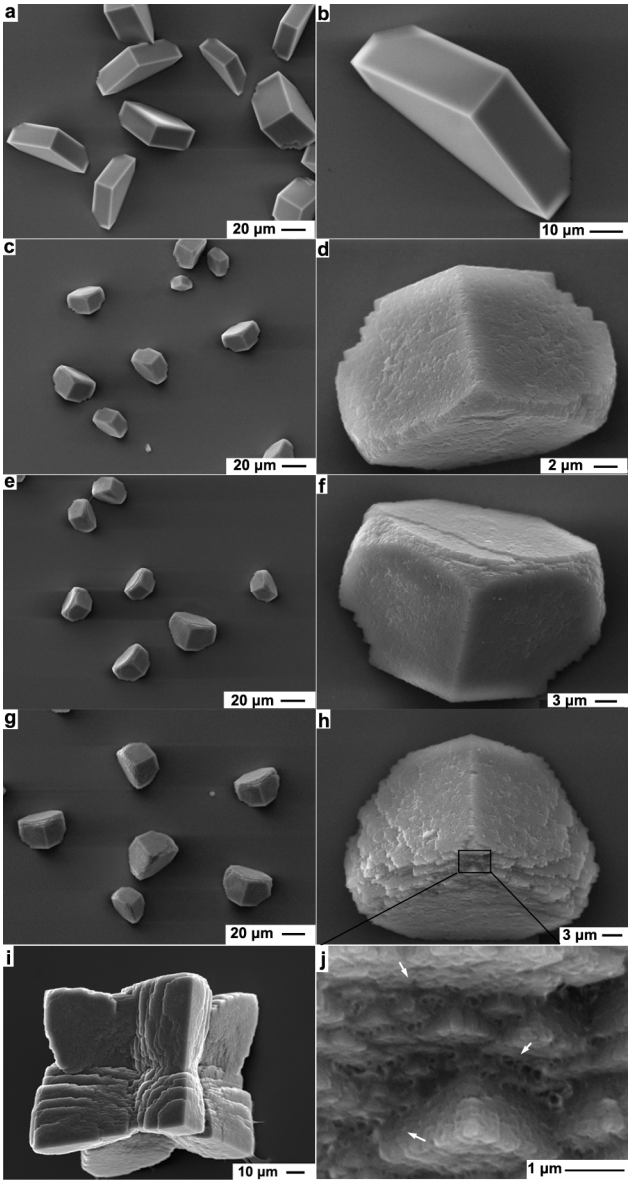

Figure 2.2: (a-h,j) SEM images of calcite crystals grown on carboxylate-terminated SAMs in a,b) solution (7 mM $CaCl_2$) ; c,d) agarose gel (1 w/v%; 7 mM $CaCl_2$); e,f) agarose gel (2 w/v%; 7 mM $CaCl_2$); g,h,j) agarose gel (3 w/v%; 7 mM $CaCl_2$). (i) A SEM image of a calcite crystal grown in bulk agarose gel (2 w/v%; 7 mM $CaCl_2$).

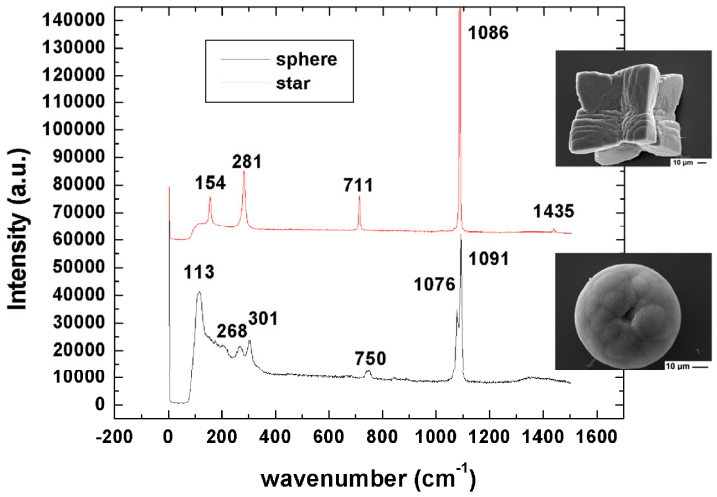

Figure 2.3: Raman spectra[1] of crystals grown in agarose gel (2 w/v%; 7 mM $CaCl_2$). Two polymorphs of calcium carbonate were detected, corresponding to star-shaped calcite (top) and spherulites of vaterite (bottom). Insets are SEM images of the gel-grown crystals.

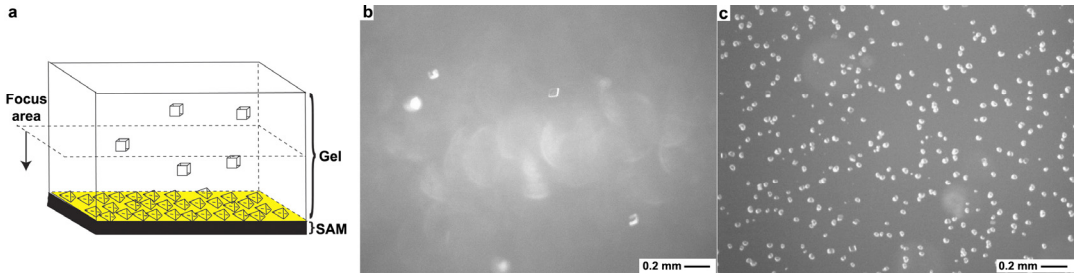

Figure 2.4: (a) A schematic representation of the method to observe the crystal in SAM/gel matrix. (b,c) Optical micrographs (transmission light) of crystals grown in SAM/gel matrix. (b) in gel and (c) on the SAM.

The 2-D ordered, anionic SAM serves as an active interface for heterogeneous nucleation so that the energetic barrier to nucleation and, thus, the threshold supersaturation required for nucleation of calcite is reduced.[27] The nucleation activity of the SAM has been discussed by several authors and may result from a small interfacial energy between the SAM and calcite due to an attractive interaction between the carboxylates on the SAM and the cationic (012) layer in calcite.[23,27] In addition, molecular dynamics simulations have indicated that the presence of a carboxylate monolayer enhances the nucleation rate of calcite as compared to the rate of homogeneous nucleation.[28]

2.3.2 Morphology of Gel-Grown Calcite

The morphology of the calcite crystals also changes upon introduction of the SAM to the agarose gel. The formation of the star-shaped calcite crystals in bulk agarose gel, as reported in the literature,[29] is attributed to the roughly spherical concentration contours of calcium and carbonate ions surrounding each rhombohedral crystal.[30] Above a certain critical size of the crystal, the difference in concentration between the vertices and the centers of the rhombohedral faces becomes significant enough that the vertices grow more rapidly, via 2-D nucleation, than the centers. This type of growth results in "skeletal" or "hopper-like" crystals.[30] Similar morphologies are not observed for the crystals grown on the anionic SAM, most likely because of the high nucleation density on the SAM (Figure 2.4). Typically, the star-shaped crystals are 50-100 microns along an edge, compared to the crystals grown on the SAM, which are 20-40 microns in length (Figure 2.7, inset). Based on our limited data set, we speculate that the short distances between the crystals on the SAM prevent them from reaching the critical size to begin the "hopper-like" growth observed in bulk gel.

2.3.3 Orientation of Crystals on the SAMs

The quality of the SAM after introduction of the gel can be evaluated indirectly by determining the orientation of the calcite crystals grown on the SAM. The nucleating plane of calcite is very sensitive to the structure of the SAM surface and the conformation of the carboxylate head-group.[22, 24] The orientations of the calcite crystals grown on the SAMs were determined by powder X-ray diffraction (PXRD) and morphological analysis (Figures 2.5 and 2.6).[31] Statistical analysis of the data (Figure 2.5, right) shows that in all experimental conditions (gel and solution), greater than 70% of the crystals have a (012) orientation. PXRD patterns, as supporting evidences, reconfirm the (012) orientation of the crystals (Figures 2.6). This orientation is in agreement with the literature on growth from solution on SAMs, and, thus, indicates that the agarose gel has not (significantly) perturbed the structure of the SAM.[32] The slight reduction in orientation at the highest gel concentration (3 w/v%) may indicate some level of disruption of the SAM structure by the gel.

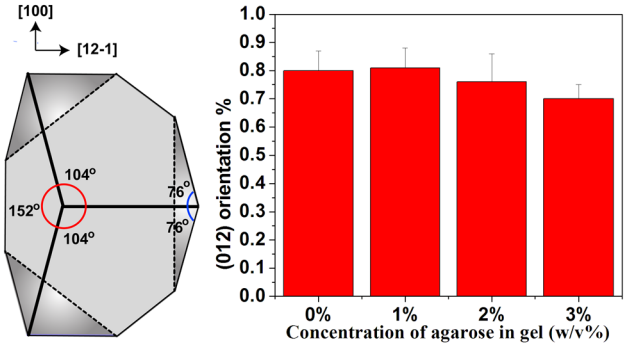

Figure 2.5: Left: Top view of a computer simulation of a calcite crystal nucleated on the (012) plane (SHAPE 7.1). The three angles (in red) between the crystal edges meeting at the upper corner of the crystal were measured to determine the crystallographic orientation direction. The crystallographic orientation of a regular {104} calcite rhombohedron unequivocally relates to these three angles and for a (012) oriented crystal, the values of the three angles are 104°, 104°, and 152°, respectively.[31] When the top corner was not clear defined, the angles in blue were measured to calculate the angles in red. Right: The results of the morphological analysis for the calcite crystals grown on carboxylate-terminated SAMs in solution (7 mM $CaCl_2$) or agarose gel (1-3 w/v%; 7 mM $CaCl_2$). Each crystal growth experiment was repeated three times and fifty crystals from each experiment were measured.

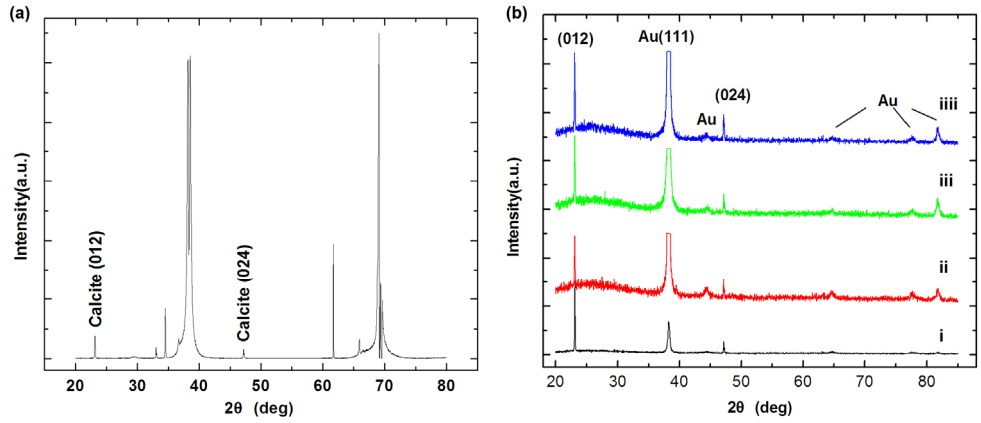

Figure 2.6: (a) A PXRD pattern of calcite crystals grown on a carboxylate-terminated SAM (16-MHDA on a gold-coated Si (100) wafer). Only two peaks are assigned to the diffraction from calcite [(012) and (024)]. All the other peaks are from the substrate [Au (111) and Si (100)]. In order to obtain a cleaner XRD patten, we also prepared16-MHDA SAMs on Au-coated glass slides (50 nm of Au on 3 nm of Cr) and used these slides as substrates for crystal growth. [See (b) for PXRD patterns.] (b) PXRD patterns of calcite crystals grown on a SAM (16-MHDA on gold-coated glass slides) in: i) solution; ii) an agarose gel (1 w/v%; 7 mM $CaCl_2$); iii) an agarose gel (2 w/v%; 7 mM $CaCl_2$); and iiii) an agarose gel (3 w/v%; 7 mM $CaCl_2$). For clarity, the signals from Au (111) in (b), (c), and (d) were truncated.

2.3.4 Effect of the Gel on Crystal Growth

The introduction of the agarose gel to the SAM changes the crystal morphologies, as described by the aspect ratios [defined as the length/width, Figure 2.7(inset)].[33] With increasing agarose concentration (1 w/v% to 3 w/v%), the aspect ratio decreases (Figure 2.7). The control crystals grown in solution have a high aspect ratio (2.1 ± 0.22), which has been attributed to a lattice match between calcite and the SAM in the [100] direction (length) but a mismatch in the [12-1] direction (width).[33] The aspect ratio drops to 1.4 ± 0.01 in 1 w/v% agarose gel, and continues to decrease

to 1.2 ± 0.04 for crystals grown in 3 w/v% agarose (Figure 2.7). From these results, it is clear that the anisotropic effect of the substrate is reduced for crystals grown in the agarose gel.

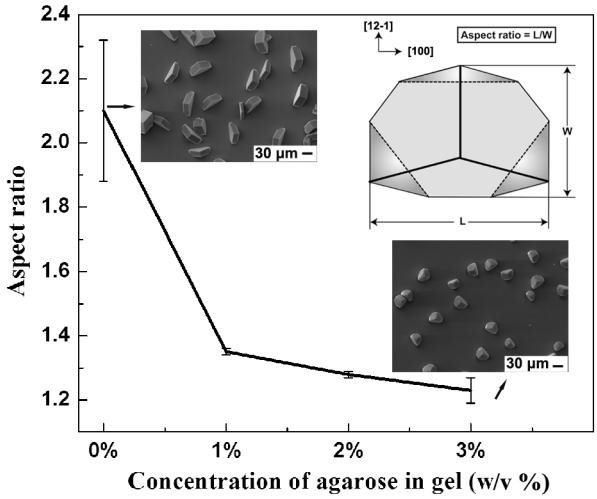

Figure 2.7: The aspect ratio (see inset) of calcite crystals nucleated on carboxylate-terminated SAMs changes as a function of the concentration of the agarose gel. Inset: Top view of a computer simulation of a calcite crystal nucleated on the (012) plane. The aspect ratio is defined as the length divided by the width.[33]

One explanation for the change in morphology is the incorporation of gel fibers *inside* of the calcite crystals.[10,17,19] Incorporated gel matrix can change the kinetics of growth, and thus the morphology, by altering the interface energy of the crystals.[19] There is evidence of incorporated organic material on the surfaces of crystals grown in the 3 w/v % agarose gels (Figure 2.2j, arrow). Gel fibers appear to bridge the macroscopic steps of the crystal, suggesting that they are inside of the crystal. To investigate further the presence of organic material inside of the crystals, we etched the gel-grown crystals in deinonized (DI) water (pH ~ 6.5) for two days. Etching is a common technique used to detect the presence of organic material inside

of biogenic minerals.[34-36] When synthetic calcite crystals are etched in DI water, shallow etch pits with {104} geometries appear on the surface (Figure 2.8(a,b)).[37] In contrast, after etching the gel-grown crystals, the surfaces of the remaining crystals are covered completely by irregular etch pits (Figure 2.8c). A magnified image of the etched surface further reveals an interpenetrating network of gel fibers and crystalline material (Figure 2.8d). Based upon these experiments, we suggest that the gel-grown crystals are composites that contain both agarose fibers and calcite.

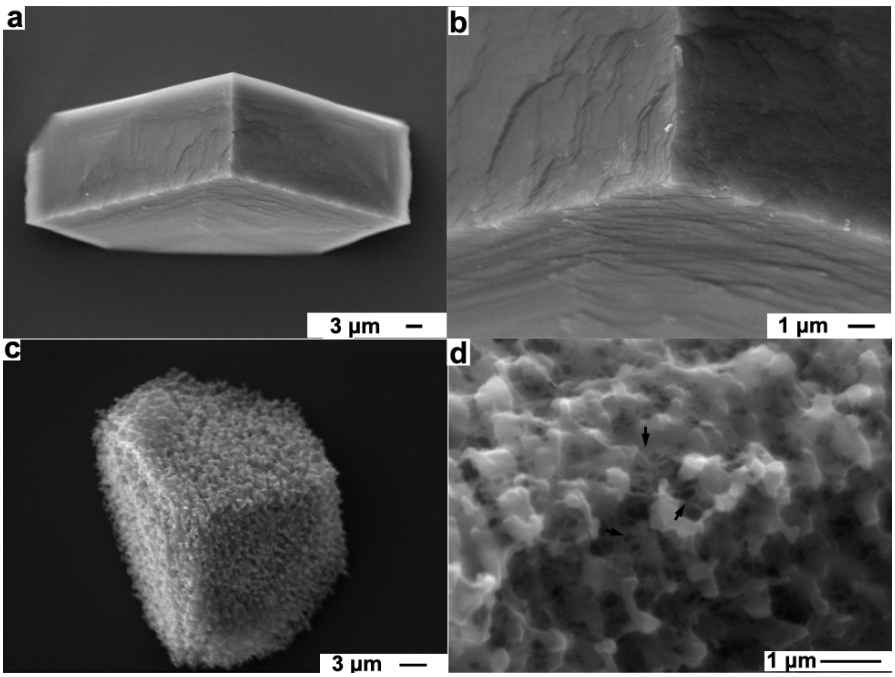

Figure 2.8: SEM images of: (a,b) A solution-grown crystal etched in DI water for two days and (c,d) a gel-grown (2 w/v% agarose) crystal etched in DI water for two days. Arrows in (d) highlight the locations of gel fibers.

2.4 Conclusion

The SAM/gel platform has the potential to allow us to control, independently, the nucleation and growth of inorganic crystals at surfaces. In this study of calcite

crystals grown on carboxylate-terminated SAMs in agarose gel, we find that at the SAM/gel interface, the SAM regulates the orientation of the calcite crystals with high fidelity (>70% have a (012) orientation). The SAM also contributes to phase selection by providing a heterogeneous substrate, thereby reducing the threshold supersaturation required for nucleation of calcite at the interface. Under these conditions, the formation of the metastable polymorph, vaterite, is suppressed.[27] The hydrogel, on the other hand, changes the growth kinetics, and thus, the morphology of the calcite crystals, as expressed by a decrease in the aspect ratio with increasing gel concentration.

This *in vitro* crystal growth system was designed based upon models of the organic matrices in which biomineralization occurs.[38] Like many biominerals, crystals grown in the gel/SAM set-up have incorporated organic material, as revealed by etching experiments. The incorporation of proteins in biominerals is hypothesized to enhance their biogenic function, such as improving the mechanical properties of the brittle minerals.[39] The structure and properties of these single-crystal composites are of great interest to biologists and materials scientists.[40-43] The combination of biologically relevant hydrogels with SAMs is a promising approach for studying multiple features of biomineralization, including the mechanisms governing protein incorporation, crystal orientation, and polymorph selectivity.

2.5 Experimental Section

2.5.1 SAM-gel matrix preparation

Two types of gold-coated substrates were used to form the SAMs. Gold-coated silicon (100) wafers (100 nm of Au on a thin Ti adhesion layer) were purchased from Platypus Technologies. Gold-coated glass slides (50 nm of Au on 3 nm of Cr) were prepared using Veeco 7700 Bell Jar Evaporator (base pressure 10^{-6} Torr) and these

substrates were only used for PXRD characterization (see Figure 2.6). Pieces of substrates were incubated overnight in a 10 mM solution of 16-mercaptohexadecanoic acid (16-MHDA; Sigma) in ethanol. After rinsing with ethanol and deionized (DI) water (18.2 mΩ, Barnstead EASYpure® RoDi), the slides were transferred to Petri dishes (35 mm x 10 mm) and covered with 3 mL of a filtered (syringe filter; 0.45 μm, Millipore), warm solution of agarose (1-3 w/v%; Type IB, Sigma) in 7 mM $CaCl_2 \bullet 2H_2O$ (99+%, Aldrich). After gelation (about 30 minutes), the Petri dishes were covered with aluminum foil with one small hole.

2.5.2 Crystallization, etching, and control experiments

The Petri dishes with the SAM-gel matrix were placed in a closed desiccator containing one vial of ammonium carbonate (Sigma). After 24 hours in the desiccator, the slides were removed from the gel and rinsed with DI water.

The crystals, still on the slides, were etched in DI water for two days. During this time, the Petri dishes with the crystals were gently rocked on a rocking platform. The slides with the etched crystals were rinsed and air-dried.

Control crystallizations were also carried out in the desiccator containing ammonium carbonate. The following controls were done: 1) Growth on a 16-MHDA SAM in a filtered (syringe filter, 0.2 μm, Millipore) 7 mM $CaCl_2$ solution; and 2) Growth in bulk gel (2 w/v % agarose) in the absence of a SAM.

2.5.3 Characterization

The morphology of the obtained crystals was examined by scanning electron microscopy (STEREOSCAN 440, LEICA, 25 KV, 600 pA) after being sputter-coated with Au/Pd. Crystal morphologies were modeled with SHAPE 7.1. A regular {104}

calcite rhombohedra was truncated by a (012) plane and aligned on that (012) face (Figure 2.5 left and Figure 2.7 inset).

The crystal phase and the crystallographic orientations of the crystals grown on the SAMs were determined by X-ray diffraction in θ-2θ scan mode from 20°-80° (Scintag Inc., Theta-Theta Diffractometer); Radiation: $CuK_{\alpha 1}$; Voltage: 45 kV; Current: 40 mA; Scan rate: 4.00 Deg/min; Step: 0.02°).

Phase composition was identified by Raman spectroscopy[44] (Renishaw InVia Reflex Raman Microscope, software: Wire 2; laser: 785 nm edge; laser power: 50%; spectral range: 0-1500 cm^{-1}).

The orientations of individual crystals were determined by measuring the three angles between the crystal edges meeting at the upper corner of the crystal. For statistics, each crystal growth experiment was repeated three times and fifty crystals from each experiment were measured. The error was set as 2°. The aspect ratio of calcite crystals were measured using ImageJ and then statistically analyzed. A sampling method similar to the one described for the orientation analysis was used for the aspect ratio measurements.

REFERENCES

1. J. Moradian-Oldak, *Matrix Biol.*, 2001, **20**, 293-305.
2. Y. Levi-Kalisman, G. Falini, L. Addadi and S. Weiner, *J. Struct. Biol.*, 2001, **135**, 8-17.
3. E. Murayama, Y. Takagi, T. Ohira, J. G. Davis, M. I. Greene and H. Nagasawa, *Eur. J. Biochem.*, 2002, **269**, 688-696.
4. F. Nudelman, B. A. Gotliv, L. Addadi and S. Weiner, *J. Struct. Biol.*, 2006, **153**, 176-187.
5. A. L. Arsenault and B. W. Robinson, *Calcif. Tissue Int.*, 1989, **45**, 111-121.
6. G. Falini, S. Fermani, M. Gazzano and A. Ripamonti, *Chemistry-a European Journal*, 1997, **3**, 1807-1814.
7. L. Fernandez-Diaz, A. Putnis, M. Prieto and C. V. Putnis, *J. Sediment. Res.*, 1996, **66**, 482-491.
8. O. Grassmann and P. Lobmann, *Chem.-Eur. J.*, 2003, **9**, 1310-1316.
9. R. I. Petrova and J. A. Swift, *J. Am. Chem. Soc.*, 2004, **126**, 1168-1173.
10. L. A. Estroff, L. Addadi, S. Weiner and A. D. Hamilton, *Org. Biomol. Chem.*, 2004, 137-141.
11. C. A. Orme, A. Noy, A. Wierzbicki, M. T. McBride, M. Grantham, H. H. Teng, P. M. Dove and J. J. DeYoreo, *Nature*, 2001, **411**, 775-779.
12. L. A. Estroff, C. D. Incarvito and A. D. Hamilton, *J. Am. Chem. Soc.*, 2004, **126**, 2-3.
13. J. J. J. M. Donners, R. J. M. Nolte and N. A. J. M. Sommerdijk, *J. Am. Chem. Soc.*, 2002, **124**, 9700-9701.
14. H. Colfen and L. M. Qi, *Chemistry-a European Journal*, 2001, **7**, 106-116.

15. S. Albeck, J. Aizenberg, L. Addadi and S. Weiner, *J. Am. Chem. Soc.*, 1993, **115**, 11691-11697.

16. G. Fu, S. Valiyaveettil, B. Wopenka and D. E. Morse, *Biomacromolecules*, 2005, **6**, 1289-1298.

17. H. K. Henisch, *Crystals in Gels and Liesegang Rings*, Cambridge University Press, New York, 1988.

18. M. Fialkowski, C. J. Campbell, I. T. Bensemann and B. A. Grzybowski, *Langmuir*, 2004, **20**, 3513-3516.

19. J. M. Garcia-Ruiz, J. A. Gavira, F. Otalora, A. Guasch and M. Coll, *Mater. Res. Bull.*, 1998, **33**, 1593-1598.

20. L. Silverman and A. L. Boskey, *Calcif. Tissue Int.*, 2004, **75**, 494-501.

21. J. Aizenberg, A. J. Black and G. M. Whitesides, *Nature*, 1999, **398**, 495-498.

22. A. M. Travaille, L. Kaptijn, P. Verwer, B. Hulsken, J. A. A. W. Elemans, R. J. M. Nolte and H. Van Kempen, *J. Am. Chem. Soc.*, 2003, **125**, 11571-11577.

23. J. Aizenberg, A. J. Black and G. M. Whitesides, *J. Am. Chem. Soc.*, 1999, **121**, 4500-4509.

24. Y. J. Han and J. Aizenberg, *Angew. Chem., Int. Ed. Engl.*, 2003, **42**, 3668-3670.

25. Y. J. Han, L. M. Wysocki, M. S. Thanawala, T. Siegrist and J. Aizenberg, *Angew. Chem., Int. Ed.*, 2005, **44**, 2386-2390.

26. The formation of vaterite, a metastable, kinetically favored phase, at the high levels of supersaturation in the gel, is in agreement with Ostwald's Rule of Stages.

27. A. M. Travaille, E. G. A. Steijven, H. Meekes and H. van Kempen, *J. Phys. Chem. B*, 2005, **109**, 5618-5626.

28. D. M. Duffy, A. M. Travaille, H. van Kempen, J. H. Harding, *J. Phys. Chem. B*, 2005, **109**, 5713-5718.

29. D. Yang, L. M. Qi and J. M. Ma, *Chem. Commun.*, 2003, 1180-1181.

30. A. A. Chernov, *Modern Crystallography III: Crystal Growth*, Springer-Verlag, New York, 1984.

31. D. D. Archibald, S. B. Qadri and B. P. Gaber, *Langmuir*, 1996, **12**, 538-546.

32. For other gel/SAM pairs we have found evidence that there can be significant interaction of the gel and SAM, destroying the oriented nucleation (Li, Keene, and Estroff, unpublished results).

33. A. M. Travaille, Ph. D. Thesis, Radboud University Nijmegen, 2005.

34. L. J. Wang, R. K. Tang, T. Bonstein, C. A. Orme, P. J. Bush and G. H. Nancollas, *J. Phys. Chem. B*, 2005, **109**, 999-1005.

35. J. Seto, Y. Zhang, P. Hamilton and F. Wilt, *J. Struct. Biol.*, 2004, **148**, 123-130.

36. R. L. Ryall, D. E. Fleming, I. R. Doyle, N. A. Evans, C. J. Dean and V. R. Marshall, *J. Struct. Biol.*, 2001, **134**, 5-14.

37. N. E. Pingitore, S. B. Fretzdorff, B. P. Seitz, L. Y. Estrada, P. M. Borrego, G. M. Crawford and K. M. Love, *Journal of Sedimentary Petrology*, 1993, **63**, 641-645.

38. L. Addadi, D. Joester, F. Nudelman and S. Weiner, *Chemistry-A European Journal*, 2006, **12**, 981-987.

39. J. Aizenberg and G. Hendler, *J. Mater. Chem.*, 2004, **14**, 2066-2072.

40. B. Pokroy, A. N. Fitch, F. Marin, M. Kapon, N. Adir and E. Zolotoyabko, *J. Struct. Biol.*, 2006, **155**, 96-103.

41. H. Colfen and S. Mann, *Angew. Chem., Int. Ed.*, 2003, **42**, 2350-2365.

42. J. Aizenberg, J. Hanson, T. F. Koetzle, S. Weiner and L. Addadi, *J. Am. Chem. Soc.*, 1997, **119**, 881-886.

43. A. Berman, L. Addadi and S. Weiner, *Nature*, 1988, **311**, 546-548.

44. C. G. Kontoyannis and N. V. Vagenas, *Analyst*, 2000, **125**, 251-255.

CHAPTER 3

POROUS CALCITE SINGLE CRYSTALS GROWN FROM A HYDROGEL MEDIUM*

3.1 Introduction

Crystals are usually homogeneous solids within which the atoms are arranged in extended, periodic arrays. Biogenic calcite crystals, however, have biomacromolecules incorporated within the otherwise regular atomic array.[1-3] This work describes a synthetic approach to single crystals with incorporated organic material. We demonstrate that calcite crystals grown in an agarose hydrogel, like some biogenic calcite crystals, have a porous internal structure due to incorporated gel fibers.

Echinoderms (e.g., sea urchins and brittle stars) are model organisms in which to study the formation of porous single crystals of calcite.[2-5] Sea urchin spines and plates are constructed from high-Mg calcite single crystals with micrometer-sized pores (10's of μm) penetrating throughout the entire crystal.[6] The sea urchin tooth is composed of single crystal plates of high-Mg calcite. A recent report described the presence of nanometer-sized pores (10-225 nm) within these crystals.[7] The incorporation of organic materials inside of these biogenic crystals results in a large diversity of morphologies, introduces lattice distortions,[8] and compensates for the intrinsic brittleness of the calcite ceramic.[9, 10]

Synthetic calcite crystals with pores (10's of μm) have been formed by confining the growth inside of polymer templates.[11, 12] Pores have also been introduced by using latex particles (10's of nm-several μm) as templates both on the

* Reproduced with permission from [H. Y. Li and L. A. Estroff, *Crystengcomm*, 2007, **9**, 1153-1155.] Copyright 2007 Royal Society of Chemistry.

surface of calcite crystals and zinc oxide crystals.[13-15] More recently, crystals with nanoscale pores (10's of nm) in 2-dimensions have been grown using a porous polymer membrane.[16] In the current work, we use an agarose hydrogel to introduce nanoscale pores (100's of nm) into calcite single crystals. Depending on the crystal-gel pair, growth in hydrogels can result in large, defect-free single crystals, cloudy single crystals, or aggregates of crystals.[17-20] We and others have reported evidence that calcite crystals can incorporate both agarose[21] and silica[22] gel materials. In the current work, we examine, in detail, the internal structure of the gel-grown calcite crystals from the micro to nanometer scale.

3.2 Results and Discussion

The calcite crystals were grown in an agarose hydrogel (1 w/v% agarose, 7 mM $CaCl_2$; Type IB agarose) using the ammonium carbonate method.[23] These crystals are faceted with the characteristic rhombohedral morphology of calcite expressed by six {104} faces (Figure 3.1a). The macroscopic morphology, however, disguises the complex internal structure that is revealed by transmission electron microscopy (TEM). The crystals were embedded in epoxy resin and cut by microtome to give thin slices (50 nm thick) that were observed by TEM. As shown in Figures 3.1b, the crystal slice is not complete, but full of pores, which means the crystal is divided into smaller crystallites (hundreds of nanometers) that are connected, partially, by crystalline bridges. The pores range in size from 60 to 364 nm with an average of 190±82 nm (determined from the caliper length of 50 pores, ImageJ).

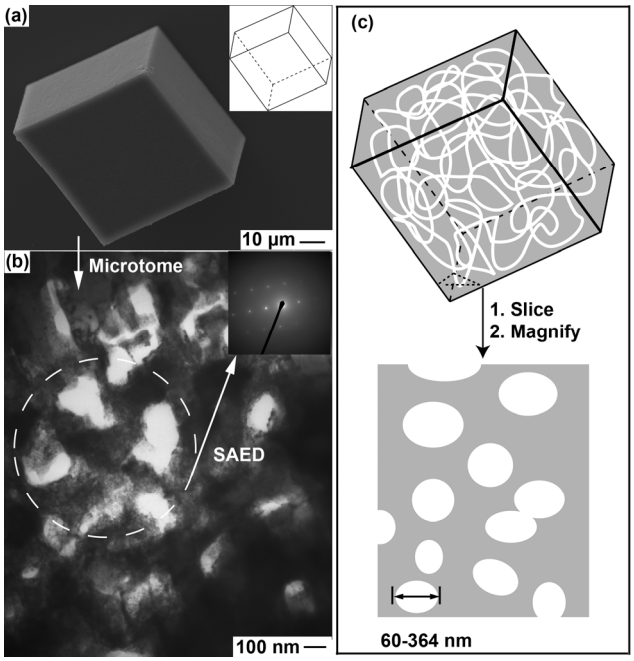

Figure 3.1: (a) A SEM image of a calcite crystal grown in an agarose gel (1 w/v%; 7 mM $CaCl_2$), inset: computer simulation of a calcite crystal expressed by 6 {104} faces; (b) A TEM image of a 50 nm thin slice of an epoxy-embedded gel-grown calcite crystal. The slice was cut by microtome. Inset: A SAED pattern of the area indicated by the dashed line. (c) A schematic representation of the internal structure of a porous single crystal filled with gel fibers.

The internal structure of the gel-grown crystals demonstrates the abnormality of these calcite crystals and raises four questions: (1) Is the porous structure observed by TEM connected coherently into a macroscopic single crystal? (2) How do these pores form inside of the crystals? (3) Are all of the gel-grown crystals porous? (4) Are the pores distributed uniformly throughout an individual crystal? The answers are provided below.

We first investigated the crystallography of the porous crystals. Individual crystals extinguish simultaneously as single crystals between crossed-polarizers

(Figure 3.2). To obtain higher resolution information about the crystallinity of the gel-grown crystals, we used selected area electron diffraction (SAED). SAED of an area including several pores in a microtomed sample produces a single set of diffraction spots **(**Figure 3.1b, inset). Over this length regime, therefore, the porous structure behaves, as a single crystal. To probe a larger area, electron back-scattered diffraction (EBSD) was used. An EBSD orientation map of a square area (50 μm x 50 μm) revealed that in this area all of the crystalline components have the same orientation (Figure 3.3). From the size of the crystallites observed by TEM, this area contains greater than 1000 crystallites. Based upon the SAED and EBSD data, we conclude that the porous structures of the gel-grown calcite crystals are connected coherently with the crystalline components inside sharing the same crystallographic orientation. Other authors have observed structures composed of oriented crystallites, sometimes referred to as mesocrystals, under a variety of experimental condition including growth in gel media or in solution with polymer additives.[19, 24-26]

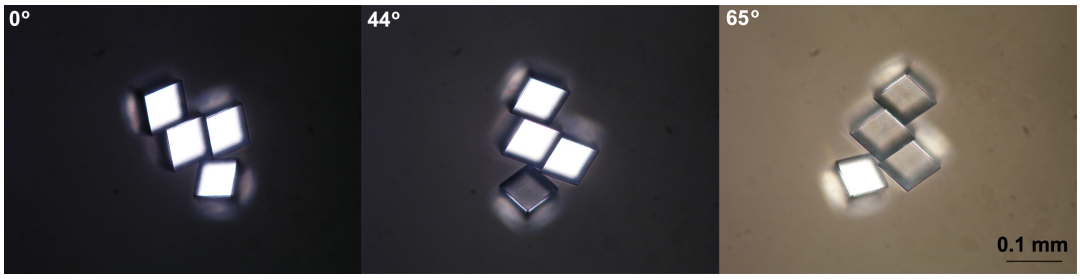

Figure 3.2: Micrograph series of crystals grown in 1 w/v% gel that are rotated under cross-polarized light. Individual rotated crystals extinguish simultaneously as single crystals.

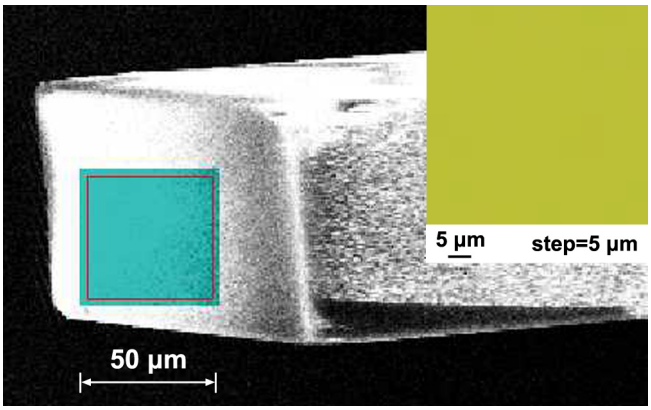

Figure 3.3: EBSD orientation map of a crystal grown in agarose gel (1 w/v%; 7 mM $CaCl_2$). The scanning area is blue-marked; the orientation mapping is shown in top right corner. Each crystallographic direction is allocated a specific color during mapping. The uniformity of the color in the inset means that all of the crystalline components in this area have the same orientation.

The origin of the pores is hypothesized to be related to the incorporation of the gel fibers inside of the crystals.[21] We used etching to test this prediction since etching is commonly used to detect organic materials inside of biominerals[4, 27] and has been previously used to examine gel-grown crystals.[20, 22, 28] Etching the gel-grown crystals in deionized (DI) water for 4 days revealed the incorporated gel fibers. SEM images of the etched crystals show that dissolution results in a porous surface morphology (Figure 3.4a, b). Fibers are found in the etch pits throughout the surface (Figure 3.4b). Etching experiments were also conducted for crystals grown in 2 w/v% agarose and the results show porous etch pits filled with fibers similar to those grown in 1 w/v% gel (Figure 3.4c, d).[29, 30] These SEM images demonstrate clearly that the gel matrix and crystalline component coexist inside of the gel-grown crystals.

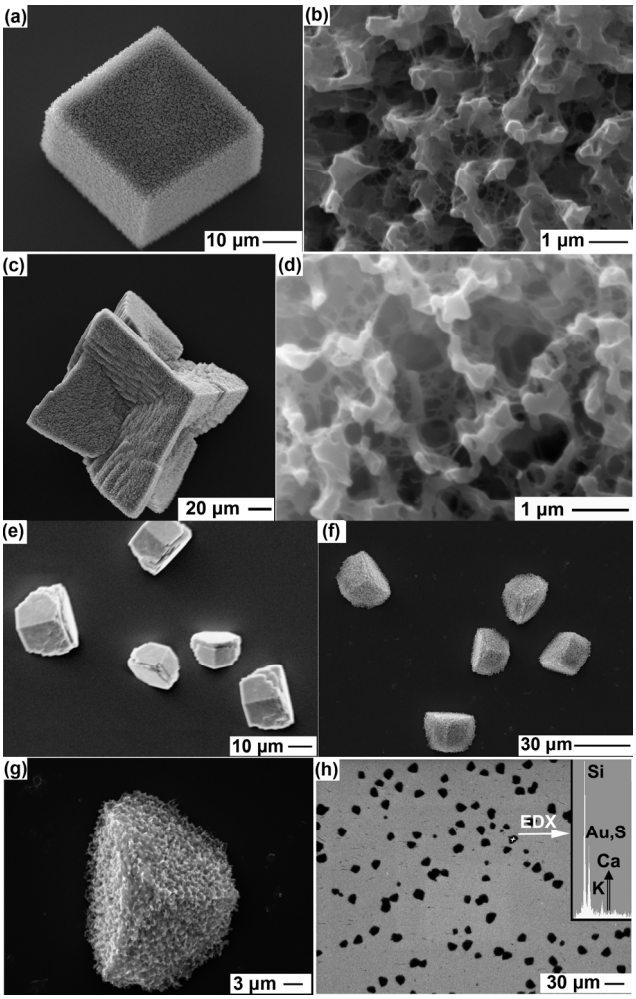

Figure 3.4: (a-d) SEM images of a calcite crystal grown in (a, b) an agarose gel (1 w/v%; 7 mM $CaCl_2$) and (c, d) an agarose gel (2 w/v%; 7 mM $CaCl_2$), after etching in DI water for 4 days; (e-g) SEM images of calcite crystals grown on a carboxylate-terminated SAM (16-MHDA) in an agarose gel (2 w/v%; 7 mM $CaCl_2$): (e) as prepared, (f, g) after etching in DI water for 2 d, (h) after etching in 0.1 M HCl for ~10 min. Inset: an EDX spectrum of the area indicated by an X. The x-axis shown is from 0 to 6 keV and Ca should show signals at 3.704 and 4.026 keV. The spectrum shows the absence of calcium. Sample (h) was imaged without an Au/Pd coating to improve the contrast between the gold background and the organic "ghosts".

Etching experiments on large numbers of gel-grown calcite crystals show that all of the gel-grown crystals incorporate the gel matrix. A large number of gel-grown crystals were prepared by introducing a SAM (16-mercaptohexadecanoic acid on gold) to the bottom of a hydrogel (2 w/v% agarose) as an effective nucleation substrate (Figure 3.4e).[21, 23] After etching in DI water for two days,[31] all of the crystals show porous etch pits similar to those grown in the bulk gel (Figure 3.4f, g).[21] After etching in 0.1 M HCl for approximately ten minutes, all of the crystals dissolve and visible "ghosts" remain with footprints similar to the shapes of the original crystals (Figure 3.4h). Energy Dispersive X-ray Analysis (EDX) taken at the center of the "ghosts" shows that there is no calcium present, therefore, the "ghosts" are composed of organic material (agarose) only.

Examination of the organic material that remains on the slides after the etching experiments suggests that the gel fibers are incorporated uniformly inside of the crystals. The crystals grown on SAMs in gel (2 and 3 w/v % agarose) were etched in DI water for four days. During this time, most of the crystals disappear and the incorporated gel matrices collapse around the residual crystals, as observed by optical microscopy (OM) (Figure 3.5). The residual crystals at the center of the "ghosts" are visible between crossed- polarizers (Figure 3.5, inset). The collapsed gel matrices have regular interference fringes when viewed with unpolarized light (Figure 3.5). The interference fringes are roughly parallel to the edges of the "ghosts" and the shapes of the fringes are similar to those of the as-prepared crystals. We infer, therefore, that the gel matrices were roughly intact inside of the crystals and were incorporated uniformly inside of the crystals under our experimental conditions.

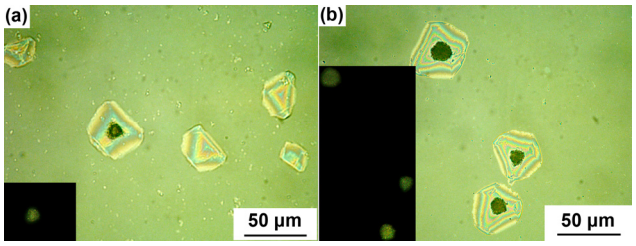

Figure 3.5: Optical microscopy images of calcite crystals grown on a SAM (16-MHDA) in (a) 2 w/v% agarose gel and (b) 3 w/v% agarose gel, after etching in DI water for 4 days. Insets: same field of view under crossed-polarizers to show the remaining crystalline material inside of the agarose "ghosts".

3.3 Conclusion

On the basis of the TEM, SEM and OM images of the as-grown and etched crystals, we suggest that during crystal growth, the growing crystals encounter the gel network and grow through the pores (~140 nm on average for 1 w/v% gel[32]), thereby incorporating the fibers inside. Based upon previous models of crystal growth in porous media,[33, 34] we are continuing to study the mechanism of the interaction between the growing crystals and the gel networks. The observed porous internal structure (Figure 3.1c), with pore sizes on the order of 100's of nanometers, is similar to biogenic calcite crystals that have incorporated biomacromolecules.[7] There is growing evidence that in some organisms these proteins either form hydrogels themselves or are in a hydrogel-like matrix associated with the biominerals.[35-37] Our work provides a platform with which to study formation mechanisms in biomineralization and properties of polymer-reinforced single crystals of calcite. This work also suggests that the gel method could be an approach to fabricate single crystals with large internal surface areas between organic and inorganic materials without destroying the integrity of the crystalline component.

3.4 Experimental Section

3.4.1 Gel preparation

The 1 w/v% agarose solution was prepared by dissolving agarose powder (Type IB, Sigma) in a hot solution of 7 mM $CaCl_2 \bullet 2H_2O$ (99+%, Sigma-Aldrich). 3 mL of the solution was then filtered (syringe filter; 0.2 μm, Nylon, Millipore), into a Petri dish (35 mm x 10 mm). After gelation (about 30 minutes), the Petri dishes were covered with aluminum foil with one small hole. The 2 w/v% gel was prepared via the same procedure except using a different filter (syringe filter; 0.45 μm, PVDF, Millipore) because the 2 w/v% agarose solution was more viscous than the 1 w/v% solution.

3.4.2 SAM-gel matrix preparation

To form the SAMs, pieces of gold-coated glass slides (40 nm of Au on 3 nm of Cr, Veeco 7700 Bell Jar Evaporator, base pressure 10^{-6} Torr) were incubated overnight in a 10 mM solution of 16-mercaptohexadecanoic acid (16-MHDA; Aldrich) in ethanol. After rinsing with ethanol and deionized (DI) water (18.2 mΩ, Barnstead EASYpure® RoDi), the slides were transferred to Petri dishes (35 mm x 10 mm) and covered with 3 mL of a filtered (syringe filter; 0.45 μm, PVDF, Millipore), warm solution of agarose (2 and 3 w/v%) in 7 mM $CaCl_2 \bullet 2H_2O$. After gelation (about 30 minutes), the Petri dishes were covered with aluminum foil with one small hole.

3.4.3 Crystallization and etching

The Petri dishes with the gel or SAM-gel matrix were placed in a closed desiccator containing one vial of ammonium carbonate [$(NH_4)_2CO_3$, Sigma-Aldrich]. After 24 hours in the desiccator, crystals grew in the bulk gel (Type I) and on the SAM in gel (Type II). Type I crystals were removed from the gel by dissolving the

agarose in boiling DI water. Type II Crystals were removed from the gels by peeling the gels away from the slides and the crystals on slides were rinsed with DI water.

The crystals were etched in DI water (Type I: etching for two days; Type II: four days. The difference in etching time is due to the different sizes of the two types of crystals.). During this time, the Petri dishes with the crystals were gently rocked on a rocking platform. After etching, the etched crystals were air-dried. For complete etching, Type II crystals were dissolved in 0.1M HCl for approximately 10 minutes. The slide was then rinsed with DI water and air-dried.

3.4.4 Characterization

The morphology of both the as-grown and the etched crystals was examined by scanning electron microscopy (SEM, STEREOSCAN 440, LEICA, 25 kV, 600 pA) after being sputter-coated with Au/Pd. The elemental composition was identified by Energy Dispersive X-ray Analysis (detector: Kevex; analyzer and software: Evex).

The internal structure of type I crystal was observed by transmission electron microscope (TEM, JEOL 1200EX, 120 kV) after being embedded in epoxy (Unicryl embedding kit, EMS, Cat #14660) and microtomed (diamond knife) into slices of 50 nm thick. The details of sample preparation are described below. Step 1: Embed the crystals in agarose hydrogel; Step 2: Sequentially replace the water in the hydrogel with ethanol/water mixtures (1:3, 1:1, 3:1) and then absolute ethanol; Step 3: Replace the ethanol in the gel with an epoxy monomer/ethanol mixture (1:1) and then pure monomer; Step 4: Polymerize the epoxy at 100^{o}C; Step 5: Microtome with diamond knife.

The crystallography of the gel-grown crystals was study by both optical microscopy (Olympus BX51) using crossed-polarizers and electron back-scattered diffraction (EBSD, detector: Nordlys II, HKL; Software: Channel 5). By using EBSD,

crystal orientation maps of a 50 micron by 50 micron, square area (Figure B.3 blue area) with a step of 5 micron was obtained. Before the EBSD experiment, the crystals on a glass slide were coated with a very thin carbon film (~several nm) by a thermal evaporator (Edwards, Auto-306). To collect the EBSD data, the sample stage was tilted at 70° from the horizontal.

The incorporated gel fibers were observed by optical microscopy (Olympus BX51) after completely etching type II crystals in 0.1 M HCl.

REFERENCES

1. H. A. Lowenstam and S. Weiner, *On Biomineralization*, Oxford University Press, New York, 1989.
2. J. Aizenberg, J. Hanson, T. F. Koetzle, S. Weiner and L. Addadi, *J. Am. Chem. Soc.*, 1997, **119**, 881-886.
3. A. Berman, L. Addadi and S. Weiner, *Nature*, 1988, **311**, 546-548.
4. J. Seto, Y. Zhang, P. Hamilton and F. Wilt, *J. Struct. Biol.*, 2004, **148**, 123-130.
5. J. Aizenberg, A. Tkachenko, S. Weiner, L. Addadi and G. Hendler, *Nature*, 2001, **412**, 819-822.
6. H. U. Nissen, *Science*, 1969, **166**, 1150-1152.
7. J. S. Robach, S. R. Stock and A. Veis, *J. Struct. Biol.*, 2005, **151**, 18-29.
8. B. Pokroy, A. N. Fitch, F. Marin, M. Kapon, N. Adir and E. Zolotoyabko, *J. Struct. Biol.*, 2006, **155**, 96-103.
9. S. Weiner, L. Addadi and H. D. Wagner, *Mater. Sci. Eng. C-Bio S*, 2000, **11**, 1-8.
10. J. Aizenberg and G. Hendler, *J. Mater. Chem.*, 2004, **14**, 2066-2072.
11. R. J. Park and F. C. Meldrum, *Adv. Mater.*, 2002, **14**, 1167-1169.
12. R. J. Park and F. C. Meldrum, *J. Mater. Chem.*, 2004, **14**, 2291-2296.
13. C. H. Lu, L. M. Qi, H. L. Cong, X. Y. Wang, J. H. Yang, L. L. Yang, D. Y. Zhang, J. M. Ma and W. X. Cao, *Chem. Mater.*, 2005, **17**, 5218-5224.
14. N. B. J. Hetherington, A. N. Kulak, K. Sheard and F. C. Meldrum, *Langmuir*, 2006, **22**, 1955-1958.
15. G. Wegner, P. Baum, M. Mullert, J. Norwig and K. Landfester, *Macromol. Symp.*, 2001, **175**, 349-355.

16. S. Ludwigs, U. Steiner, A. N. Kulak, R. Lam and F. C. Meldrum, *Adv. Mater.*, 2006, **18**, 2270-2273.

17. H. K. Henisch, *Crystals in Gels and Liesegang Rings*, Cambridge University Press, New York, 1988.

18. Y. Oaki and H. Imai, *Cryst. Growth Des.*, 2003, **3**, 711-716.

19. O. Grassmann, R. B. Neder, A. Putnis and P. Lobmann, *Am. Mineral.*, 2003, **88**, 647-652.

20. S. Busch, U. Schwarz and R. Kniep, *Adv. Funct. Mater.*, 2003, **13**, 189-198.

21. H. Y. Li and L. A. Estroff, *J. Am. Chem. Soc.*, 2007, **129**, 5480-5483.

22. H. J. Nickl and H. K. Henisch, *J. Electrochem. Soc.*, 1969, **116**, 1258-1270.

23. J. Aizenberg, A. J. Black and G. M. Whitesides, *J. Am. Chem. Soc.*, 1999, **121**, 4500-4509.

24. R. L. Penn and J. F. Banfield, *Science*, 1998, **281**, 969-971.

25. H. Colfen and M. Antonietti, *Angew. Chem., Int. Ed.*, 2005, **44**, 5576-5591.

26. A. N. Kulak, P. Iddon, Y. T. Li, S. P. Armes, H. Colfen, O. Paris, R. M. Wilson and F. C. Meldrum, *J. Am. Chem. Soc.*, 2007, **129**, 3729-3736.

27. L. J. Wang, R. K. Tang, T. Bonstein, C. A. Orme, P. J. Bush and G. H. Nancollas, *J. Phys. Chem. B*, 2005, **109**, 999-1005.

28. L. A. Estroff, L. Addadi, S. Weiner and A. D. Hamilton, *Org. Biomol. Chem.*, 2004, 137-141.

29. Crystals grown in 2 w/v% agarose gel are star-shaped, as previously reported. See references 21 and 30.

30. D. Yang, L. M. Qi and J. M. Ma, *Chem. Commun.*, 2003, 1180-1181.

31. The etching time of the crystals grown on the SAM in gel is shorter since they are smaller than the crystals grown in bulk gel.

32. C. I. D. Bica, R. Borsali, E. Geissler and C. Rochas, *Macromolecules*, 2001, **34**, 5275-5279.

33. V. Ia. Khaimov-Mal'kov, *Soviet Physics: Crystallography*, 1958, **3**, 487-493.

34. J. A. Gavira and J. M. Garcia-Ruiz, *Acta Crystallogr.D*, 2002, **58**, 1653-1656.

35. J. Moradian-Oldak, *Matrix Biol.*, 2001, **20**, 293-305.

36. Y. Levi-Kalisman, G. Falini, L. Addadi and S. Weiner, *J. Struct. Biol.*, 2001, **135**, 8-17.

37. E. Murayama, Y. Takagi, T. Ohira, J. G. Davis, M. I. Greene and H. Nagasawa, *Eur. J. Biochem.*, 2002, **269**, 688-696.

CHAPTER 4

VISUALIZING THE 3D INTERNAL STRUCTURE OF CALCITE SINGLE CRYSTALS GROWN IN AGAROSE HYDROGELS*

4.1 Abstract

Single crystals are usually faceted solids with homogeneous chemical compositions. Biogenic and synthetic calcite single crystals, however, have been found to incorporate macromolecules, spurring investigations of how large molecules are distributed within the crystals without substantially disrupting the crystalline lattice. Here, electron tomography reveals how random three dimensional networks of agarose nanofibers are incorporated into single crystals of synthetic calcite by allowing both high- and low-energy fiber/crystal interface facets to satisfy network curvatures. These results suggest that physical entrapment of polymer aggregates is a viable mechanism by which macromolecules can become incorporated inside inorganic single crystals. As such, this work has implications for understanding the structure and formation of biominerals as well as towards the development of new high-surface area, single-crystal composite materials.

4.2 Introduction

Biominerals, such as sea urchin skeletal parts and the calcite prisms in mollusk shells, are examples of organic-inorganic single-crystal composites with improved mechanical properties as compared with pure crystals.[1-7] Sea urchin spines and plates are high-magnesium calcite single crystals, which incorporate not only micrometer-sized cellular tissue networks but also smaller intracrystalline proteins.[1, 4] Similarly,

* Reproduced with permission from [H. Y. Li, H. L. Xin, D. A. Muller and L. A. Estroff, *Science*, 2009, **326**, 1244-1247.]. Copyright 2009 American Association for the Advancement of Science.

prisms from the calcitic layer of mollusk shells (such as *Atrina rigida*) are single crystals of calcite with an incorporated organic matrix composed of proteins and other biomacromolecules.[6, 7] Several techniques have been used to investigate how these macromolecules are distributed inside the single crystals without substantially disrupting the crystalline lattice. On the basis of coherence-length measurements on biogenic calcite crystals, Berman et al. suggested that intracrystalline proteins were concentrated at the mosaic block boundaries,[8] whereas transmission electron microscopy (TEM) observation of sea urchin teeth has indicated that organic material may be isolated in nanometer-sized cavities.[5] Synchrotron powder diffraction studies of a variety of biogenic calcite crystals indicate that the intra-crystalline organics induce anisotropic lattice distortions, suggesting that individual proteins may be incorporated as impurities in the crystalline lattice.[9] In addition to biogenic crystals, synthetic calcite crystals also incorporate polymers when grown in the presence of polymer networks, porous membranes, or colloidal particles.[10-15] Although it is evident that polymers are occluded in all of these crystals, the mode of distribution of the macromolecules within the crystals (such as individual molecules vs. aggregates) and the structure of the polymer/crystal interface are still both poorly characterized and understood.

There are several challenges to the study of the internal structure of inorganic crystals with incorporated organic macromolecules at atomic resolution and in three dimensions by use of traditional EM and X-ray diffraction techniques. These difficulties arise from the small sizes of the incorporated organic molecules and/or aggregates, the radiation sensitivity (for example, electron damage) of the materials, and the lack of well-developed methods for preparing electron transparent samples from micron-sized specimens suitable for high-resolution imaging. Aided by advances in focused ion beam (FIB) sample preparation technique, annular dark-field scanning

transmission electron microscopy (ADF-STEM), and ADF electron tomography for three-dimensional (3D) imaging, we have visualized the internal structure of calcite crystals ($CaCO_3$; trigonal system, space group $R\bar{3}c$) grown in agarose (a linear polysaccharide consisting of alternating 1,3-linked β-D-galactopyranose and 1,4-linked 3,6-anhydro-α-L-galactopyranose) hydrogels.

Calcite, the most abundant biomineral, has interested scientists because of the exquisite control biological organisms exert over its macro- and microscopic structure and the corresponding advanced mechanical properties of these organic/inorganic composite materials.[1-9] Biogenic minerals, including calcite, are often associated with a fibrous, hydrated, organic matrix. For these reasons, we chose to study the growth of calcite crystals in agarose hydrogels. Similar to biogenic calcite, these gel-grown crystals incorporate the agarose polymers, providing a model system with which to study the internal structure of organic/inorganic composites.[10, 11]

4.3 Results and Discussion

Calcite crystals were grown by using the ammonium carbonate method in agarose hydrogels (1 w/v %).[11] The gel-grown crystals are faceted, with the characteristic rhombohedral morphology of calcite expressed by six $\{10\bar{1}4\}$ faces (Figure 4.1, A and B).[10, 11] For STEM investigations, electron-transparent sections of the crystals were prepared by using a dual-beam FIB (Figure 4.2). Because of the radiation sensitivity of the samples, the final surfaces of the sections were finished by means of a 2-keV low-dose ion-polishing step in order to remove the damaged layer left behind by previous high-kilo-electron volt fast milling procedures. The resulting ion-thinned area has a wedge shape giving a usable working thickness ranging from ~20 nm to 1 μm.

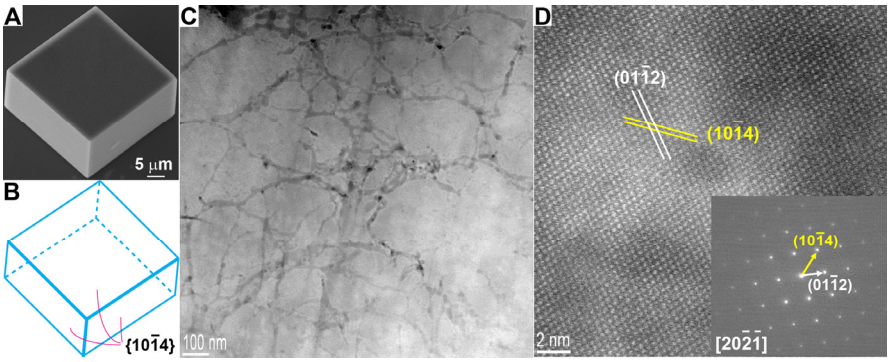

Figure 4.1: (A) A SEM image of a gel-grown calcite crystal. (B) A model of a calcite crystal expressed by six $\{10\bar{1}4\}$ faces. (C) A LAADF-STEM image of a thin section cut from a gel-grown calcite crystal by means of FIB. (D) A LAADF-STEM lattice image viewed down the $[20\bar{2}\,\bar{1}]$ zone axis of calcite single crystals. (Inset) A SAED pattern of the cut section. The examined area (diameter of 800 nm) contains both crystals and fibers.

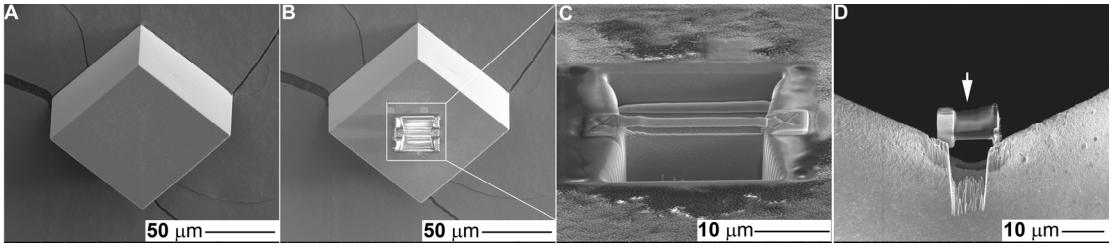

Figure 4.2: SEM images showing the sequence of preparing an electron-transparent TEM sample by FIB: (A) A calcite crystal before FIB-milling; (B, C) Two trenches were ion milled, leaving behind a slab (1.5 μm thick) of calcite attached to the bulk material. The specific trench orientation was chosen for the slab surface to lie approximately perpendicular to the $[20\bar{2}\,\bar{1}]$ zone axis; (D) A FIB-thinned TEM sample marked by arrow was mounted on a copper grid by Omniprobe.

After comparing ADF-STEM and TEM images, we selected ADF-STEM for high-resolution imaging and tomography for its more effective suppression of diffraction contrast and the better fulfillment of the projection requirement (the signal is a monotonic function of the projected mass thickness of the sample), which is an essential requirement for imaging directly interpretable and qualitatively reliable tomographic reconstructions. We optimized imaging conditions before the calcite sample loading to reduce radiation damage. Tilt-series images (for tomographic reconstruction) were recorded in areas that were 200 to 500 nm thick, where the features of interest (the incorporated organic fibers) are abundantly sampled and the imaging quality is not substantially degraded by beam divergence and beam spreading.[16]

Low-angle ADF-STEM (LAADF-STEM) images of a thin section of gel-grown calcite reveal an interconnected network of darker fibers (average diameter of 13 ± 5 nm) within a brighter matrix (Figure 4.1C). These fibrous structures are assigned to be the agarose fibers on the base of the difference in the elastic scattering cross-section of the two materials. The lower average atomic number (Z) of the organic polymer as compared with that of the calcite results in the observed difference in Z-contrast between the two materials.

In order to examine the 3D structure of the polymer network, tomographic reconstructions were generated from a tilt series of high-angle ADF-STEM (HAADF-STEM) images.[17] The result shows that the incorporated polymer aggregates form a 3D random network penetrating throughout the section of the calcite crystal (Figure 4.3A and B). The preservation of the fiber network indicates that the agarose fibers are relatively rigid and that calcite grows around the fibers without substantially disrupting the fiber aggregates.[18] Although the examined section was lifted out from near the surface of a gel-grown crystal (~10 μm penetration of ~60 μm total height),

we believe for two reasons that the images are representative of the interior of the whole crystal. First, the network persists over our largest field of view (~4 μm by 4 μm) (Figure 4.4). Second, as we have reported previously, gentle etching of fractured crystals revealed that polymer fibers are distributed throughout the crystal.[18]

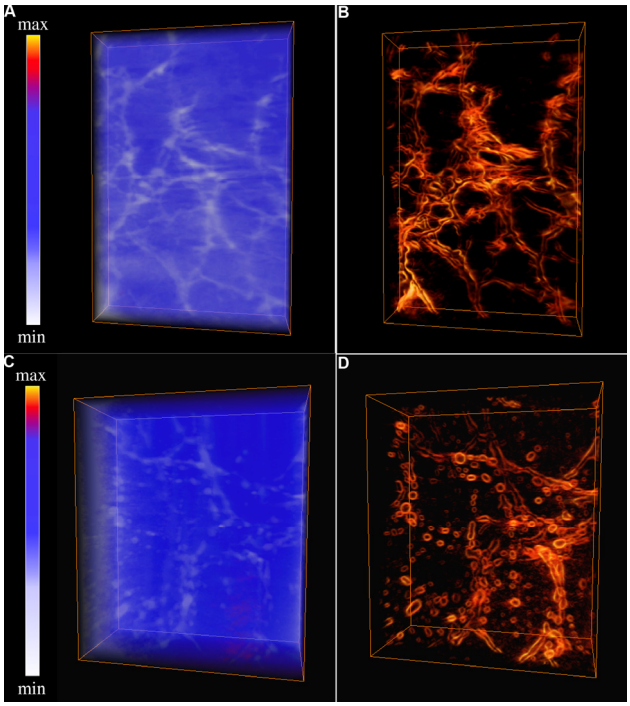

Figure 4.3: (A-D) Tomographic reconstructions of (A, B) an agarose network inside a section of as-prepared crystal and (C, D) cavities inside a section of heated crystal shown as direct volume renderings (A, C) and the respective images after applying a Sobel filter (B, D) to enhance the interfaces. (A, C) The intensity is linearly mapped to colors from the minimum to the maximum according to the color scale given on the left. Fibers and cavities are rendered as white channels and voids, and bulk calcite is rendered blue in the final visualizations. (B, D) In order to highlight the fiber/crystal and cavity/crystal interfaces, a 3-D Sobel filter (a local gradient filter which has the effect of enhancing edges, and suppresses slowly-varying backgrounds) was applied to the reconstructions to show the interface-enhanced rendition of the internal structure. The view is digitally reconstructed from a tilt series of HAADF-STEM images recorded from approximately -70° to +70° [-68° to +60° for the as-prepared crystal (A, B); -55° to +61° for the heated crystal (C, D)] at 2° intervals. The dimensions of the bounding box of the 3-D reconstruction are 1453 nm x 975 nm x 220 nm for (A, B) and 1405 nm x 1196 nm x 554 nm for (C, D).

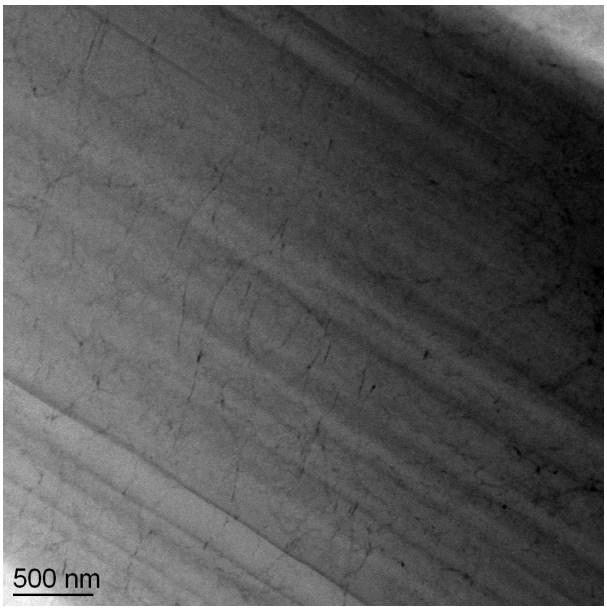

Figure 4.4: An HAADF-STEM image of a thin section cut from a gel-grown calcite crystal by FIB. The fiber network persists over the field of view (~ 4 μm x 4 μm).

Despite the presence of the organic networks, the crystals maintain their single-crystal nature. Selected-area electron diffraction (SAED) of a large area (diameter of 800 nm), including fibers, gives a single set of diffraction spots (Figure 4.1D, inset). In addition, high-resolution LAADF-STEM images directly show the regular 2D lattice image viewed down the $[20\bar{2}\,\bar{1}]$ zone axis of calcite (Figure 4.1D).

The incorporation of polymer fibers into single crystals of calcite introduces interfaces between the organic fibers and the inorganic crystals. Indexing the facets that form the internal interfaces shows that the interfaces are a mixture of $\{10\bar{1}4\}$ low-energy facets and $\{01\bar{1}2\}$ high-energy (homocharged) facets (Figure 4.5). In addition to these facets, there are other high-energy faces that could not be indexed. If the sample had been imaged at varied orientations (zones), very possibly we would observe additional high-energy faces forming the crystal/polymer interfaces.

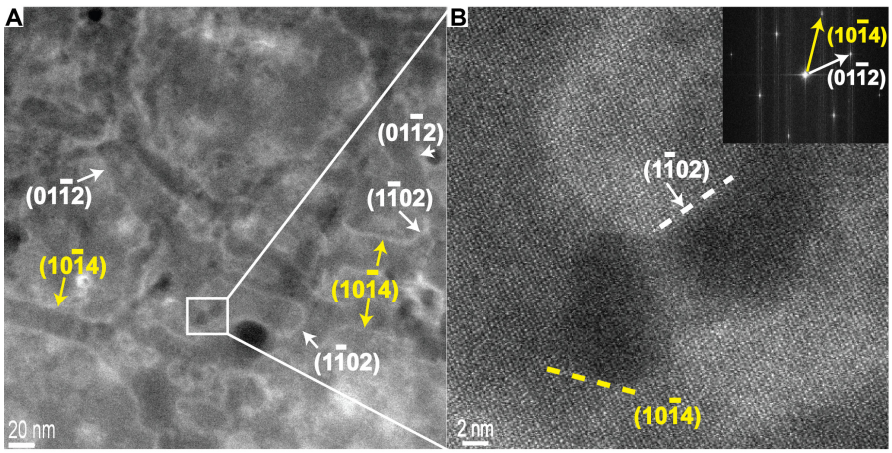

Figure 4.5: (A and B) LAADF-STEM images of a thin section cut from a gel-grown calcite crystal by means of FIB. In (B), the lattice fringes are continuous across the fiber because there is a considerable volume of crystal above and/or below the fiber. (Inset) Fast fourier transforms (FFT) of (B). The vertical streaking in the FFT is due to scan noise. On the base of the FFT, interfaces between the crystal and fibers are partially indexed. For clarity, faces in the $\{10\bar{1}4\}$ family are indicated in yellow, whereas faces in the $\{01\bar{1}2\}$ family are highlighted in white.

At the length scale of hundreds of nanometers (Figures. 4.1C and 4.3B), the interfaces are curved and thus are defined by the contours of the flexible polymer fibers. Because the fibers are interconnected as 3D random networks, at large length scales the interfaces are 3D random curved surfaces. At smaller length scales (tens of nanometers), however, the interfaces appear to be faceted and thus are defined by the faceted habit of the crystal (Figure 4.5). A combination of high- and low-energy facets is observed surrounding the fibers. Facets in addition to the $\{10\bar{1}4\}$ facets are required to satisfy the local curvature of the fibers and to minimize the interface area.

There are several possible mechanisms with which to explain the appearance of high-energy facets surrounding the agarose fibers. We will consider two general

categories: physical and chemical mechanisms. Chemical (or epitaxial) mechanisms, usually involving molecular recognition between an organic additive and a specific face of calcite, are commonly invoked to explain the expression of non-$\{10\bar{1}4\}$ surfaces in calcite crystals.[19-25]. For example, $\{01\bar{1}2\}$ faces are seldom expressed, except in the presence of homocharged (anionic) surfaces, which are believed to template the formation of a layer of calcium ions with the same structure as the $\{01\bar{1}2\}$ faces.[26-28] It is possible that the agarose fibers may in a similar way stabilize or template the formation of the $\{01\bar{1}2\}$ faces. However, the external morphology of the gel-grown calcite crystals (six $\{10\bar{1}4\}$ faces) suggests that the uncharged polysaccharide, agarose, has a weak affinity for calcite (Figure 4.1, A and B). Furthermore, even though both the external and internal surfaces are exposed to the agarose polymers, high-energy facets only appear at the internal surfaces.

As an alternative or supplement to a chemical mechanism, we propose that the coexistence of singular $\{10\bar{1}4\}$ faces at the external surface and the nonsingular faces at the internal surfaces (Figure 4.5) possibly originates from the different geometry (convex versus concave) of the growth fronts. According to the theory of crystal growth, the external morphology of crystals is defined by slow-growing (usually low-energy) faces, as depicted by kinetic Wulff diagrams. The external facets, by definition, are convex growth fronts. The picture changes for internal surfaces, which are concave. It is predicted that such concave growth fronts will instead be dominated by fast-growing (usually high-energy) faces (Figure 4.6).[29] The external surfaces of calcite crystals are convex; therefore, the low-energy (usually slow-growing) $\{10\bar{1}4\}$ faces dominate the final morphology (Figure 4.1, A and B, and Figure 4.6B). In contrast, the internal growth fronts are concave because the crystals must grow around the fibers to incorporate them, satisfying the curvature of the fibers (Figure 4.6A). Consequently, we would predict the appearance of multiple, high energy facets at the

internal interfaces, which is consistent with the observation of the high-energy (usually fast-growing) faces, including $\{01\bar{1}2\}$ faces at the calcite-agarose interfaces (Figure 4.5 and Figure 4.6, A and C). As described earlier, although, $\{01\bar{1}2\}$ faces are exemplified as high-energy (fast-growing) facets there are other high-energy facets present. Although this physical model is consistent with our observations, further work is required to determine the formation mechanism (or mechanisms) of the high-energy facets, including possible contributions from molecular recognition processes, which might favor one set of facets over another.

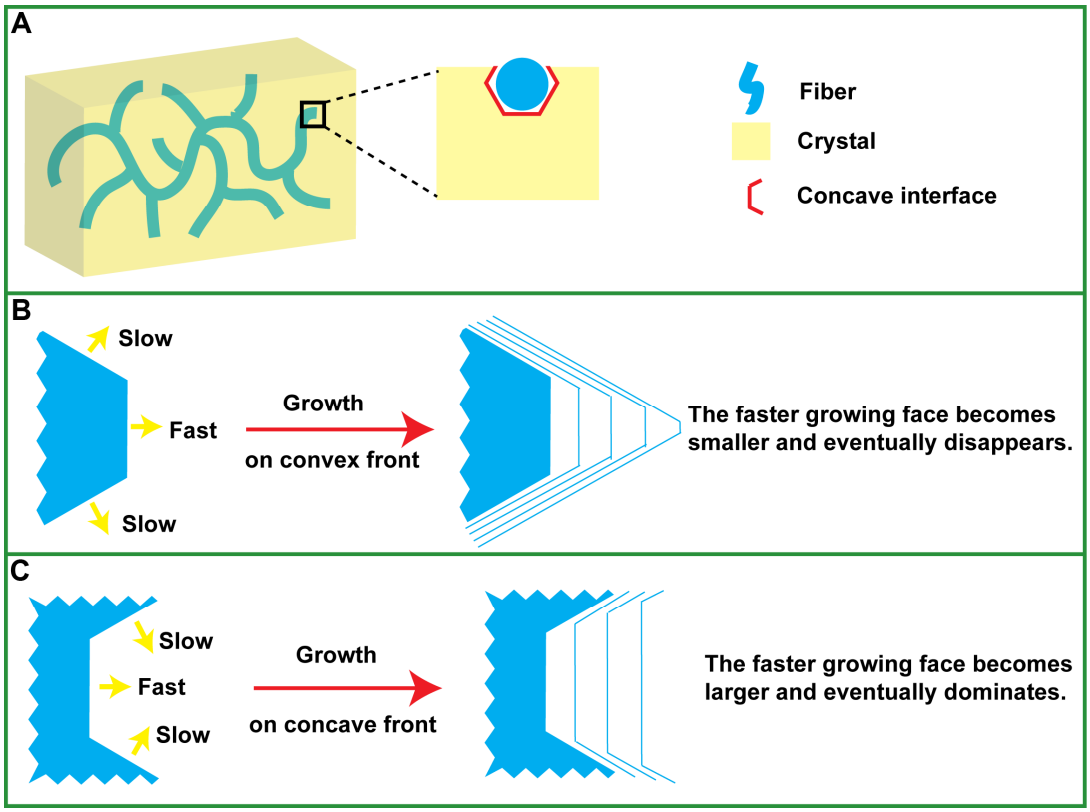

Figure 4.6: (A) A schematic representation of a crystal with incorporated polymer networks. Incorporation of polymer fibers results in a concave interface between the crystal and the fibers. (B, C) schematic representations of shape evolution at convex (B) and concave (C) growth fronts. During crystal growth, the growth fronts move forward as marked by the blue lines.

In order to investigate the stability of the internal porous structure, we removed the organic network by heating the crystals at 400 $^{\circ}$C under a flowing air atmosphere for one hour. The removal of agarose fibers at this temperature was confirmed through thermogravimetric analysis (TGA) (Figure 4.7).[18] Detailed ADF-STEM observations show the differences between the internal structure of the crystals before and after heating (Figure 4.8). After pyrolysis, cavities are observed instead of continuous fiber-like interfaces, as highlighted by the arrows in Figure 4.8A. Tomographic

reconstructions show in three dimensions that these cavities often are arranged in lines (Figure 4.3, C and D). This observation suggests that the original, continuous channels fragmented into discrete cavities after the polymer fibers were removed. This surface evolution could be due to reorganization of the internal surfaces to reduce surface area. ADF-STEM images of individual cavities reveal that the high-energy $\{01\bar{1}2\}$ facets are still present at the internal surfaces after removal of the organic material (Figure 4.8, B to D). SAED and LAADF-STEM lattice images show that even after pyrolysis, the crystals behave as single crystals (Figure 4.8, E and F). Therefore, crystalline integrity and high-energy internal facets are both preserved after pyrolysis. The internal surfaces, however, become isolated and disconnected from the external surfaces and are no longer accessible.

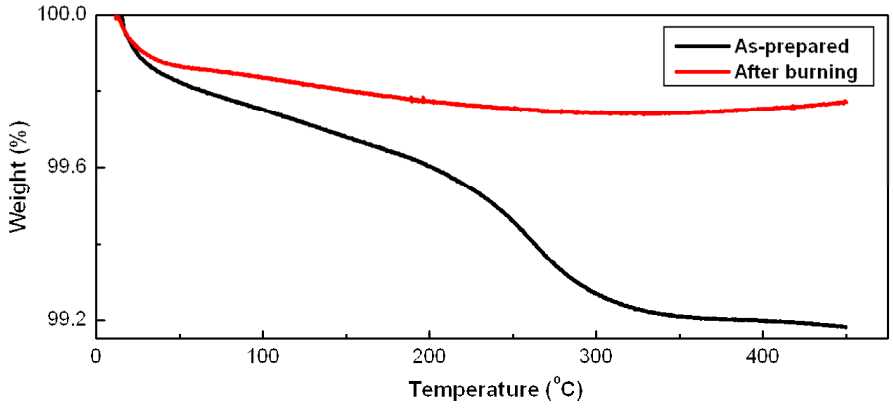

Figure 4.7: TGA curves for calcite crystals before (black) and after (red) heat treatment. In the black curve, the clear step transition of decomposition indicates the existence of agarose fibers inside of the crystals and the amount of the agarose is calculated to be around 0.56 wt%. In the red curve, no step transition of decomposition was detected. Therefore, after heat treatment, there is no detectable agarose residue.

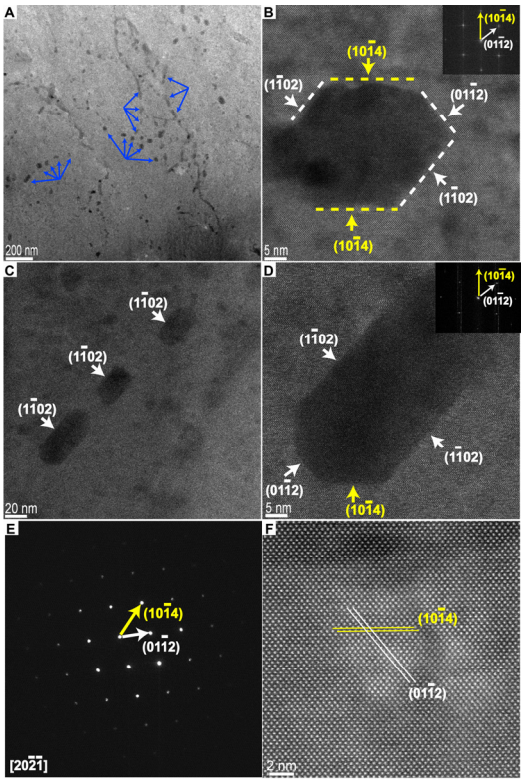

Figure 4.8: (A to D) ADF-STEM images of a thin section (prepared by means of FIB) cut from a gel-grown calcite crystal after heating. The (B) inset shows an FFT of (B), and the (D) inset shows an FFT of (D). On the basis of the FFT, the interfaces between the crystal and cavities are partially indexed. For clarity, faces in the $\{10\bar{1}4\}$ family are indicated in yellow, whereas faces in the $\{01\bar{1}2\}$ family are highlighted in white. (A) and (B) were taken in LAADF imaging mode in order to give a better signal-to-noise ratio and higher contrast between the calcite and the cavities in thin regions of the section. (C) and (D) were taken in HAADF imaging mode in order to eliminate diffraction contrast allowing the calcite/cavity interfaces to be imaged sharply in thicker regions of the sample. (E) A SAED pattern of the section. The examined area (diameter of 800 nm) contains both crystals and internal cavities. (F) An LAADF-STEM image showing the lattice of a heated calcite crystal viewed along the $[20\bar{2}\,\bar{1}]$ zone axis.

4.4 Conclusion

In summary, we have identified the mode of distribution of agarose fibers inside calcite single crystals and observed the polymer/crystal interfaces at high resolution. In these synthetic single crystals, the incorporated macromolecular aggregates are distributed as a 3D network of nanofibers as opposed to isolated molecules or individual fibers. The internal, curved polymer/crystal interfaces are formed by a combination of high- and low-energy facets. These results support physical entrapment of polymer aggregates[18] as a possible mechanism by which macromolecules can become incorporated inside inorganic single-crystals. In contrast to other mechanisms, which invoke a specific chemical interaction between the organic component and the growing crystal,[4, 15] physical entrapment can occur for a wide range of organic material. This work suggests an approach for modifying the internal structures of crystals and synthesizing single-crystal composites with large, potentially accessible, internal surface areas. Potential uses for the gel method include the preparation of materials that require both high crystallinity and high surface areas such as photovoltaic materials.[30]

4.5 Experimental Section

4.5.1 Gel preparation

The 1 w/v% agarose solution was prepared by dissolving agarose powder (Type IB, Sigma, Product #: A0576) in a hot solution of 5 mM $CaCl_2 \cdot 2H_2O$ (99+%, Sigma-Aldrich). 3 mL of the agarose solution was then filtered (syringe filter; 0.2 μm, Nylon, Millipore), into a Petri dish (35 mm x 10 mm). After gelation at ambient temperature (about 30 minutes), the Petri dishes were covered with aluminum foil with one small hole.

4.5.2 Crystallization and heat treatment

The Petri dishes with the gels were placed in a closed desiccator containing one vial of ammonium carbonate [$(NH_4)_2CO_3$, Sigma-Aldrich]. After 24 hours in the desiccator, crystals grew in the bulk gel and were removed from the gel by dissolving the agarose in boiling deionized (DI) water (18.2 mΩ, Barnstead EASYpure® RoDi). The obtained crystals were dried overnight in an oven (~80°C) after being rinsed with DI water and ethanol.

Pyrolysis was conducted in an oven (furnace: Lab-Temp; controller: Deltech Inc.) using a 5 $^{o}C\ min^{-1}$ ramp to 400 ^{o}C. The temperature was then held at 400 °C for 1 h under a flowing air atmosphere.

4.5.3 SEM and TGA

The morphologies of the crystals were examined by scanning electron microscopy (SEM, STEREOSCAN 440, LEICA, 25 kV, 600 pA) after being sputter-coated with Au/Pd.

The amount of incorporated materials is measured by thermogravimetric analysis (TGA). TGAs of both the as-prepared and the heated crystals (~ 10 mg) were conducted with a thermogravimetric analyzer (TA Instruments Q500) under a flowing air atmosphere and with a heating rate of 5°C per minute from ambient temperature to 450°C.

4.5.4 ADF-STEM

Electron-transparent transmission electron microscopy (TEM) samples were prepared by a dual-beam focused ion beam (FIB) system (FEI Strata 400 with Omniprobe). Due to the radiation sensitivity of calcite and the organic fibers, the final surfaces of the sections were finished by a 2-keV low-dose ion-polishing step to

remove the damaged layer left behind by previous high-keV fast milling procedures.[31] The resulting ion-thinned area had a wedge shape giving a usable working thickness ranging from ~20 nm to 1 μm for imaging.

Internal structures of both the as-prepared and the heat-treated crystals were investigated by annular-dark-field scanning transmission electron microscopy (ADF-STEM) (FEI Tecnai F20 field emission gun, 200 kV, with Fischione annular-dark-field detector). Selected area electron diffraction (SAED) patterns were also obtained on the same equipment (FEI Tecnai F20). Two different projector settings were used in our experiments to collect different portions of scattered electrons on the annular-dark-field detector. The high-angle annular-dark-field (HAADF) mode has a nominal camera length of 100 mm that collects scattered electrons from 65 mrad to 330 mrad. The low-angle annular-dark-field (LAADF) mode has a nominal camera length of 300 mm, recording scattered electrons from 22 mrad to 110 mrad. Because the HAADF mode records electrons that scatter to relatively high angles, it is less sensitive to diffraction contrast and reflects the projected mass contrast (Z-contrast) of the underlying material. On the other hand, LAADF is more sensitive to diffraction contrast. For example, strained materials show up brighter than unstrained materials in LAADF mode but not in HAADF mode (In Figure 4.5A, the fiber/calcite interfaces are outlined brighter due to the strain field[32] at the boundary).

4.5.5 ADF-STEM tomography

The internal three dimensional (3-D) structure of the calcite crystals was reconstructed by HAADF-STEM tomography. A series of HAADF-STEM images were acquired at successively increasing tilt angles from approximately -70° to +70° (-68° to +60° for the as-prepared sample; -55° to +61° for the heated sample) at 2° intervals. The computed reconstructions based on the tilt series were performed using

a custom-written IDL (Interface Descriptor Language, a scripting language package similar to Matlab) script code employing the simultaneous iterative reconstruction technique[33] with an iteration number of 15. All images were re-binned by two before they were input for reconstruction due to memory limits in 32-bit IDL. The reconstructions were directly volume rendered by the Voxel function in Avizo 5.0 as shown in Figure 4.3 A and C. While the voids and channels are visible in the reconstructions, we also used a 3-D Sobel filter in Avizo 5.0 to highlight the boundaries (Figure 4.3 B and D). The Sobel filter is a standard filter implemented in commercial imaging processing software like Avizo. It takes the local gradient of the image, effectively removing slowly-varying backgrounds. The resulting volume rendered images show bright boundaries tracing the interfaces between high and low intensity objects[34].

REFERENCES

1. Y. Politi, T. Arad, E. Klein, S. Weiner and L. Addadi, *Science*, 2004, **306**, 1161-1164.
2. J. Aizenberg, D. A. Muller, J. L. Grazul and D. R. Hamann, *Science*, 2003, **299**, 1205-1208.
3. J. Aizenberg, A. Tkachenko, S. Weiner, L. Addadi and G. Hendler, *Nature*, 2001, **412**, 819-822.
4. J. Aizenberg, J. Hanson, T. F. Koetzle, S. Weiner and L. Addadi, *J. Am. Chem. Soc.*, 1997, **119**, 881-886.
5. J. S. Robach, S. R. Stock and A. Veis, *J. Struct. Biol.*, 2005, **151**, 18-29.
6. F. Nudelman, H. H. Chen, H. A. Goldberg, S. Weiner and L. Addadi, *Faraday Discuss.*, 2007, **136**, 9-25.
7. A. Berman, J. Hanson, L. Leiserowitz, T. F. Koetzle, S. Weiner and L. Addadi, *Science*, 1993, **259**, 776-779.
8. A. Berman, L. Addadi, A. Kvick, L. Leiserowitz, M. Nelson and S. Weiner, *Science*, 1990, **250**, 664-667.
9. B. Pokroy, A. N. Fitch, F. Marin, M. Kapon, N. Adir and E. Zolotoyabko, *J. Struct. Biol.*, 2006, **155**, 96-103.
10. H. Y. Li and L. A. Estroff, *J. Am. Chem. Soc.*, 2007, **129**, 5480-5483.
11. H. Y. Li and L. A. Estroff, *Crystengcomm*, 2007, **9**, 1153-1155.
12. S. Sindhu *et al.*, *Adv. Funct. Mater.* **17**, 1698 (2007).
13. R. J. Park and F. C. Meldrum, *Adv. Mater.*, 2002, **14**, 1167-1169.
14. C. Li and L. M. Qi, *Angew. Chem., Int. Ed.*, 2008, **47**, 2388-2393.
15. A. N. Kulak, P. Iddon, Y. T. Li, S. P. Armes, H. Colfen, O. Paris, R. M. Wilson and F. C. Meldrum, *J. Am. Chem. Soc.*, 2007, **129**, 3729-3736.

16. J. K. Hyun, P. Ercius and D. A. Muller, *Ultramicroscopy*, 2008, **109**, 1-7.

17. P. A. Midgley and M. Weyland, *Ultramicroscopy*, 2003, **96**, 413-431.

18. H. Y. Li and L. A. Estroff, *Adv. Mater.*, 2009, **21**, 470-473.

19. J. J. De Yoreo and P. M. Dove, *Science*, 2004, **306**, 1301-1302.

20. C. A. Orme, A. Noy, A. Wierzbicki, M. T. McBride, M. Grantham, H. H. Teng, P. M. Dove and J. J. DeYoreo, *Nature*, 2001, **411**, 775-779.

21. S. Mann, D. D. Archibald, J. M. Didymus, T. Douglas, B. R. Heywood, F. C. Meldrum and N. J. Reeves, *Science*, 1993, **261**, 1286-1292.

22. L. A. Estroff, C. D. Incarvito and A. D. Hamilton, *J. Am. Chem. Soc.*, 2004, **126**, 2-3.

23. N. Sommerdijk and G. de With, *Chem. Rev.*, 2008, **108**, 4499-4550.

24. E. M. Pouget, P. H. H. Bomans, J. Goos, P. M. Frederik, G. de With and N. Sommerdijk, *Science*, 2009, **323**, 1555-1458.

25. R. Q. Song, A. W. Xu, M. Antonietti and H. Colfen, *Angew. Chem., Int. Ed.*, 2009, **48**, 395-399.

26. J. Aizenberg, A. J. Black and G. M. Whitesides, *Nature*, 1999, **398**, 495-498.

27. A. M. Travaille, L. Kaptijn, P. Verwer, B. Hulsken, J. A. A. W. Elemans, R. J. M. Nolte and H. Van Kempen, *J. Am. Chem. Soc.*, 2003, **125**, 11571-11577.

28. D. Volkmer, M. Fricke, C. Agena and J. Mattay, *J. Mater. Chem.*, 2004, **14**, 2249-2259.

29. D. X. Du, D. J. Srolovitz, M. E. Coltrin and C. C. Mitchell, *Phys. Rev. Lett.*, 2005, **95**.

30. I. Gur, N. A. Fromer, M. L. Geier and A. P. Alivisatos, *Science*, 2005, **310**, 462-465.

31. L. A. Giannuzzi, R. Geurts, Ringalda J, *Microsc. Microanal.,* 2005, **11 (Suppl 2),** 828

32. Z. H. Yu, D. A. Muller and J. Silcox, *J. Appl. Phys.*, 2004, **95**, 3362-3371.

33. P. A. Midgley and M. Weyland, *Ultramicroscopy*, 2003, **96**, 413-431.

34. R. O. Duda and P. E. Hart, *Pattern classification and scene analysis*, Wiley, New York, 1973.

CHAPTER 5

CRYSTAL GROWTH IN GELS: AN APPROACH TO MAKE POROUS SINGLE CRYSTALS

5.1 Introduction

Porous materials usually have poor crystallinity and single-crystalline materials usually do not exhibit porosity. Combining porosity and single-crystallinity is still challenging for material synthesis. Our previous work shows that calcite crystals grown from agarose hydrogels incorporate the agrose networks, resulting in polymer/single-crystal composites (Chapters 2-4).[1] In this work, we demonstrate that removal of the agarose networks from the composites leads to porous single crystals of calcite. The results suggest that crystal preparation in gel media is an approach to make advanced materials that combine porosity with single-crystallinity.

Porous materials, as the name suggests, have large internal surface area to make contact with foreign molecules, and thus have promise for applications in catalysis, absorption, sensing, drug delivery, and optoelectronics.[2-9] Templating is a typical method to create pore space within solids. For example, using block-polymers or colloidal particles as templates, porous materials have been made with the pore spaces defined at different and even hierarchical length scales.[10, 11] In addition to the internal surfaces, the frameworks supporting the pore space also essentially determine the properties of porous materials. Frameworks with different composition have been prepared and investigated, ranging from insulating, semiconducting, and conducting materials. Crystalline frameworks are often desired due to their intrinsic properties such as electronic, magnetic, and mechanical properties. Efforts have been made to improve the crystallinity of framework materials from amorphous, semicrystalline, and polycrystalline states.[12-17] Nevertheless, further increasing the crystallinity to a

single crystal is still challenging as, phenomenologically, templated porous materials tend to have low crystallinity, while single-crystal materials tend to be faceted and homogeneous (without pores).

In Nature, organisms construct crystals (biominerals) with porous structures. Surprisingly, many of these biominerals are endowed with porosity as well as single-crystallinity. Typical examples are the skeletal materials of echinoderms (e.g., sea urchins and brittle stars).[18-20] Sea urchin spines and plates are composed of high-Mg calcite single crystals with micrometer-sized pores (10's of μm) penetrating throughout the entire crystal. In addition, smaller-sized (10-225 nm) pores have been found in the components of sea urchin teeth that are also made of high-Mg calcite single crystals.[21] These examples from Nature show the possibility of combining single-crystallinity with porosity together to create advanced materials. Synthetically, 3-dimensional (3D) macroporous (10's of μm pores) single crystals of calcite have been prepared using polymer replicas of sea urchin plates as sacrificial templates.[18, 22] More recently, pore size down to 100's and 10's of nm have been achieved in calcite single crystals templated by colloidal crystals and block-copolymer membranes.[23, 24] These methods all involve a relatively elaborate process of template preparation and a simpler approach is desired.

Gels have been used to grow a variety of crystals for more than one century.[25] In 1969, Nickl and Henisch found that calcite crystals grown from silica gels incorporate the gel networks.[26] More recently, the gel-incorporation phenomenon becomes more general to gel-grown crystals. Proteins, calcite, α-glycine, and calcium tartrate tetrahydrate crystals have been reported to incorporate silica, gelatin, agar and agarose gel networks.[27-32] Among these systems, calcite crystals grown from agarose gels have been investigated thoroughly from the internal agarose/calcite interfacial structure to the mechanisms of gel incorporation. The results shows that the calcite

crystals incorporate the gel networks without losing their long-range order (single-crystal nature).[1, 33, 34] Potentially, the gel-method will become a promising approach to prepare porous single-crystals. If the incorporated networks are removed from the crystals, porous single-crystals will be obtained. In this work, we remove the agarose networks from gel-grown calcite single crystals, use focused ion beam (FIB) and transmission electron microscopy (TEM) to visualize the obtained internal porous structure, and measure the specific surface area of the accessible internal pores.

5.2 Results and Discussion

Calcite crystals were grown in agarose hydrogels (1 w/v % agarose IB, 5 mM $CaCl_2$) using the ammonium carbonate method.[33] The obtained crystals are isolated from the gel media and observed by scanning electron microscopy (SEM). These crystals are faceted, with the characteristic rhombohedral morphology of calcite single crystal expressed by six $\{10\bar{1}4\}$ faces (Figure 5.1a). Although the gel-grown crystals resemble the pure single crystals, they are actually polymer/single-crystal composites with agarose polymer networks penetrating inside of a calcite single-crystal matrix (Figure 5.1c).[1]

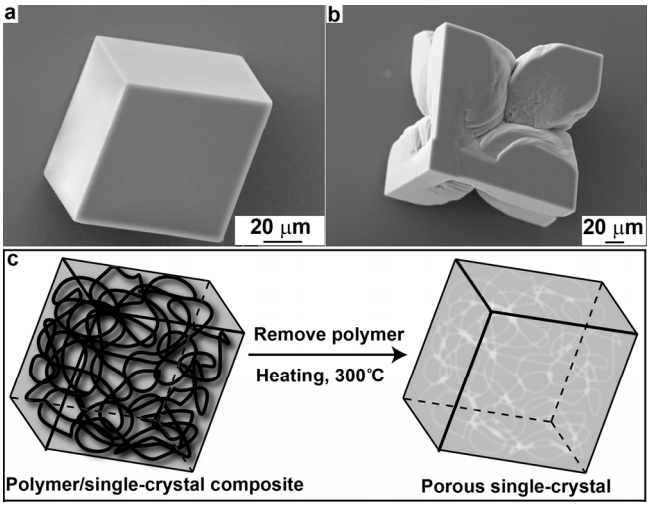

Figure 5.1: a,b) Representative SEM images of calcite crystals grown in agarose gels (1 w/v% Agarose IB) containing a) 5 mM $CaCl_2$ and b) 500 mM $CaCl_2$. c) A schematic representation of the gel-grown calcite crystals before and after gel networks removal.

In order to obtain accessible porous internal space, the agarose networks were removed from the crystal matrix by heating the crystals at 300 $^{\circ}$C under a flowing air atmosphere for one hour. Thermogravimetric analysis (TGA) was used to confirm the removal of the agarose networks. TGA of the as prepared gel-grown crystals shows a clear step transition which is identified as the decomposition of agarose polymers.[34] In constrast, TGA of the heated crystals does not show the above mentioned step transition, indicating that the agarose polymers were successfully removed by the heat treatment (Figure 5.2). Although TGA shows no detectable agarose in the heated crystals, there is possibly a small amount of decomposition product remaining since the crystals changed color from white to light brown after heating.

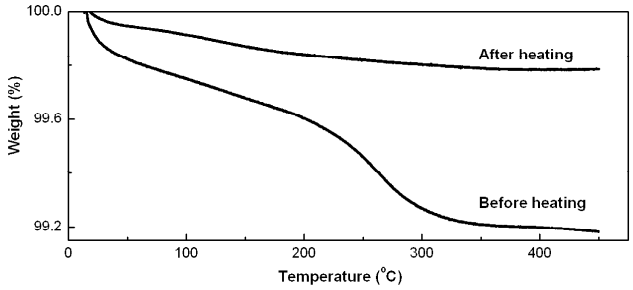

Figure 5.2: TGA curves for gel-grown calcite crystals before and after heat treatment (300°C).

In a previous study (Chapter 4)[1], we showed that heating the crystals at a higher temperature (400 °C) also removed the agarose polymers without disrupting the crystalline lattice. The internal surfaces of these crystals, however, evolved from continuous channels into isolated cavities, became disconnected from the external surfaces, and were no longer accessible. In order to examine the morphology of the internal channels under the current experimental conditions (300 °C heating), we visualized the internal structure of the heated crystals using TEM. Electron-transparent TEM samples were prepared by a dual-beam FIB system (Figure 5.3a, b). TEM images show continuous channels inside of the crystal matrix (Figure 5.3c). The diameter of the channels is 15 ± 6 nm which is close to the diameter (13 ± 5 nm) of the agarose fiber before heating (see Figure 4.1).[1] Therefore, at 300 °C, heating removes the polymers without significantly changing the internal surfaces of the crystals (Figure 5.1c).

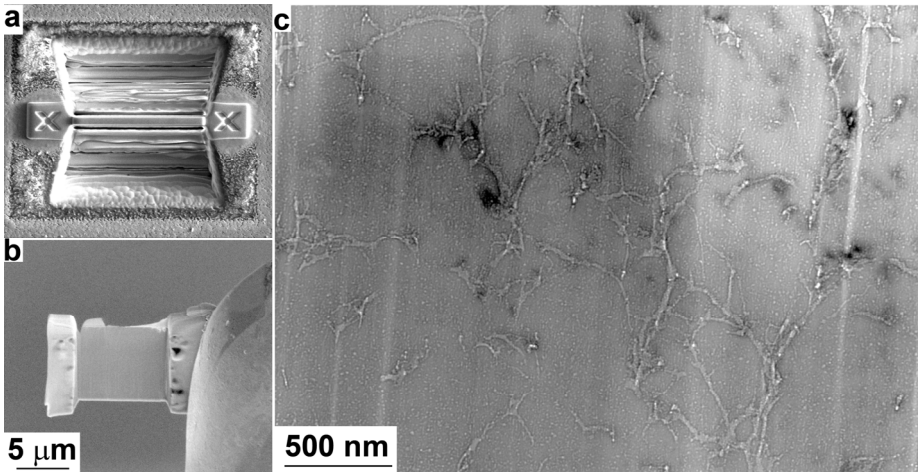

Figure 5.3: a, b) SEM images showing the sequence of preparing an electron-transparent TEM sample by FIB: a) Two trenches were ion milled, leaving behind a slab (1.5 μm thick); b) The slab was mounted on a copper grid for TEM observation, after being lift-out from the trenches and FIB-thinned. c) A TEM image of the FIB-prepared thin section of a heated gel-grown crystal.

Nitrogen physisorption was used to confirm that the interal porous surface was accessible and to determine the specific surface area using the Brunauer, Emmett and Teller (BET) method. For measurement, more than 1 gram of crystals was prepared using a high concentration of reactant (500 mM $CaCl_2$). The obtained crystals have a "hopper-like" shape (Figure 5.1b) which evolves from a rhombohedron (Figure 5.1a) when the corners and edges grow faster than the center of faces of the rhombohedron.[29, 35] Nitrogen adsorption-desorption isotherms of the as-prepared crystals show that there is no clear nitrogen absorption, indicating that the external surfaces of the crystals do not contribute significantly to the adsorption (Figure 5.4a). In sharp contrast, after removing the polymers by heating (at 300^{o}C), the crystals exhibit clear absorption (Figure 5.4b). Therefore, nitrogen physisorption shows that at least some of the porous internal space is connected to the external space of the

crystals and the internal surfaces are accessible. Although, the internal surface area is not as high as porous calcite crystals prepared by the mesocrystal method or precipitation in presence of specific polymers,[36, 37] the gel-grown porous calcite crystals have higher crystallinity (single-crystallinity). In addition, the internal surface area increases with the polymer concentration of gels we use to grow the crystals. When a 3 w/v% gel is used, the specific surface area increases to 5.8 $m^2 g^{-1}$ (Figure 5.4c).

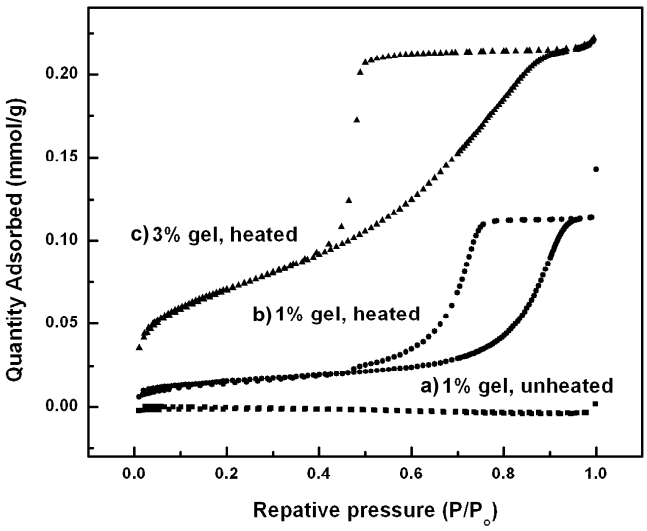

Figure 5.4: a, b) Nitrogen adsorption-desorption isotherms of calcite crystals grown from gels (1 w/v% Agarose IB, 500 mM $CaCl_2$) before (a) and after (b) heating. c) Nitrogen adsorption-desorption isotherms of calcite crystals grown from gels (3 w/v% Agarose IB, 500 mM $CaCl_2$) after heating.

5.3 Conclusion

Heating of gel-grown agarose/calcite-crystal composites at 300^{o}C removes the agarose from the composites, resulting in internal nano-channels (diameter: 15 ± 6 nm) and open porosity. These results demonstrate that crystal growth in gel media,

which is a traditional, well-developed method for crystal preparation, is an approach to prepare materials with both high crystallinity (single-crystallinity) and high surface area (much higher than homogeneous single crystals).

5.4 Experimental section

5.4.1 Gel preparation

The 1 w/v% agarose solution was prepared by dissolving agarose powder (Type IB, Sigma) in a hot solution of 5 mM or 500 mM $CaCl_2 \cdot 2H_2O$ (99+%, Sigma-Aldrich). 3 mL of the solution was then filtered (syringe filter; 0.2 μm, Nylon, Millipore) into a Petri dish (35 mm x 10 mm). After gelation (about 30 minutes), the Petri dishes were covered with aluminum foil with one small hole. The 3 w/v% gel was prepared via the same procedure except using a different filter (syringe filter; 0.45 μm, PVDF, Millipore) because the 3 w/v% agarose solution was more viscous than the 1 w/v% solution.

5.4.2 Crystallization and heat treatment

The Petri dishes with the gel were placed in a closed desiccator containing one vial of ammonium carbonate (Sigma-Aldrich). After a period of time (24 hours for gels with 5 mM $CaCl_2$, 10 days for gels with 500 mM $CaCl_2$) in the desiccator, crystals grew in the bulk gel and were removed from the gel by dissolving the agarose in boiling deionized (DI) water (18.2 MΩ, Barnstead EASYpure® RoDI). The obtained crystals were then rinsed with DI water and ethanol.

Pyrolysis was conducted in an oven (furnace: Lab-Temp; controller: Deltech Inc.) using a 5 $^{o}C\ min^{-1}$ ramp to 300 ^{o}C. The temperature was then held at 300 °C for 1 h under a flowing air atmosphere.

5.4.3 *Characterization*

The morphologies of the as-grown crystals were examined by scanning electron microscopy (STEREOSCAN 440, LEICA) after being sputter-coated with Au. The internal structure of the crystals after pyrolysis was investigated by annular dark-field scanning transmission electron microscopy (ADF-STEM) (FEI Tecnai F20 field emission gun, 200 kV, with Fischione annular-dark-field detector) and electron-transparent transmission electron microscopy (TEM) samples were prepared by a dual-beam focused ion beam (FIB) system (FEI Strata 400 with Omniprobe).

Thermogravimetric analysis (TGA) of the crystals was conducted with a Thermogravimetric Analyzer (TA Instruments Q500) under a flowing air atmosphere and with a heating rate of 5°C per minute from ambient temperature to 450°C. About 10 mg of crystals were used for each run after drying overnight in an oven (~80°C). Nitrogen physisorption was performed on a Micromeritics ASAP 2020 with an equilibration time of 10 s.

REFERENCES

1. H. Y. Li, H. L. Xin, D. A. Muller and L. A. Estroff, *Science*, 2009, **326**, 1244-1247.
2. M. E. Davis, *Nature*, 2002, **417**, 813-821.
3. J. S. Beck, J. C. Vartuli, W. J. Roth, M. E. Leonowicz, C. T. Kresge, K. D. Schmitt, C. T. W. Chu, D. H. Olson, E. W. Sheppard, S. B. McCullen, J. B. Higgins and J. L. Schlenker, *J. Am. Chem. Soc.*, 1992, **114**, 10834-10843.
4. T. Asefa, M. J. MacLachlan, N. Coombs and G. A. Ozin, *Nature*, 1999, **402**, 867-871.
5. F. Schuth and W. Schmidt, *Adv. Mater.*, 2002, **14**, 629-638.
6. Y. Y. Li, F. Cunin, J. R. Link, T. Gao, R. E. Betts, S. H. Reiver, V. Chin, S. N. Bhatia and M. J. Sailor, *Science*, 2003, **299**, 2045-2047.
7. Y. Ding, M. W. Chen and J. Erlebacher, *J. Am. Chem. Soc.*, 2004, **126**, 6876-6877.
8. S. Bag, P. N. Trikalitis, P. J. Chupas, G. S. Armatas and M. G. Kanatzidis, *Science*, 2007, **317**, 490-493.
9. M. Nedelcu, J. Lee, E. J. W. Crossland, S. C. Warren, M. C. Orilall, S. Guldin, S. Huttner, C. Ducati, D. Eder, U. Wiesner, U. Steiner and H. J. Snaith, *Soft Matter*, 2009, **5**, 134-139.
10. P. D. Yang, T. Deng, D. Y. Zhao, P. Y. Feng, D. Pine, B. F. Chmelka, G. M. Whitesides and G. D. Stucky, *Science*, 1998, **282**, 2244-2246.
11. M. Kamperman, A. Burns, R. Weissgraeber, N. van Vegten, S. C. Warren, S. M. Gruner, A. Baiker and U. Wiesner, *Nano Lett.*, 2009, **9**, 2756-2762.
12. P. D. Yang, D. Y. Zhao, D. I. Margolese, B. F. Chmelka and G. D. Stucky, *Nature*, 1998, **396**, 152-155.

13. S. C. Warren, L. C. Messina, L. S. Slaughter, M. Kamperman, Q. Zhou, S. M. Gruner, F. J. DiSalvo and U. Wiesner, *Science*, 2008, **320**, 1748-1752.

14. J. Lee, M. C. Orilall, S. C. Warren, M. Kamperman, F. J. Disalvo and U. Wiesner, *Nat. Mater.*, 2008, **7**, 222-228.

15. S. Inagaki, S. Guan, T. Ohsuna and O. Terasaki, *Nature*, 2002, **416**, 304-307.

16. J. H. Ba, J. Polleux, M. Antonietti and M. Niederberger, *Adv. Mater.*, 2005, **17**, 2509-2512.

17. O. D. Velev, P. M. Tessier, A. M. Lenhoff and E. W. Kaler, *Nature*, 1999, **401**, 548-548.

18. R. J. Park and F. C. Meldrum, *Adv. Mater.*, 2002, **14**, 1167-1169.

19. J. Aizenberg, J. Hanson, T. F. Koetzle, S. Weiner and L. Addadi, *J. Am. Chem. Soc.*, 1997, **119**, 881-886.

20. J. Aizenberg, A. Tkachenko, S. Weiner, L. Addadi and G. Hendler, *Nature*, 2001, **412**, 819-822.

21. J. S. Robach, S. R. Stock and A. Veis, *J. Struct. Biol.*, 2005, **151**, 18-29.

22. R. J. Park and F. C. Meldrum, *J. Mater. Chem.*, 2004, **14**, 2291-2296.

23. C. Li and L. M. Qi, *Angew. Chem., Int. Ed.*, 2008, **47**, 2388-2393.

24. A. S. Finnemore, M. R. J. Scherer, R. Langford, S. Mahajan, S. Ludwigs, F. C. Meldrum and U. Steiner, *Adv. Mater.*, 2009, **21**, 3928-3932.

25. H. K. Henisch, *Crystals in Gels and Liesegang Rings*, Cambridge University Press, New York, 1988.

26. H. J. Nickl and H. K. Henisch, *J. Electrochem. Soc.*, 1969, **116**, 1258-1270.

27. J. M. Garcia-Ruiz, J. A. Gavira, F. Otalora, A. Guasch and M. Coll, *Mater. Res. Bull.*, 1998, **33**, 1593-1598.

28. J. A. Gavira and J. M. Garcia-Ruiz, *Acta Crystallogr.D*, 2002, **58**, 1653-1656.

29. H. Y. Li and L. A. Estroff, *J. Am. Chem. Soc.*, 2007, **129**, 5480-5483.

30. H. Y. Li and L. A. Estroff, 2009, **submitted** (see Chapter 8).

31. Y. X. Huang, J. Buder, R. Cardoso-Gil, Y. Prots, W. Carrillo-Cabrera, P. Simon and R. Kniep, *Angew. Chem., Int. Ed.*, 2008, **47**, 8280-8284.

32. Y. Oaki, S. Hayashi and H. Imai, *Chem. Commun.*, 2007, 2841-2843.

33. H. Y. Li and L. A. Estroff, *Crystengcomm*, 2007, **9**, 1153-1155.

34. H. Y. Li and L. A. Estroff, *Adv. Mater.*, 2009, **21**, 470-473.

35. D. Yang, L. M. Qi and J. M. Ma, *Chem. Commun.*, 2003, 1180-1181.

36. A. W. Xu, M. Antonietti, S. H. Yu and H. Colfen, *Adv. Mater.*, 2008, **20**, 1333-1338.

37. J. G. Yu, J. C. Yu, L. Z. Zhang, X. C. Wang and L. Wu, *Chem. Commun.*, 2004, 2414-2415.

CHAPTER 6

CALCITE GROWTH IN HYDROGELS: ASSESSING THE MECHANISM OF POLYMER NETWORK INCORPORATION INTO SINGLE CRYSTALS*

6.1 Introduction

Synthetic and biogenic calcite ($CaCO_3$) crystals are known to incorporate biomacromolecules[1] and other organic molecules[2] while still diffracting X-rays as single crystals. This work evaluates the parameters that control the incorporation of polymer networks during calcite crystal growth in agarose hydrogels. We find that the crystallization pressure promotes the exclusion of the gel network while faster growth rates favor the incorporation. These two competing factors determine how much of the gel network is incorporated into the calcite crystals. Insights provided by this work may help to elucidate the formation mechanism(s) of biogenic single crystals with incorporated organic material.

In Nature, organisms fabricate inorganic single crystals with occluded proteins and polysaccharides, resulting in biominerals with improved mechanical properties.[1, 3, 4] Typical examples are the skeletal parts of echinoderms (e.g., sea urchins and brittle stars) and the prismatic layer of mollusk shells.[4-9] One component of sea urchin teeth is high-Mg calcite plates that are single crystals with 20 v/v% cavities with diameters ranging from 10 to 225 nm. These cavities were suggested to be filled with a hydrated organic phase.[7] The calcite prisms in the prismatic layer of *Atrina rigida* also behave as single crystals, which contain an organic matrix composed primarily of chitin fibers.[8, 9] Similar to biogenic calcite crystals with incorporated polymer, there are several reports of synthetic calcite crystals with incorporated material including

* Reproduced with permission from [H. Y. Li and L. A. Estroff, *Adv. Mater.*, 2009, **21**, 470-473.]. Copyright 2009 Wiley-VCH.

poly[(methyl methacrylate)-co-(ethyl acrylate)] porous membranes,[10, 11] poly(styrene) films with nanopores,[12] colloidal particles,[13, 14] silica hydrogels,[15, 16] and agarose hydrogels.[17, 18] In many of these examples, the authors have demonstrated that the calcite crystals diffract electrons and/or X-rays as single crystals, despite the presence of the organic material.[4, 5, 8, 11, 14, 18]

To date, the mechanisms for the incorporation of polymer networks into calcite single crystals are poorly understood. A related phenomenon, the incorporation of foreign particles into crystals, has been described.[19-23] When a growth front approaches a foreign particle, which wets the crystal surface, the particle will be incorporated into the crystal. If the mutual wetting is poor, however, the particle will be repelled by a positive "disjoining force" and move forward, together with the growth front.[23] The disjoining force is counteracted by a hydrodynamic force that increases with increasing growth rate. At faster growth rates and thus stronger hydrodynamic forces, the particle will be pressed into the crystal; whereas at slower growth rates, the particle will be pushed ahead by the growing front. An equally important effect of the growth rate is that faster growth rates increase transport resistance by allowing less time for molecules or ions to diffuse into the gap between the growth front and the particle. This effect further promotes incorporation of foreign particles at fast growth rates.

If instead of individual particles, interconnected polymer networks such as hydrogels are present during crystal growth,[15] additional factors have to be considered.[24] As a crystal grows, it exerts a pressure on its surroundings, which depends on the supersaturation of the solution.[25, 26] The gel network can respond to this pressure by rearranging; this ability to rearrange is related to the modulus of the gel network and the rate of crystal growth. If the gel network is strong enough to resist the "crystallization pressure," the crystal will be forced to grow around the gel fibers

and, hence, incorporate them.[16, 18, 27] Alternatively, if the gel is weak, the growing crystals will damage the network and exclude the fibers.[15, 24]

In the current work, we examine the growth of calcite crystals in agarose hydrogels in the context of the previous work describing the interactions between growth fronts and foreign materials (particles and networks). We evaluate the mechanism of hydrogel network incorporation into calcite crystals and elucidate the effects of gel concentration, gel strength, and growth rate on the amount of incorporated gel.

6.2 Results and Discussion

Calcite crystals grown in agarose hydrogels (0.25-1 w/v% Agarose IB, 5 mM $CaCl_2$) using the ammonium carbonate method[28] are faceted with the characteristic rhombohedral morphology of calcite expressed by six {104} faces (Figure 6.1a). As we have reported previously, gently etching the crystals with deionized (DI) water reveals the incorporated gel fibers.[17, 18] SEM images of fractured and etched surfaces show gel fibers emerging from irregular etch pits (Figure 6.1b-f). The density of etch pits and the number of visible fibers decrease with decreasing agarose concentration (Figure 6.1c-f).

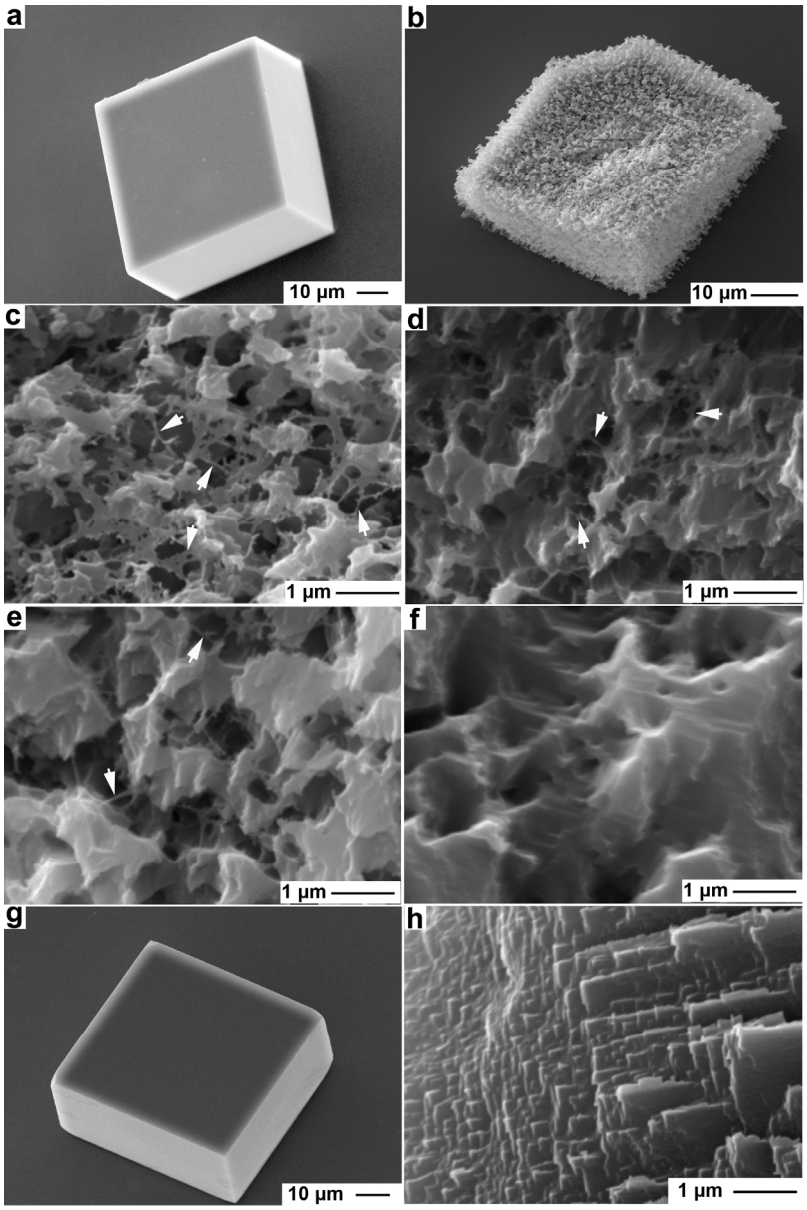

Figure 6.1: a,b) Representative SEM images of (a, g) as grown and (b-f, h) fractured and etched calcite crystals grown in (a-c) an agarose gel (1 w/v% Agarose IB; 5 mM $CaCl_2$), (d) an agarose gel (0.75 w/v% Agarose IB; 5 mM $CaCl_2$), (e) an agarose gel (0.5 w/v% Agarose IB; 5 mM $CaCl_2$), (f) an agarose gel (0.25 w/v% Agarose IB; 5 mM $CaCl_2$), and (g, h) an agarose gel (1 w/v% Agarose IX; 5 mM $CaCl_2$). White arrows highlight the incorporated gel fibers. Note: agarose IB and agarose IX are two types of agarose (see text for details.).

The amount of material incorporated in the crystals was quantified by thermogravimetric analysis (TGA). For all samples, there is a clear step transition of decomposition with an onset temperature between 225°C and 250°C (a representative trace is shown in Figure 6.2a(ii)). For consistency across samples, the weight loss above 150°C, the temperature where the decomposition begins to accelerate as shown by derivative thermogravimetric (DTG) analysis [Figure 6.2a(iiii)], was calculated. This weight loss increases roughly linearly from 0.17 ± 0.04 to 0.56 ± 0.06 wt% with increasing agarose concentration in the growth medium, from 0.25 to 1.0 w/v% (Figure 6.2b, squares).

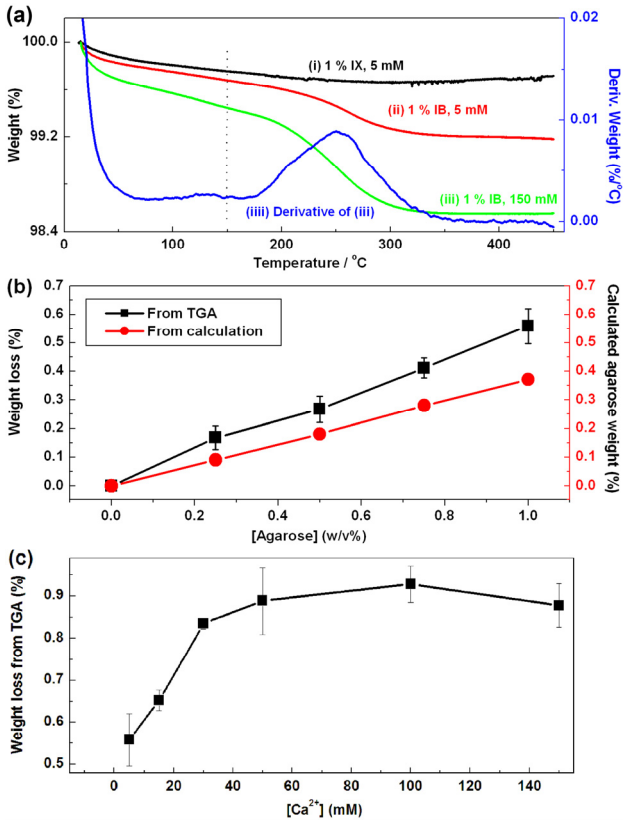

Figure 6.2: a) Typical (i-iii) TGA and (iiii) DTG curves for calcite crystals grown in i) 1 w/v% Agarose IX, 5 mM $CaCl_2$, ii) 1 w/v% Agarose IB, 5 mM $CaCl_2$, and iii, iiii) 1 w/v% Agarose IB, 150 mM $CaCl_2$; b) The relationship between the agarose concentration in the growth media (0.25-1 w/v% Agarose IB, 5 mM $CaCl_2$) and the weight loss above 150 ^oC calculated from TGA (squares) and from equation 1 (circles); c) The relationship between the $CaCl_2$ concentration in the growth media (1 w/v% Agarose IB, $CaCl_2$: 5-150 mM) and the weight loss above 150 ^oC calculated from TGA. Each experiment was repeated 3 times and the mean values are plotted in b) and c).

If the growing crystals incorporate all of the agarose fibers within a given volume, but exclude all of water from that same volume, the mass fraction of incorporated agarose (W_a) in the crystal is given by equation (1),

$$W_a = C/\left[C + \rho_c\left(1 - C/\rho_a\right)\right] \quad (1)$$

where C is the concentration of agarose in the growth media (g mL^{-1}), ρ_a is the density of agarose, 1.64 g cm^{-3},[29] and ρ_c is the density of calcite, 2.71 g cm^{-3}. The values obtained from eq. 1 are plotted in Figure 6.2b (circles). By comparison, the experimental mass fractions determined from TGA are 44-86% higher than the calculated values. One explanation for this discrepancy is that some of the bound water molecules associated with the agarose chains are also incorporated into the crystals.[30]

In order to investigate the role of crystallization pressure on the incorporation, we used a different agarose gel, with a lower fracture strength, as the growth medium. The strength of agarose gels can be changed by partial hydroxyethylation of the polysaccharide units.[31] The substitution on the sugar rings disrupts the molecular packing of the agarose chains and frustrates gel formation. One of these modified agaroses, Agarose IX, is over 10 times weaker than Agarose IB as measured by compression testing (Figure 6.3). Calcite single crystals grown from this gel (1.0 w/v% Agarose IX; 5 mM $CaCl_2$) were obtained with characteristic rhombohedral morphologies (Figure 6.1g). After etching in DI water for four days, the fractured surfaces of the crystals show angular etch pits without any incorporated gel fibers (Figure 6.1h). Correspondingly, TGA of the crystals has no step transition of decomposition over the entire temperature range (ambient temperature to 450 ^{o}C) (Figure 6.2a(i)).

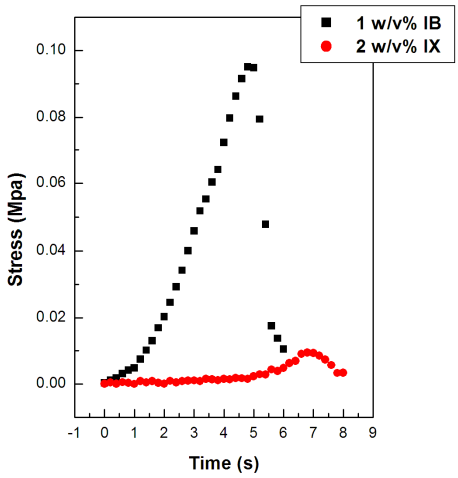

Figure 6.3: Representative results of the compression tests of hydrogels of 1 w/v% Agarose IB (squares) and 2 w/v% Agarose IX (circles).[†] Gel strength is defined as the maximum stress that the sample could sustain before fracture. Each measurement was repeated 3 times and the average gel strengths are 98 ± 3 kPa for the gel of 1 w/v% Agarose IB and 9.8 ± 0.4 kPa for the gel of 2 w/v% of Agarose IX. So the former is 10 times stronger than the latter. Since gel strength will increase with increasing agarose concentration, a gel of 2 w/v% of Agarose IX should be stronger than a gel of 1 w/v% Agarose IX. Therefore, we conclude that a gel of 1 w/v% Agarose IB is over ten times stronger than a gel of the same concentration of Agarose IX.

The morphologies of calcite crystals grown from both Agarose IB and Agarose IX gels are similar (Figure 6.1a, g), while their internal structures are different. The retention of rhombohedral morphologies for crystals grown in both gels suggests that neither of the agarose gels has a strong affinity for the calcite (i.e., agarose does not

[†] We did not measure the gel strength of gels with 1 w/v% Agarose IX because they are too weak to handle.

wet the calcite surface very well). One explanation for the difference in the internal structures is that the weaker gel (1.0 w/v% Agarose IX) is not able to sustain the crystallization pressure and is thus pushed away by the growth fronts. In contrast, the stronger gel (1.0 w/v% Agarose IB) is able to resist the crystallization pressure and the crystals are forced to grow around the fibers and incorporate them.

The growth rate, which is related to the supersaturation, can affect the incorporation of isolated particles during crystal growth.[19-23] To test this variable for gel growth, we grew calcite in 1 w/v% Agarose IB gels with varying [Ca^{2+}] (5-150 mM).[32] With increasing concentration of $CaCl_2$, the crystal morphology gradually evolves from the characteristic rhombohedra to "hopper-like" shapes (Figure 6.4). This shape evolution suggests that with increasing [Ca^{2+}] (growth rate), the 2-D nucleation rates at the corners and edges are increasing.[19] Analysis of these crystals with TGA shows that as the [Ca^{2+}] increases, the amount of material incorporated by the crystals increases from 0.56 ± 0.06 wt% to approximately 0.9 wt%, at which point the weight loss plateaus (Figure 6.2c). This asymptotic behavior suggests that the gel fibers (with bound water) are not all incorporated at slower growth rates (lower [Ca^{2+}]).

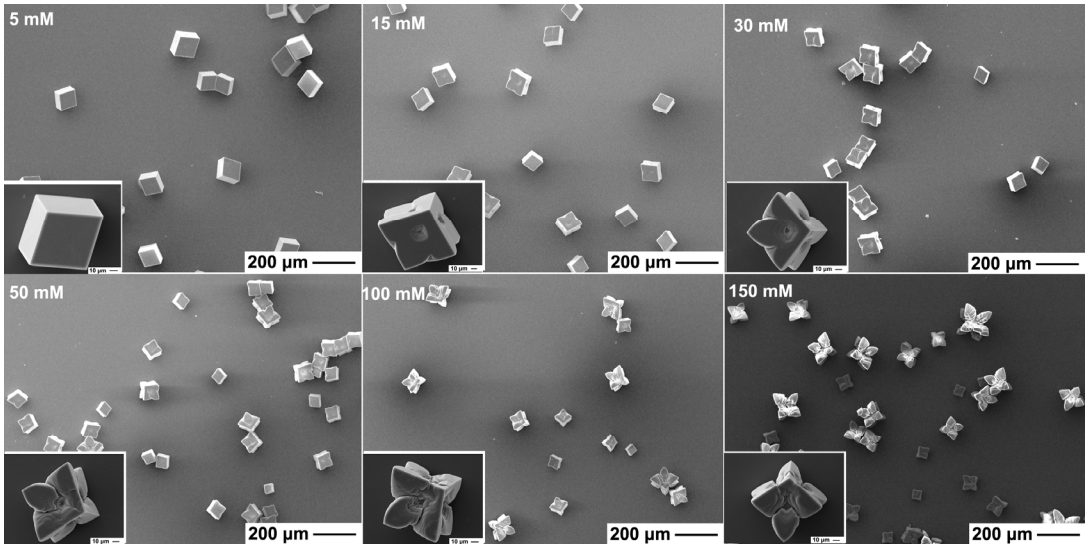

Figure 6.4: SEM images of calcite crystals grown in 1 w/v% Agarose IB gels with varying [Ca^{2+}] (5-150 mM). Insets: images at high magnification, scale bar 10 µm.

One possible explanation for the trend in Figure 6.2c is that the agarose gel network is not homogeneous in structure and contains components with different strengths. Studies of agarose gel structure by scattering and rheological techniques suggest the existence of free and /or dangling chains in addition to the network fibers.[33, 34] At slower growth rates (low [Ca^{2+}]), some of the gel components with lower strengths (free/dangling chains) are expelled by the growing crystals while those with higher strengths (network fibers) are incorporated. As [Ca^{2+}] and growth rate increase, more and more of the weaker parts are incorporated since faster growth rates favor incorporation of foreign material due to the stronger hydrodynamic forces and increased transport resistance.[19-23] When [Ca^{2+}] and growth rate increase to a critical value,[19, 20] the entire gel network is incorporated, reaching a saturation value of approximately 0.9 wt% for a 1 w/v% Agarose IB gel.

Based upon these observations, we propose the following explanations for how the agarose network, with bound water, is incorporated into the calcite crystals (Figure

6.5). The gel fibers limit mass transport of ions to the nearby growth fronts. At the same time, the growing crystals exert a crystallization pressure on the gel network. The competition between these two effects leads to three principally different scenarios: (1) A weak gel network (e.g., Agarose IX) will be pushed away by the crystallization pressure. Crystals grown in this network will not incorporate any material (Figure 6.5a). (2) A strong gel network with fast growth rates (e.g., Agarose IB and high [Ca^{2+}]) will be completely incorporated (Figure 6.5c). (3) An intermediate case is a strong gel network at slower growth rates (e.g., Agarose IB and low [Ca^{2+}]). Crystals grown in these conditions will partially incorporate the gel network. The amount of incorporated material increases with increasing growth rate (Figure 6.5b).

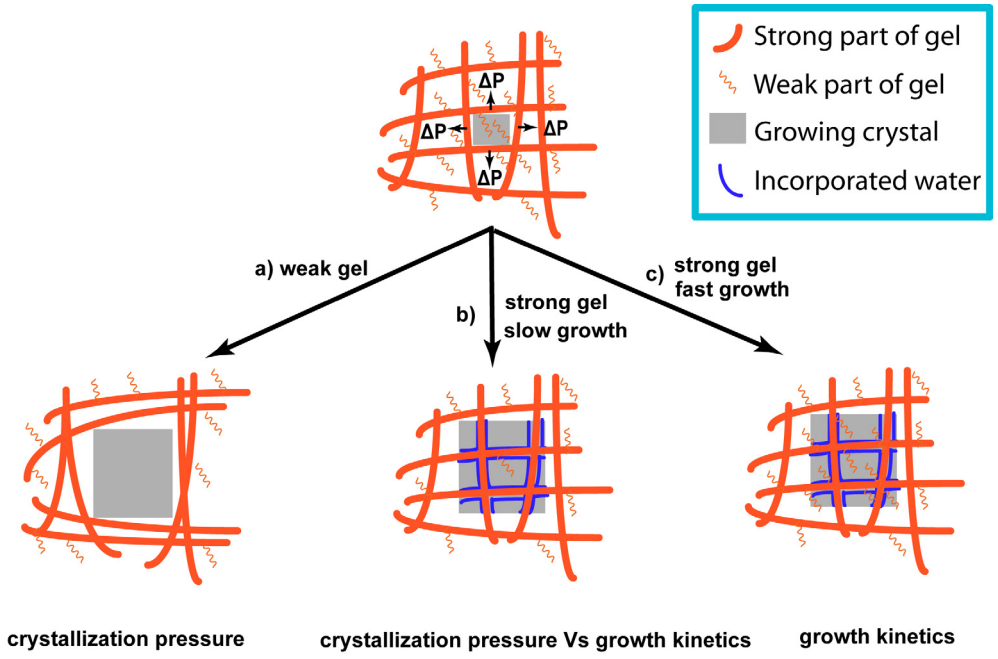

Figure 6.5: A schematic representation of the proposed mechanisms by which the agarose network and water are incorporated during crystal growth. For further details, see the text.

6.3 Conclusion

In conclusion, we have examined the variables critical for controlling the incorporation of gel networks into crystals. In particular, this work demonstrates the crucial effect of growth kinetics on the incorporation of the gel networks. This effect had previously only been demonstrated for the incorporation of individual particles and was not appreciated for gel networks. By controlling both gel strength and crystal growth kinetics, we have achieved complete incorporation and total exclusion of the gel network for a single gel-crystal pair (calcite and agarose). These results have the potential to lead to design criteria for polymer-reinforced crystalline materials with unique structure-property relationships.

6.4 Experimental section

6.4.1 Gel preparation

Two types of agarose (Type IB and Type IX, Sigma) are used to prepare the hydrogels. Agarose solutions (0.25-1 w/v %) were prepared by dissolving agarose powder in a hot solution of 5-150 mM $CaCl_2 \cdot 2H_2O$ (99+%, Sigma-Aldrich). The agarose solution (3 mL) was then filtered (syringe filter; 0.2 μm, Nylon, Millipore) into a Petri dish (35 mm x 10 mm). The solutions containing Agarose IB (gel point: ~36 °C) were cooled at ambient temperature for gelation (about 30 minutes); the solutions containing Agarose IX (gel point: 8-17 °C) were cooled in a refrigerator for gelation (30 minutes) and then equilibrated at ambient temperature for another 30 minutes. After gelation, the Petri dishes were covered with aluminum foil with one small hole.

6.4.2 Crystallization

The Petri dishes with the gel were placed in a closed desiccator containing one vial of ammonium carbonate (Sigma-Aldrich). After 24 hours in the desiccator, crystals grew in the bulk gel and were removed from the gel by dissolving the agarose in boiling deionized (DI) water (18.2 MΩ, Barnstead EASYpure® RoDI). The obtained crystals were then rinsed with DI water and ethanol.

Calcite crystals grown on glass substrates in solution were used as a control. Glass slides were cleaned by sonication in ethanol (15 minutes) and DI water (15 minutes). After rinsing with DI water, each clean slide was placed in a Petri dish with filtered 5 mM $CaCl_2 \cdot 2H_2O$ solution (syringe filter; 0.2 μm, Nylon, Millipore). After crystallization, the slides were sonicated in ethanol to remove the crystals from the glass slides.

6.4.3 Characterization

To observe the incorporated gel fibers, the crystals were fractured by clean razors and then etched in DI water for four days. After etching, the etched crystals were air-dried for characterization. The morphologies of both the as-grown and the etched crystals were examined by scanning electron microscopy (STEREOSCAN 440, LEICA) after being sputter-coated with Au. Thermogravimetric analysis (TGA) of the crystals was conducted with a Thermogravimetric Analyzer (TA Instruments Q500) under a flowing air atmosphere and with a heating rate of 5°C per minute from ambient temperature to 450°C. 10 ± 2 mg of crystals were used for each run after drying overnight in an oven (~80°C). Each TGA experiment was repeated 3 times.

Compression test was used to measure the gel strength. Agarose solutions were poured into Teflon molds (cylinder: 10 mm in diameter and 10 mm in height). The molds were covered with a glass plate and allowed to cool. The solutions containing

Agarose IB (gel point: ~36 °C) were cooled at ambient temperature about 30 minutes; while the solutions containing Agarose IX (gel point: 8-17 °C) were cooled in a refrigerator (0°C) for 30 minutes and then equilibrated at ambient temperature for another 30 minutes. The gels were removed from the molds immediately prior to use. Compression was applied to the agarose cylinder using an Instron Universal Tester (Model 5569) at a crosshead speed of 50 mm/min. The force exerted on the probe was recorded as a function of time. Stress was calculated as $\sigma = F/A_0$, where F is the applied force and A_0 is the original cross-sectional area. Gel strength was defined as the maximum stress that the sample could sustain before fracture. Gel strengths of hydrogels made from 1 w/v% Agarose IB and 2 w/v% Agarose IX were measured. Each measurement was repeated 3 times.

REFERENCES

1. P. M. Dove, J. J. DeYoreo and S. Weiner, eds., *Biomineralization*, The Mineralogical Society of America, Washington, DC, 2003.
2. a) H. Colfen and S. Mann, *Angew. Chem., Int. Ed.*, 2003, **42**, 2350-2365; b) H. Colfen and S. Mann, *Angew. Chem.,* 2003, **115**, 2452-2468.
3. S. Weiner, L. Addadi and H. D. Wagner, *Mater. Sci. Eng. C-Bio S*, 2000, **11**, 1-8.
4. A. Berman, J. Hanson, L. Leiserowitz, T. F. Koetzle, S. Weiner and L. Addadi, *Science*, 1993, **259**, 776-779.
5. J. Aizenberg, J. Hanson, T. F. Koetzle, S. Weiner and L. Addadi, *J. Am. Chem. Soc.*, 1997, **119**, 881-886.
6. J. Aizenberg, A. Tkachenko, S. Weiner, L. Addadi and G. Hendler, *Nature*, 2001, **412**, 819-822.
7. J. S. Robach, S. R. Stock and A. Veis, *J. Struct. Biol.*, 2005, **151**, 18-29.
8. B. Pokroy, A. N. Fitch, F. Marin, M. Kapon, N. Adir and E. Zolotoyabko, *J. Struct. Biol.*, 2006, **155**, 96-103.
9. F. Nudelman, H. H. Chen, H. A. Goldberg, S. Weiner and L. Addadi, *Faraday Discuss.*, 2007, **136**, 9-25.
10. R. J. Park and F. C. Meldrum, *J. Mater. Chem.*, 2004, **14**, 2291-2296.
11. R. J. Park and F. C. Meldrum, *Adv. Mater.*, 2002, **14**, 1167-1169.
12. S. Ludwigs, U. Steiner, A. N. Kulak, R. Lam and F. C. Meldrum, *Adv. Mater.*, 2006, **18**, 2270-2273.
13. C. H. Lu, L. M. Qi, H. L. Cong, X. Y. Wang, J. H. Yang, L. L. Yang, D. Y. Zhang, J. M. Ma and W. X. Cao, *Chem. Mater.*, 2005, **17**, 5218-5224.

14. a) C. Li and L. M. Qi, *Angew. Chem., Int. Ed.*, 2008, **47**, 2388-2393; b) C. Li and L. M. Qi, *Angew. Chem.,* 2008, **120**, 2422-2427.

15. H. K. Henisch, *Crystals in Gels and Liesegang Rings*, Cambridge University Press, New York, 1988.

16. H. J. Nickl and H. K. Henisch, *J. Electrochem. Soc.*, 1969, **116**, 1258-1270.

17. H. Y. Li and L. A. Estroff, *J. Am. Chem. Soc.*, 2007, **129**, 5480-5483.

18. H. Y. Li and L. A. Estroff, *Crystengcomm*, 2007, **9**, 1153-1155.

19. A. A. Chernov, *Modern Crystallography III: Crystal Growth*, Springer-Verlag, New York, 1984.

20. A. A. Chernov, D. E. Temkin and A. M. Mel'nikova, *Sov. Phys. Crystallogr.*, 1976, **21**, 369-374.

21. D. R. Uhlmann, B. Chalmers and K. A. Jackson, *J. Appl. Phys.*, 1964, **35**, 2986-2993.

22. M. O. Kliya and I. G. Sokolova, *Sov. Phys. Crystallogr.* , 1958, **3**, 217-221.

23. A. A. Chernov and D. E. Temkin, in *Current Topics in Materials Science*, ed. E. Kaldis, North-Holland, New York, 1977, pp. 3-77.

24. V. I. Khaimov-Mal'kov, *Sov. Phys.: Crystallogr.*, 1958, **3**, 487-493.

25. L. A. Rijniers, H. P. Huinink, L. Pel and K. Kopinga, *Phys. Rev. Lett.*, 2005, **94**.

26. R. J. Flatt, M. Steiger and G. W. Scherer, *Environ. Geol.*, 2007, **52**, 221-237.

27. J. A. Gavira and J. M. Garcia-Ruiz, *Acta Crystallogr.D*, 2002, **58**, 1653-1656.

28. J. Aizenberg, A. J. Black and G. M. Whitesides, *J. Am. Chem. Soc.*, 1999, **121**, 4500-4509.

29. T. C. Laurent, *Biochim. Biophys. Acta*, 1967, **136**, 199-205.

30. S. Arnott, A. Fulmer, W. E. Scott, I. C. M. Dea, R. Moorhouse and D. A. Rees, *J. Mol. Biol.*, 1974, **90**, 269-284.

31. K. B. Guiseley, (Union, ME), MARINE COLLOIDS INC, US Patent 3956273, 1976.

32. The supersaturation can not be directly determined since [CO_3^{2-}] continuously increases over the course of the experiment.

33. M. Ramzi, C. Rochas and J. M. Guenet, *Macromolecules*, 1998, **31**, 6106-6111.

34. J. M. Guenet and C. Rochas, *Macromol. Symp.*, 2006, **242**, 65-70.

CHAPTER 7

CRYSTAL GROWTH IN GELS: COMPETITIONS AT THE GROWTH FRONTS

7.1 Abstract

The phenomenon of matrix-incorporation has been identified in both biominerals and gel-grown crystals, spurring investigation into the mechanisms by which organic matrixes can become incorporated inside of inorganic single-crystals. Here, we study gel-incorporation inside calcite single-crystals grown in agarose hydrogels by examining the effects of reactant concentration and gel concentration on gel-incorporation. By systematically changing both concentrations, the gel-grown crystals exhibit two distinct characteristics in thermogravimetric analysis (TGA): with and without transition step of agarose decomposition. These two characteristics suggest that by changing these two variables, the crystals are switched between two states: with and without gel-incorporation. Scanning electron microscopy (SEM) images of gently-etched crystals support the TGA data. Based on these results, a gel-incorporation mechanism is proposed, suggesting that a force competition and a mass competition at the growth fronts. The balance between these competitions determines if a growing crystals will or will not incorporate the gel matrix. This work has implications for the study of how biogenic single-crystals incorporate the surrounding organic matrix.

7.2 Introduction

Synthetic and biogenic calcite ($CaCO_3$) crystals are known to incorporate organic molecules while still diffracting X-rays and/or electron beams as single-crystals. Although the incorporation phenomenon has been widely addressed and studied,[1-12] the incorporation mechanism(s) is still poorly understood.[13] This work

demonstrates that by controlling the growth conditions (reactant concentration and gel concentration), single crystals can be grown in a gel with and without gel-incorporation. This study provides further understanding of the interactions between growing crystals and their surrounding matrix.

7.2.1 Gel-grown crystals

The gel method for growing crystals is a widely used approach, which has a long history of more than one centaury (see Chapter 1).[14] A large number of single-crystals have been grown via the gel method.[14] Among these gel-grown crystals, several are found to be exceptional in the sense that they incorporate the gel media and become gel/single-crystal composites. Initially, in 1969, Nickl and Henisch reported that calcite crystals grown from silica gels incorporated the silica matrix.[15] Subsequently, Garcia-Ruiz et al. found that gel-grown protein (lysozyme, ferritin and thaumatin) crystals can incorporate the gel (silica and/or agarose) matrix.[16, 17] More recently, Huang et al. showed that when grown in gelatin gels, calcite crystals also incorporate the gel material.[18] We have demonstrated that calcite crystals grown in agarose gels incorporate the polymer network, and that the crystals maintain their long-range order (single-crystal nature) (See Chapter 3 and 4).[19-21] In addition to calcite, we found that both α-glycine and calcium tartrate tetrahydrate single-crystals also incorporated agarose gels (See Chapter 8).[22] The phenomenon of gel-incorporation indicates that the gel method is not only an approach for the preparation of single-crystals but also a direction to synthesize single-crystal composites and porous single-crystals.[21, 22] Although the examples of gel-incorporated crystals are limited, as compared with the large number of gel-grown crystals, these gel-incorporated crystals are very diversified including crystals of inorganics and organics,

small molecules and macromolecules. Therefore, the gel-incorporation phenomenon could be more general than as we have previously known.

7.2.2 Possible incorporation mechanisms

One of the possible factors that determine the gel-incorporation is gel strength. Before gel-incorporation was first reported by Nickl and Henisch, Khaimov-Mal'kov had proposed that a growing crystal exerted a crystallization pressure on the surrounding gel media. His work suggested that whether or not the crystal incorporated the gel was determined by whether or not the gel was strong enough to resist the crystallization pressure.[23] If the gel network was strong, then the crystal would grow around it, whereas if it was weak, it would be broken or pushed away. Following this hypothesis, Garcia-Ruiz et al. calculated the magnitude of the crystallization pressure from growing protein crystals on agarose gel networks and found that the pressure was much higher than the gel strengths, suggesting that the crystals would always break or push away the gel media.[17] In the experiments, however, the pressure did not disrupt the gel as expected and the authors only obtained crystals with gel-incorporation. Very recently, we have investigated calcite crystal growth in agarose gels and achieved complete incorporation and total exclusion of the gel network for a strong (agarose IB) and a weak (agarose IX) gel, respectively (see Chapter 6).[13] Although the weak agarose is chemically modified (partial hydroxyethylation) as compared with the strong agarose, they are chemically similar. Our results support experimentally the importance of gel strength on gel-incorporation.

Another possible factor affecting gel-incorporation is the crystal growth rate. The effect of growth rate has been demonstrated for the incorporation of individual particles. Multiple experiments show that crystallization in the presence of foreign

particles has two states.[24-26] At low growth rates, growing crystals do not incorporate the particles, but once the growth rate increases beyond a critical value, incorporation of particles takes place. This transition between the two states was mainly explained via a force competition between a "disjoining force" and a hydrodynamic force at the growth front.[24, 27, 28] The former usually tends to push away the particles, while the latter favors the incorporation and is proportional to growth rate. The transition exists at the critical growth rate where the hydrodynamic force is high enough to overcome the disjoining force. In addition, faster growth rates further promote incorporation of the particles by allowing less time for molecules or ions to diffuse into the growth fronts screened by the particles. Similar effects of growth rate might apply to gel-incorporation in gel-grown crystals. Our previous results have indicated that when the growth rate increases, calcite crystals grown in agarose gels incorporate more and more agarose, until saturation is reached (see Chapter 6).[13]

The above incorporation mechanisms predict competitions at the growth fronts for gel-grown crystals. The crystals should switch between two states of gel-incorporation (with or without) when gel strength and/or growth rate changes. Until now, this kind of transition has not, to the best of our knowledge, been demonstrated experimentally for a single gel-crystal pair. In this work, we examine calcite crystal growth in agarose gels and systematically adjust the gel and reactant concentration to directly affect the gel strength and growth rate. We have observed the predicted transition between the two states, verifying the hypothesized incorporation mechanism(s) and improving our understanding of the gel-incorporation phenomenon.

7.3 Results and Discussion

7.3.1 Effects of growth rate on incorporation

Agarose hydrogels were used as growth media. Agarose is a polysaccharide, and in the gel state agarose polymers form interconnected fibrous networks.[21, 29] Calcite crystals were grown in 0.75 w/v % agarose (agaroe IX from Sigma) hydrogels containing $CaCl_2$ solutions by using the ammonium carbonate method.[20, 30] Crystal growth rate was increased by increasing the concentration of $CaCl_2$ ($[CaCl_2]$) from 5 mM to 50 mM. At low $[CaCl_2]$, the crystals exhibit characteristic the rhombohedral morphology of calcite expressed by six {104} faces (Figure 7.1a). With increasing $[CaCl_2]$, the crystal morphology gradually evolves into "hopper-like" shapes, suggesting 2D nucleation take place at the corners and edges of the crystals.[14, 24]

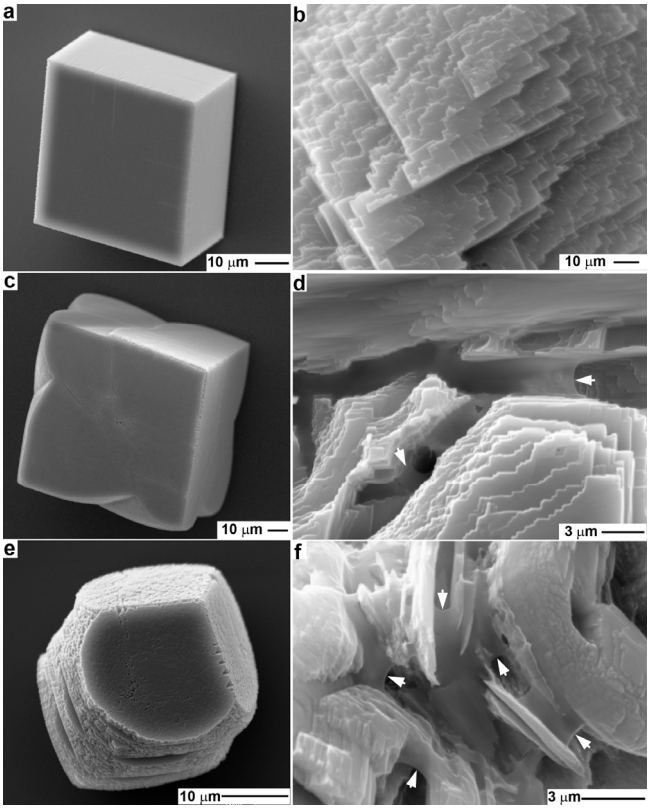

Figure 7.1: Scanning electron microscopy (SEM) images of a, c, e) as prepared and b, d, f) etched calcite crystals grown in a, b) an agarose gel (0.75 w/v% agarose, 5 mM $CaCl_2$), c, d) an agarose gel (0.75 w/v% agarose; 50 mM $CaCl_2$), and e, f) an agarose gel (2 w/v% agarose; 5 mM $CaCl_2$). Arrows highlight the incorporated agarose polymers that are revealed by etching.

The gel-grown crystals were examined by thermogravimetric analysis (TGA) (Figure 7.2a).[13] In TGA, agarose polymers decompose above 200 °C and the resulting curves show clear transition steps. Qualitatively, whether or not a transition step exists in TGA curves of the gel-grown crystals indicates whether or not there is a measurable amount of incorporated agarose polymers. Quantitatively, the weight loss corresponding to the transition step quantifies the amount of incorporated agarose polymers. At low [$CaCl_2$] (5 mM or 10 mM) and slow growth rates, TGA of the

crystals shows no clear decomposition of agarose; while at higher [$CaCl_2$] (15 mM to 50 mM) and faster growth rates, TGA indicates clear transition steps of decomposition (Figure 7.2a). Weight loss above 150°C was plotted as a function of the [$CaCl_2$] (Figure 7.2b). At 5 mM and 10 mM of [$CaCl_2$], the weight loss is around 0.1 wt%. As [$CaCl_2$] is increased above 15 mM, the weight loss increases to 0.26 ± 0.05 wt% to 0.3 ± 0.06 wt%. These values are close to the calculated value (0.28 wt%) for crystals incorporating all of the agarose fibers they encounter.[13, 24]

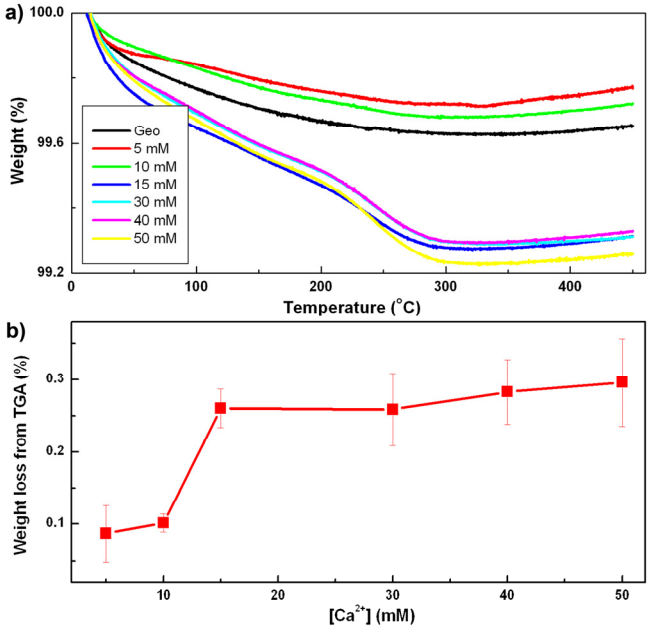

Figure 7.2: a) Typical TGA curves for geological calcite and calcite crystals grown in 0.75 w/v% agarose IX gels containing increasing [$CaCl_2$] (5-50 mM); b) The relationship between the [$CaCl_2$] in the gels and the weight loss above 150 °C calculated from TGA. Each experiment was repeated 3 times and the mean values are plotted.

Apparently, crystals grown at low and high [$CaCl_2$] (growth rates) exhibit two distinct TGA curves corresponding to two states of gel incorporation. At higher

[$CaCl_2$] (≥ 15 mM), crystals grow relatively fast and incorporate most of the agarose fibers they encounter. To further examine the crystals, they were etched in deionized (DI) water at 4 ^oC. SEM images of the etched crystals reveal the incorporated agarose polymers existing in the etch pits (Figure 7.1d). In contrast, at lower [$CaCl_2$] (5 mM and 10 mM), crystals grow slower and push away most of the surrounding agarose fibers. SEM images of the etched surface show angular etch pits without visible agarose polymers (Figure 7.1b). The weight loss (~0.1 wt%) might be due to the absorbance of small molecules such as water at the crystal surfaces. When geological calcite was used as control crystals, TGA showed a weight loss of 0.08 wt% (Figure 7.2a). At low [$CaCl_2$] (5 mM and 10 mM), although most of the agarose is pushed away, a small amount of polymer might be trapped in the crystals, as evidenced by SEM images showing that there is tiny amount of organic materials around etched crystals (Figure 7.3).

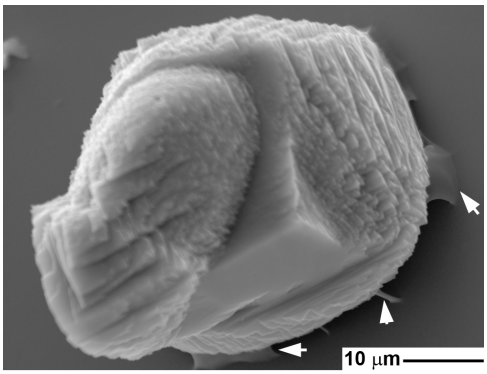

Figure 7.3: A SEM image of an etched calcite crystal grown in an gel (0.75 w/v% agarose IX, 5 mM $CaCl_2$). The image was recorded after the sample was tilted 25 degrees in the microscope, showing organic materials (arrows) surrounding the etched crystals. This small amount of organic materials might be trapped agarose polymers. A top view of the same crystal is shown in Figure 7.1b.

7.3.2 Effects of gel strength on incorporation

Gel strength increases with increasing agarose concentration in gels (gel concentration). The effects of gel strength on incorporation is studied by examining calcite crystals grown in agarose hydrogels with a fixed [$CaCl_2$] (5 mM), but different gel concentrations ranging from 0.75 w/v % to 2 w/v%. In contrast to our previous work where we change gel type (thus change chemical structures) to change gel strength, this experiment keeps the gel type constant, eliminating any potential difference in gel chemistry that might affects incorporation. With increasing gel concentration, the crystals gradually develop curved surfaces at the corners (Figure 7.1a, e). This change in morphology is possibly due to agarose-crystal interactions that affect the growth kinetics anisotropically, similar to the effects of varied additives on calcite morphology.[1, 31-33]

The crystals were examined by TGA. At low gel concentrations (0.75 - 1.25 w/v%), TGA shows no clear transition step of agarose decomposition and the weight loss is around 0.1 wt% (Figure 7.4). At higher gel concentrations (1.5 w/v% and 2 w/v%), clear transition steps of agarose decomposition indicate the existence of incorporated agarose inside crystals and the weight losses are 0.28 ± 0.06 wt% for 1.5 w/v% gel and 0.47 ± 0.13 wt% for 2 w/v% gel (Figure 7.4).

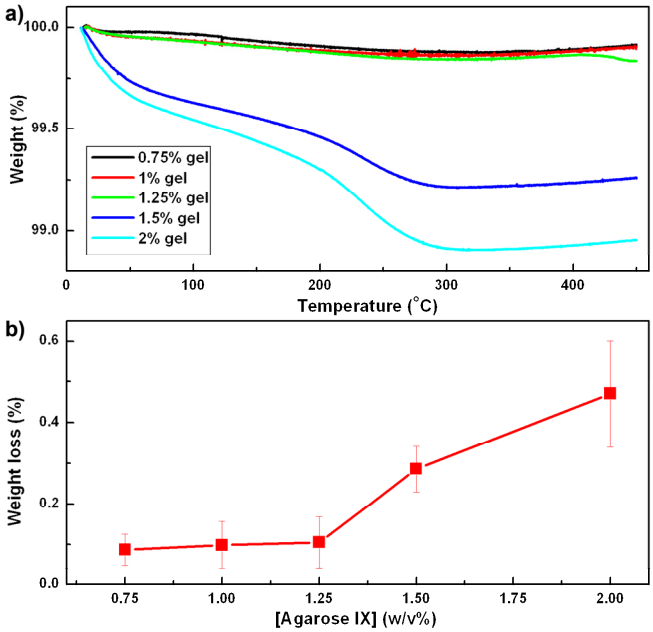

Figure 7.4: a) Typical TGA curves for calcite crystals grown in agarose gels with fixed [$CaCl_2$] (5 mM) but different gel concentrations (0.75 w/v % to 2 w/v%); b) The relationship between the gel concentration and the weight loss above 150 ^{o}C calculated from TGA. Each experiment was repeated 3 times and the mean values are plotted.

The dependence of the amount of incorporated agarose on gel concentration and gel strength is nonlinear (Figure 7.4). At low gel concentrations and low gel strength, there is almost no incorporated agarose inside the crystals (Figure 7.1b). In contrast, at higher gel concentrations and higher gel strength, crystals incorporate agarose gels as evidenced by SEM images revealing the incorporated agarose polymers in the etch pits of etched crystals (Figure 7.1f).

7.3.3 Competitions at the growth fronts

The effects of growth rate and gel strength on gel incorporation indicate that calcite single-crystals grown in agarose IX gels have two states: with and without gel-

incorporation. The transition of crystals between these two states suggests that there are competitions between factors favoring and disfavoring gel-incorporation and that these competing factors are dependent on crystal growth rate and gel strength. Increase of both growth rate and gel strength favors the gel-incorporation. On the one hand, the effect of growth rate on gel-incorporation is similar to that on particle-incorporation[24-26] and is consistent with the force competition model previously suggested by Chernov and Temkin[27] for crystallization in the presence of particles. On the other hand, the effect of gel strength on gel-incorporation verifies the importance of gel resistance to the crystallization pressure implied by Khaimov-Mal'kov.[23] Taking these two contributions into consideration, we propose the following mechanism for gel-incorporation.

As a growing crystal approaches a gel fiber with poor mutual wetting, at the growth front, there is a force competition between a disjoining force, a hydrodynamic force, and the resistance of the gel network (Figure 7.5a).[23, 27] The former force disfavors the gel-fiber incorporation, while the other two favor it. The hydrodynamic force is proportional to the crystal growth rate and the resistance of gel network increases with gel strength. When growth rate or gel strength is high enough, the cooperation of the hydrodynamic force and the resistance of gel network will withstand the disjoining force and the gel fibers will be incorporated. Otherwise, the disjoining force will overcome the combination of the other two and the gel fibers will be pushed away.

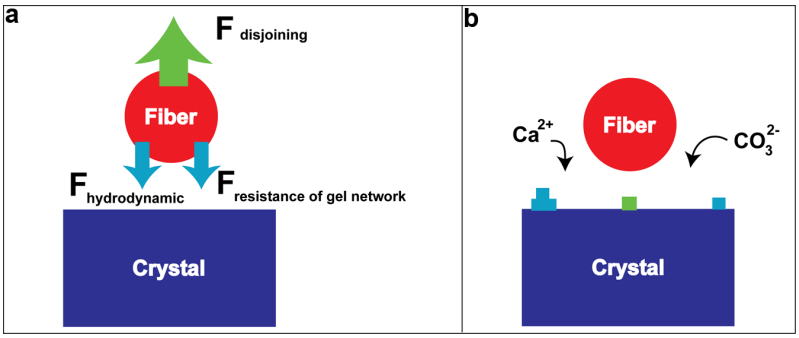

Figure 7.5: A schematic representation of the proposed gel-incorporation mechanism with a) a force competition and b) a mass competition at the growth front nearby an agarose gel fiber. For further details, see the text.

In addition to the force competition, we suggest that there is also a mass competition (Figure 7.5b).[24] The agarose fibers screen the growth fronts beneath them from mass transport so that these growth fronts have higher transport resistance than the nearby growth fronts that are free of screening. Both the screened and unscreened growth fronts advance, competing for "nutrients". Crystal growth at the screened growth fronts disfavors the gel-incorporation, while growth at the unscreened growth front favors it. The faster the growth rate, the higher the transport resistance for the screened growth fronts because less time is allowed for ions to diffuse into the gap between the growth front and the fiber. Therefore, high growth rate favors gel-incorporation because of this mass competition.

7.4 Conclusion

Based on qualitative evidence from SEM and quantitative evidence from TGA, we have demonstrated that for a single gel-crystal pair (calcite and agarose IX), gel-grown crystals can be switched between two states of gel-incorporation (with and without) by changing the crystal growth rate or the gel strength. These transitions can

be explained by a proposed mechanism emphasizing a force competition and a mass competition. These results help to understand matrix-incorporation in biominerals and gel-grown crystals.

7.5 Experimental section

7.5.1 Gel preparation

Agarose solutions (0.75-2 w/v %) were prepared by dissolving agarose powder (Type IX, Sigma, gel point: 8-17 °C) in a hot solution of 5-50 mM $CaCl_2 \cdot 2H_2O$ (99+%, Sigma-Aldrich). The warm agarose solution (3 mL) was filtered (syringe filter; 0.2 μm, Nylon, Millipore) into a Petri dish (35 mm x 10 mm) that was then cooled in a refrigerator (about 0 ^oC) for gelation (30 minutes) and equilibrated at ambient temperature for another 30 minutes. After gelation, the Petri dishes were covered with aluminum foil with one small hole.

7.5.2 *Crystallization and etching*

The Petri dishes with the gels were placed in a closed desiccator containing one vial of ammonium carbonate (Sigma-Aldrich). After 48 hours in the desiccator, crystals grew in the bulk gels and were removed from the gels by dissolving the agarose in boiling deionized (DI) water (18.2 MΩ, Barnstead EASYpure® RoDI) for three times. The obtained crystals were then rinsed with DI water and ethanol.

To observe the incorporated agarose polymers, the crystals were etched in DI water at about 4 ^oC (refrigerator). Crystals grown in 0.75 w/v% gels were etched for 18 days and crystals grown in 2 w/v% gels were etched for 10 days. After etching, the etched crystals were air-dried for characterization.

7.5.3 Characterization

The morphologies of both the as-grown and the etched crystals were examined by scanning electron microscopy (STEREOSCAN 440, LEICA, 25 kV, 600 pA) after being sputter-coated with Au/Pd. Thermogravimetric analysis (TGA) of the crystals was conducted with a Thermogravimetric Analyzer (TA Instruments Q500) under a flowing air atmosphere and with a heating rate of 5°C per minute from ambient temperature to 450°C. 10-20 mg of crystals was used for each run after drying overnight in oven (~80°C). Each TGA experiment was repeated 3 times. TGA of geological calcite (calcite Iceland spar, Carolina Biological) was used as control.

REFERENCES

1. P. M. Dove, J. J. DeYoreo and S. Weiner, eds., *Biomineralization*, The Mineralogical Society of America, Washington, DC, 2003.
2. K. Gries, R. Kroger, C. Kubel, M. Fritz and A. Rosenauer, *Acta Biomater.*, 2009, **5**, 3038-3044.
3. F. Nudelman, H. H. Chen, H. A. Goldberg, S. Weiner and L. Addadi, *Faraday Discuss.*, 2007, **136**, 9-25.
4. J. S. Robach, S. R. Stock and A. Veis, *J. Struct. Biol.*, 2005, **151**, 18-29.
5. J. Aizenberg, D. A. Muller, J. L. Grazul and D. R. Hamann, *Science*, 2003, **299**, 1205-1208.
6. J. Aizenberg, J. Hanson, T. F. Koetzle, S. Weiner and L. Addadi, *J. Am. Chem. Soc.*, 1997, **119**, 881-886.
7. A. S. Finnemore, M. R. J. Scherer, R. Langford, S. Mahajan, S. Ludwigs, F. C. Meldrum and U. Steiner, *Adv. Mater.*, 2009, **21**, 3928-2932.
8. C. Li and L. M. Qi, *Angew. Chem., Int. Ed.*, 2008, **47**, 2388-2393.
9. R. J. Park and F. C. Meldrum, *J. Mater. Chem.*, 2004, **14**, 2291-2296.
10. N. B. J. Hetherington, A. N. Kulak, K. Sheard and F. C. Meldrum, *Langmuir*, 2006, **22**, 1955-1958.
11. R. Munoz-Espi, A. Chandra and G. Wegner, *Cryst. Growth Des.*, 2007, **7**, 1584-1589.
12. C. H. Lu, L. M. Qi, H. L. Cong, X. Y. Wang, J. H. Yang, L. L. Yang, D. Y. Zhang, J. M. Ma and W. X. Cao, *Chem. Mater.*, 2005, **17**, 5218-5224.
13. H. Y. Li and L. A. Estroff, *Adv. Mater.*, 2009, **21**, 470-473.
14. H. K. Henisch, *Crystals in Gels and Liesegang Rings*, Cambridge University Press, New York, 1988.

15. H. J. Nickl and H. K. Henisch, *J. Electrochem. Soc.*, 1969, **116**, 1258-1270.

16. J. M. Garcia-Ruiz, J. A. Gavira, F. Otalora, A. Guasch and M. Coll, *Mater. Res. Bull.*, 1998, **33**, 1593-1598.

17. J. A. Gavira and J. M. Garcia-Ruiz, *Acta Crystallogr.D*, 2002, **58**, 1653-1656.

18. Y. X. Huang, J. Buder, R. Cardoso-Gil, Y. Prots, W. Carrillo-Cabrera, P. Simon and R. Kniep, *Angew. Chem., Int. Ed.*, 2008, **47**, 8280-8284.

19. H. Y. Li and L. A. Estroff, *J. Am. Chem. Soc.*, 2007, **129**, 5480-5483.

20. H. Y. Li and L. A. Estroff, *Crystengcomm*, 2007, **9**, 1153-1155.

21. H. Y. Li, H. L. Xin, D. A. Muller and L. A. Estroff, *Science*, 2009, **326**, 1244-1247..

22. H. Y. Li and L. A. Estroff, 2009, **submitted** (see Chapter 8).

23. V. I. Khaimov-Mal'kov, *Sov. Phys.: Crystallogr.*, 1958, **3**, 487-493.

24. A. A. Chernov, *Modern Crystallography III: Crystal Growth*, Springer-Verlag, New York, 1984.

25. M. O. Kliya and I. G. Sokolova, *Sov. Phys. Crystallogr.* , 1958, **3**, 217-221.

26. D. R. Uhlmann, B. Chalmers and K. A. Jackson, *J. Appl. Phys.*, 1964, **35**, 2986-2993.

27. A. A. Chernov and D. E. Temkin, in *Current Topics in Materials Science*, ed. E. Kaldis, North-Holland, New York, 1977, pp. 3-77.

28. A. A. Chernov, D. E. Temkin and A. M. Mel'nikova, *Sov. Phys. Crystallogr.*, 1976, **21**, 369-374.

29. S. Arnott, A. Fulmer, W. E. Scott, I. C. M. Dea, R. Moorhouse and D. A. Rees, *J. Mol. Biol.*, 1974, **90**, 269-284.

30. J. Aizenberg, A. J. Black and G. M. Whitesides, *J. Am. Chem. Soc.*, 1999, **121**, 4500-4509.

31. J. J. De Yoreo and P. M. Dove, *Science*, 2004, **306**, 1301-1302.

32. K. J. Davis, P. M. Dove, L. E. Wasylenki and J. J. De Yoreo, *Am. Mineral.*, 2004, **89**, 714-720.

33. C. A. Orme, A. Noy, A. Wierzbicki, M. T. McBride, M. Grantham, H. H. Teng, P. M. Dove and J. J. DeYoreo, *Nature*, 2001, **411**, 775-779.

CHAPTER 8

GEL INCORPORATION INSIDE OF ORGANIC SINGLE CRYSTALS GROWN IN AGAROSE HYDROGELS

8.1 Introduction

Crystal growth in gels has interested scientists for more than one century.[1] As "the best and most versatile growth media" for crystal, gels have advantages over controlling both nucleation and growth during crystallization.[1] In a gel, nucleation is suppressed and only a limited number of nuclei grow into large crystals in a stable, diffusion-dominated mass-transport environment. A large variety of gel-grown crystals have been prepared and studied.[1] Among these crystals, calcite was found, surprisingly, by Henisch et al. to incorporate the silica-gel media and become a gel/single-crystal composite.[2] More recently, we have demonstrated that calcite crystals grown in agarose gels also incorporate the polymer network, and that these crystals maintain their long-range order (single-crystal nature).[3] In this respect, the gel-grown calcite crystals, as Henisch pointed out, are similar to biogenic calcite single crystals which have biomacromolecules such as proteins and polysaccharides occluded.[4] Calcite was, therefore, thought to be "unique" in the sense that it incorporates gel media while others do not. This apparent uniqueness was maintained until Garcia-Ruiz et al. reported that gel-grown protein single crystals trapped silica gels and agarose gels.[5] Until now, however, types of crystals known to incorporate gels have been limited.

The discovery of single crystals with incorporated polymer networks challenges our traditional understanding of single crystals, which are usually defined as faceted solids with homogeneous compositions. It also provides a potential approach to prepare new composite materials with complementary properties of rigid

single crystals and flexible polymers. Nevertheless, given that a very limited number of crystals (only calcite and a few proteins) have been demonstrated to incorporate a gel matrix, it is necessary to know how general this gel-incorporation phenomenon is. In this work, we investigate two model crystals to see whether or not they incorporate the gel matrix when grown within agarose hydrogels. Glycine and calcium tartrate tetrahydrate (CTT) crystals are typical models for the study of crystal growth. Glycine is used for polymorph and orientation selection studies,[6] while CTT is for study of crystal growth in gels.[1, 7]

8.2 Results and Discussion

Glycine crystals were grown in 1 w/v % agarose hydrogel by diffusing ethanol vapor into the hydrogel, which was made from a glycine solution (60 mg/mL). Millimeter-sized solids were obtained (Figure 8.1a) and a block of solid was randomly cut for crystallographic investigation using single crystal X-ray diffraction (XRD) (Table 8.1). The results show that the block of solid diffracts X-rays as a single crystal, and the solved unit cell parameters are consistent with reported data for the α-phase of glycine.[8] Therefore, the individual as-grown solid is a single crystal of α-glycine. The internal structure of the single crystals was studied by observing gently etched crystals using field emission scanning electron microscopy (FESEM). After etching in ethanol for 4 days, fiber networks are visible inside of etch pits (Figure 8.1b, c). Since etching reveals the gel networks inside of the crystals, we conclude that gel-grown α-glycine single crystals incorporate the gel polymers.

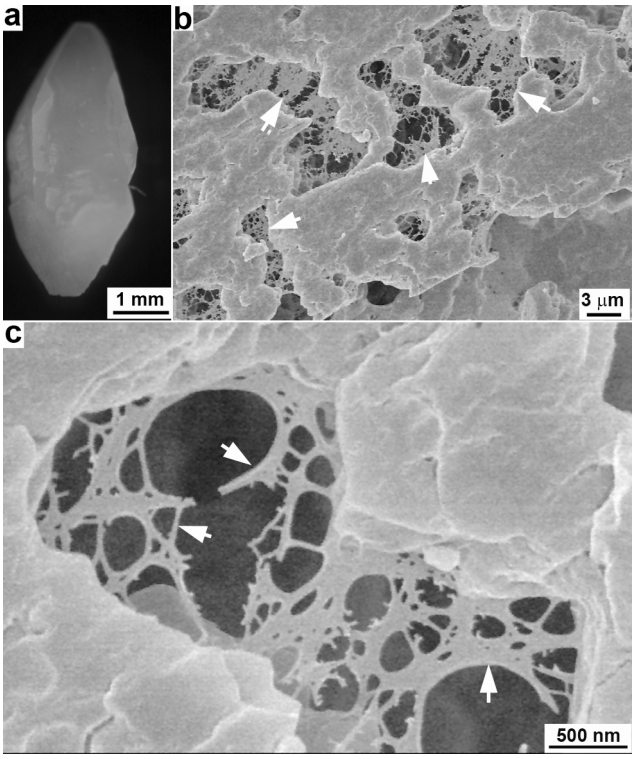

Figure 8.1: (a) An optical microscopy (OM) image of a α-glycine crystal grown from a 1 w/v% agarose hydrogel; (b, c) FESEM images of a gel-grown α-glycine crystal after etching in ethanol for 4 days. White arrows highlight the incorporated gel fibers.

Table 8.1: Unit cell dimensions of α-glycine and CTT crystals.

	α-glycine		CTT	
	Present work	Ref.[8]	Present work	Ref.[9]
a (Å)	5.1050 ± 0.0028	5.1020 ± 0.0008	9.1847 ± 0.0031	9.24 ± 0.02
b (Å)	11.8830 ± 0.0059	11.9709 ± 0.0017	10.5439 ± 0.0036	10.63 ± 0.02
c (Å)	5.4760 ± 0.0026	5.4575 ± 0.0015	9.5835 ± 0.0033	9.66 ± 0.02
α (Deg.)	90	90	90	90
β (Deg.)	111.8640 ± 0.0119	111.705 ± 0.017	90	90
γ (Deg.)	90	90	90	90

CTT crystals were prepared by diffusing an aqueous sodium tartrate solution (40 mM) into a 1 w/v % agarose hydrogel, which already contained calcium chloride (40 mM). Millimeter-sized solids precipitate at the solution/gel interface after 15 days (Figure 8.2a). The half of the crystal that grew into the gel (Figure 8.2a, right) is more opaque than the part of the crystal that grew into solution (Figure 8.2a, left). Similar methods as used for the glycine crystals were utilized to study the crystallography and internal structure of the opaque gel-grown CTT crystals. A block of solid from the opaque side was cut and examined by single crystal XRD. The results shows that the block of solid diffracts X-rays as a single crystal of CTT (Table 8.1).[9] Gently etching the crystals in DI water for 2 days reveals that there are film-like materials inside of the etch pits (Figure 8.2d & e, arrows). These materials are identified as the incorporated gel polymers. Another piece of evidence to support gel incorporation, is that after a block of crystal (Figure 8.2b) was totally dissolved in a 0.1 M HCl solution, a transparent, gel-like material (Figure 8.2c) similar to the shape of the original crystal remained. Therefore, gel-grown CTT single crystals also incorporate the gel polymers.

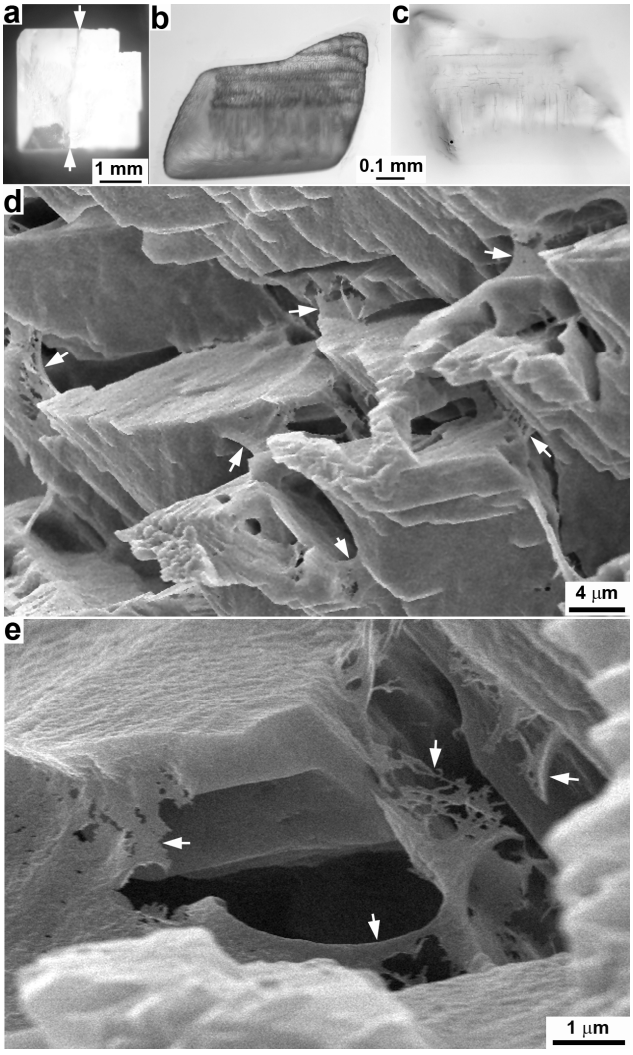

Figure 8.2: (a) An OM image of a CTT crystal grown from a 1 w/v% agarose hydrogel. White arrows highlight the interface between opaque and clear parts of the crystal. See text for details; (b, c) OM images of a block of gel-grown CTT crystal after dissolving in 0.1 M HCl solution for (b) 10 min and (c) 24 hours. Image "c" is roughly mirror symmetric but not overlapping to "b" because the gel material flipped over before imaging; (d, e) FESEM images of a gel-grown CTT crystal after etching in DI water for 2 days. White arrows highlight the incorporated gel polymers.

CTT crystals grown from silica hydrogels have been studied intensively as a model crystal and described not to incorporate the silica gel media.[1, 7] However, this work shows that CTT crystals incorporate agarose gels. The discrepancy might be due to different gel compostions and/or different growth kinetics between the silica and agarose gel systems. When a crystal grows in a gel media, whether it will incorporate the gel matrix or not is mainly determined by three factors: wetting between the crystal and gel matrix, growth rate, and strength of gel network.[10] Very possibly, by selecting gel-crystal pairs and growth conditions, more and more crystals will be found to incorporate gel media.

8.3 Conclusion

In summary, we grew α-glycine and CTT single crystals in agarose hydrogels and found that agarose polymers were incorporated into the crystals without significantly disrupting the crystalline lattices. This work extends the generality of gel-incorporated single crystals grown from hydrogels and shows that the gel method is a promising method to prepare single-crystal composite materials, and to construct sinlge crystal with internal porous structures.

8.4 Experimental section

8.4.1 Glycine crystallization

Agarose solutions (1 w/v %) were prepared by dissolving agarose powder (Type IB, Sigma) in a hot solution of glycine (60 mg/mL, J.T.Baker). The agarose solution (3 mL) was then filtered (syringe filter; 0.2 μm, Nylon, Millipore) into a 20 mL vial. After gelation (about 30 minutes), ethanol (6 mL) was filtered into the vial that was then sealed and laid upside down immediately (Figure 8.3). After 3 days,

crystals form in the gel, and 10 days later, crystals were manually removed using tweezers.

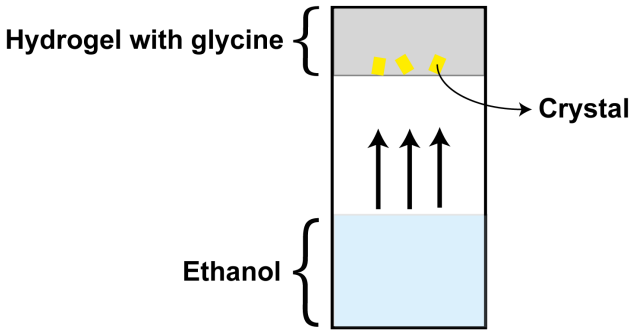

Figure 8.3: A schematic representation of the crystallization of glycine in an agarose hydrogel. An agarose hydrogel containing glycine solution was formed on the bottom of a vial. After ethanol was filtered in, the vial was sealed and laid upside down immediately to separate the gel and ethanol. The slow diffusion of ethanol (g) into the hydrogel resulted in the crystallization of glycine. Due to the syneresis (exudation) of glycine solution from the hydrogels, some precipitate also formed on the wall of the vial. Only the crystals forming in the hydrogel was used for this study. (The drawing is not to scale.)

8.4.2 Calcium tartrate tetrahydrate (CTT) crystallization

Agarose solutions (1 w/v %) were prepared by dissolving agarose powder (Type IB, Sigma) in a hot solution of 40 mM $CaCl_2•_2H_2O$ (99+%, Sigma-Aldrich). The agarose solution (5 mL) was then filtered (syringe filter; 0.2 µm, Nylon, Millipore) into a 15 mL centrifuge tube. After gelation (about 30 minutes), 5 mL of 40 mM sodium tartrate solution was filtered into the tube. After 2-3 days, crystals form at the solution/gel interface, and 15 days later, crystals were taken out using tweezers. The half of the crystal that grew into the gel (Figure 8.2a, right) is more opaque than the part of the crystal that grew into solution (Figure 8.2a, left).

8.4.3 Etching

In order to observe the incorporated gel fibers, the crystals were etched. Glycine crystals were etched in ethanol for four days. The half of the CTT crystal that grew into the gel was cut with clean razors and a block of the cut crystal was then etched in DI water for two days. After etching, the etched crystals were air-dried for characterization. CTT crystals were also etched in 0.1 M HCl solution and observed in-situ by optical microscopy.

8.4.4 Characterization

Single-crystal X-ray diffraction was used to investigate the crystallography of the crystals. A small block of crystal was cut and transferred to the goniometer head of a Bruker X8 APEX2 diffractometer equipped with a molybdenum X-ray tube (λ = 0.71073 Å). Diffraction points (155 points in 60 frames for glycine crystal; 707 points in 120 frames for calcium tartrate tetrahydrate crystal) were collected in frames with 0.5^{o}/frame. The unit cell was obtained using Apex V2.1 program.

The as-grown crystals were imaged by optical microscopy (Olympus SZ) equipped with a digital camera (Olympus C-7070). The CTT crystals during HCl etching were imaged by optical microscopy (Leica DM EP) equipped with a digital camera (Leica DFC 290). The morphologies of the etched crystals were investigated by field emission scanning electron microscopy (Hitachi S4500, 5 kV for glycine, 10 kV for CTT) after being sputter-coated with Pd-Au.

REFERENCES

1. H. K. Henisch, *Crystals in Gels and Liesegang Rings*, Cambridge University Press, New York, 1988.
2. H. J. Nickl and H. K. Henisch, *J. Electrochem. Soc.*, 1969, **116**, 1258-1270.
3. (*a*) H. Y. Li and L. A. Estroff, *J. Am. Chem. Soc.*, 2007, **129**, 5480-5483; (*b*) H. Y. Li and L. A. Estroff, *Crystengcomm*, 2007, **9**, 1153-1155; (*c*) H. Y. Li, H. L. Xin, D. A. Muller and L. A. Estroff, 2009, *Science*, **326**, 1244-1247.
4. (*a*) P. M. Dove, J. J. DeYoreo and S. Weiner, eds., *Biomineralization*, The Mineralogical Society of America, Washington, DC, 2003; (*b*) F. Nudelman, H. H. Chen, H. A. Goldberg, S. Weiner and L. Addadi, *Faraday Discuss.*, 2007, **136**, 9-25; (*c*) J. S. Robach, S. R. Stock and A. Veis, *J. Struct. Biol.*, 2005, **151**, 18-29; (*d*) J. Aizenberg, D. A. Muller, J. L. Grazul and D. R. Hamann, *Science*, 2003, **299**, 1205-1208; (*e*) J. Aizenberg, A. Tkachenko, S. Weiner, L. Addadi and G. Hendler, *Nature*, 2001, **412**, 819-822; (*f*) R. J. Park and F. C. Meldrum, *Adv. Mater.*, 2002, **14**, 1167-1169; (*g*) R. J. Park and F. C. Meldrum, *J. Mater. Chem.*, 2004, **14**, 2291-2296.
5. (*a*) J. M. Garcia-Ruiz, J. A. Gavira, F. Otalora, A. Guasch and M. Coll, *Mater. Res. Bull.*, 1998, **33**, 1593-1598; (*b*) J. A. Gavira and J. M. Garcia-Ruiz, *Acta Crystallogr.D*, 2002, **58**, 1653-1656.
6. (*a*) B. D. Hamilton, M. A. Hillmyer and M. D. Ward, *Cryst. Growth Des.*, 2008, **8**, 3368-3375; (*b*) B. D. Hamilton, I. Weissbuch, M. Lahav, M. A. Hillmyer and M. D. Ward, *J. Am. Chem. Soc.*, 2009, **131**, 2588-2596; (*c*) A. Y. Lee, I. S. Lee, S. S. Dette, J. Boerner and A. S. Myerson, *J. Am. Chem. Soc.*, 2005, **127**, 14982-14983; (*d*) J. F. Kang, J. Zaccaro, A. Ulman and A. Myerson, *Langmuir*, 2000, **16**, 3791-

3796; (*e*) I. Weissbuch, V. Y. Torbeev, L. Leiserowitz and M. Lahav, *Angew. Chem., Int. Ed.*, 2005, **44**, 3226-3229.

7. (*a*) H. K. Henisch, J. Dennis and J. I. Hanoka, *J. Phys. Chem. Solids*, 1965, **26**, 493-500; (*b*) J. I. Hanoka, *J. Appl. Phys.*, 1969, **40**, 2694-2696; (*c*) H. K. Henisch, J. I. Hanoka and J. Dennis, *J. Electrochem. Soc.*, 1965, **112**, 627-629.
8. R. E. Marsh, *Acta Crystallogr.*, 1958, **11**, 654-663.
9. G. K. Ambady, *Acta Crystallogr. B,* 1968, **B 24**, 1548-1557.
10. (*a*) A. A. Chernov and D. E. Temkin, in *Current Topics in Materials Science*, ed. E. Kaldis, North-Holland, New York, 1977, pp. 3-77; (*b*) V. I. Khaimov-Mal'kov, *Sov. Phys.: Crystallogr.*, 1958, **3**, 487-493; (*c*) H. Y. Li and L. A. Estroff, *Adv. Mater.*, 2009, **21**, 470-473.

CHAPTER 9

CONCLUSIONS

We have established a model system in which calcite crystals are grown in agarose hydrogels. This model has been used to study the incorporation of matrix molecules, which is known in both biogenic and synthetic single-crystals. We demonstrated that calcite crystals grown in agarose gels can have two forms: pure single-crystal and polymer/single-crystal composite. The form of the crystals can be switched from the former single-crystal to the latter composite by increasing the growth rate and/or gel strength. The internal structure of the polymer/single-crystal composites are determined both by the polymer and by the crystal. At the length scale of hundreds of nanometers, the interfaces are curved, defined by the contour of agarose fibers; at tens of nanometers, the interfaces are faceted, defined by the faceted habit of the crystal. Finally, in addition to calcite, both α-glycine and calcium tartrate tetrahydrate crystals grown in agarose gels form polymer/single-crystal composites.

This work is relevant to the study of biomineralization, in particular the structures and formation mechanisms of biominerals. The gel-incorporated calcite single crystals are structurally similar to biogenic calcite single-crystal composites. The matrix-incorporation mechanisms suggested by this work might apply to the biomineralization process. Specifically, this research implies that when a growing biomineral incorporates its surrounding matrix, the factors contributing to the incorporation may be physical factors such as the growth rate and/or the mechanical strength of the organic matrix. In future work, these synthetic crystals can provide a platform for studying the mechanisms that lead to enhanced mechanical properties of biogenic polymer-reinforced crystalline materials.

This work sheds new light on the traditional understanding of crystal growth in gels, showing that the gel method is an approach to prepare single-crystal composites. The resulting interpenetrating structures imply that the composites are endowed with properties contributed from both components, such as possibly advanced mechanical properties as compared with the pure single-crystals. Removal of the incorporated polymers lead to porous single-crystals, suggesting that the gel method could be used to prepare crystalline materials that require both high crystallinity (single-crystallinity) and high surface area such as photovoltaic materials.